

Prof. Yu Huang  
State Key Lab of Loess and Quaternary Geology  
Institute of Earth Environment, Chinese Academy  
of Sciences, Xi'an, 710061, China  
Tel./Fax: (86) 29-62336261  
E-mail: [huangyu@ieecas.cn](mailto:huangyu@ieecas.cn)

Aug. 25, 2022

Dear Prof. Kourtchev,

**Revision for Manuscript ACP-2022-376**

We thank you very much for giving us the opportunity to revise our manuscript. We highly appreciate the reviewers for their comments and suggestions on the manuscript entitled “**Oligomer formation from the gas-phase reactions of Criegee intermediates with hydroperoxide esters: mechanism and kinetics**”. We have made revisions of our manuscript carefully according to the comments and suggestions of reviewers. The revised contents are marked in blue color. The response letter to reviewers is attached at the end of this cover letter.

We hope that the revised manuscript can meet the requirement of Atmospheric Chemistry & Physics. Any further modifications or revisions, please do not hesitate to contact us.

Look forward to hearing from you as soon as possible.

Best regards,

Yu Huang

## Comments of reviewer #1

1. The authors should explain their variational TST calculations for barrierless reactions (p.7) in more detail, particularly since they consistently predict higher CI + HCOOH rate constants than experiment (p.10-11).

**Response:** In the original manuscript, the rate coefficients for the barrierless reactions are calculated by employing the variational transition state theory (VTST), and the rate coefficients for the bimolecular reactions with the tight transition states are computed by using the canonical transition state theory (CTST) along with one-dimensional asymmetric Eckart tunneling correction. For the initiation reactions of distinct stabilized Criegee intermediates (SCIs) with HCOOH, there are four possible pathways, namely (1) 1,4 O-H insertion (Entry 1), (2) 1,2 O-H insertion (Entry 2), (3) C-H insertion (Entry 3), and (4) C=O cycloaddition (Entry 4), in which Entry 1 is barrierless and Entry 2-4 have the tight transition states. The total rate coefficient for the reaction of SCIs with HCOOH is equal to the sum of the rate coefficient of each pathway. For the barrierless 1,4 O-H insertion reaction, the VTST is approximated with a Morse potential function,  $V(R) = D_e\{1 - \exp[-\beta(R - R_e)]\}^2$ , along with an anisotropy potential function to stand for the minimum energy path, which is used to calculate the rate coefficients (Raghunath et al., 2017). Here,  $D_e$  is the bond energy excluding the zero-point energy,  $R$  is the reaction coordinate, and  $R_e$  is the equilibrium value of  $R$ . It is assumed that the stretching potential in an anisotropy potential is used in conjunction with a potential form of  $V_{\text{anisotropy}} = V_0[1 - \cos^2(\theta_1 - \theta_{1e}) \times \cos^2(\theta_2 - \theta_{2e})]$  (Raghunath et al., 2017). Here,  $V_0$  is the stretching potential, which stands for by a Morse potential,  $\theta_1$  and  $\theta_{1e}$  represent the rotational angle between fragment 1 and the reference axis and the equilibrium bond angle of fragment 1,  $\theta_2$  and  $\theta_{2e}$  stand for the rotational angle between fragment 2 and the reference axis and the equilibrium bond angle of fragment 2. The association curve for the reaction of 1,4 O-H insertion of SCIs into HCOOH is computed at the M06-2X/6-311+G(2df,2p) level of theory to cover a range from 0.97 to 1.97 Å at step size 0.1 Å for O-H bond and from 1.44 to 2.44 Å at step size 0.1 Å for C-O bond, while other structural parameters are fully optimized. The computed potential energies are fitted to the Morse potential function. However, the calculated rate coefficients for the reactions of SCIs with HCOOH are higher than the prior experimental measurements. The reason is ascribed to the fact that the approximation of VTST using a Morse potential function in conjunction with an anisotropy potential function is unsuitable to predict the rate coefficients for the barrierless 1,4 O-H insertion

reaction.

In the revised manuscript, the rate coefficients for the barrierless reactions are computed by employing the inverse Laplace transformation (ILT) method, and the rate coefficients for the bimolecular reactions with the tight transition states are calculated by utilizing CTST in conjunction with Eckart tunneling correction. The ILT and CTST/Eckart calculations are performed by using the MESMER 6.0 and KiSTheP 2019 programs, respectively (Glowacki et al., 2012; Canneaux et al., 2013). In the ILT treatment, the rotational constants, vibrational frequencies, molecular weights, energies and other input parameters are obtained from the M06-2X/6-311+G(2df,2p) or M06-2X/ma-TZVP methods. For the barrierless reaction of 1,4 O-H insertion of SCIs into HCOOH, SCIs and HCOOH are assigned as the deficient and excess reactants, respectively. The concentration of HCOOH is given a value of  $5.0 \times 10^{10}$  molecules  $\text{cm}^{-3}$  in the simulation, which is taken from the typical concentration of HCOOH in the tropical forest environments (Vereecken, 2012).  $\text{N}_2$  is applied as the buffer gas. A single exponential down model is employed to simulate the collision transfer ( $\langle \Delta E \rangle_{\text{down}} = 200 \text{ cm}^{-1}$ ). The collisional Lennard-Jones parameters are estimated with the empirical formula described by Gilbert and Smith (1990).

The rate coefficients of each elementary pathway included in the initiation reactions of distinct SCIs with HCOOH are calculated in the temperature range of 273-400 K, as listed in Table S3-S6. As shown in Table S3, the total rate coefficients  $k_{\text{tot-CH}_2\text{OO}}$  of  $\text{CH}_2\text{OO}$  reaction with HCOOH are in excess of  $1.0 \times 10^{-10} \text{ cm}^3 \text{ molecule}^{-1} \text{ s}^{-1}$ , and they exhibit a slightly negative temperature dependence in the temperature range studied.  $k_{\text{tot-CH}_2\text{OO}}$  is estimated to be  $1.4 \times 10^{-10} \text{ cm}^3 \text{ molecule}^{-1} \text{ s}^{-1}$  at 298 K, which is in good agreement with the experimental values reported by Welz et al. (2014) ( $[1.1 \pm 0.1] \times 10^{-10}$ ), Chung et al. (2019) ( $[1.4 \pm 0.3] \times 10^{-10}$ ), and Peltola et al. (2020) ( $[1.0 \pm 0.03] \times 10^{-10}$ ).  $k(\text{TS}_{\text{ent1}})$  is approximately equal to  $k_{\text{tot-CH}_2\text{OO}}$  in the whole temperature range, and it decreases in the range of  $1.7 \times 10^{-10}$  (273 K) to  $1.2 \times 10^{-10}$  (400 K)  $\text{cm}^3 \text{ molecule}^{-1} \text{ s}^{-1}$  with increasing temperature.  $k(\text{TS}_{\text{ent1}})$  is several orders of magnitude greater than  $k(\text{TS}_{\text{ent2}})$ ,  $k(\text{TS}_{\text{ent3}})$  and  $k(\text{TS}_{\text{ent4}})$  over the temperature range from 273 to 400 K. The result again shows that the barrierless 1,4 O-H insertion reaction is predominant. Similar conclusion is also obtained from the results of the rate coefficients for the reactions of HCOOH with *anti*- $\text{CH}_3\text{CHOO}$ , *syn*- $\text{CH}_3\text{CHOO}$  and  $(\text{CH}_3)_2\text{COO}$  (Table S4-S6). At ambient temperature, the total rate coefficients of HCOOH reactions with *anti*- $\text{CH}_3\text{CHOO}$ , *syn*- $\text{CH}_3\text{CHOO}$  and  $(\text{CH}_3)_2\text{COO}$  are estimated to be 5.9, 2.7 and  $4.8 \times 10^{-10} \text{ cm}^3 \text{ molecule}^{-1} \text{ s}^{-1}$ ,

respectively, which are consistent with the prior experimental measurements of  $5 \pm 3$ ,  $2.5 \pm 0.3$  and  $4.5 \times 10^{-10} \text{ cm}^3 \text{ molecule}^{-1} \text{ s}^{-1}$  (Welz et al., 2014; Chung et al., 2019; Sipilä et al., 2014).

**Table S3** Rate coefficients ( $\text{cm}^3 \text{ molecule}^{-1} \text{ s}^{-1}$ ) of each elementary pathway involved in the initiation reaction of  $\text{CH}_2\text{OO}$  with  $\text{HCOOH}$  computed at different temperatures

T/K	$k(\text{TS}_{\text{ent1}})$	$k(\text{TS}_{\text{ent2}})$	$k(\text{TS}_{\text{ent3}})$	$k(\text{TS}_{\text{ent4}})$	$k_{\text{tot-CH}_2\text{OO}}$
273	$1.7 \times 10^{-10}$	$3.6 \times 10^{-12}$	$1.0 \times 10^{-22}$	$3.6 \times 10^{-12}$	$1.8 \times 10^{-10}$
280	$1.6 \times 10^{-10}$	$2.9 \times 10^{-12}$	$1.2 \times 10^{-22}$	$3.1 \times 10^{-12}$	$1.7 \times 10^{-10}$
298	$1.4 \times 10^{-10}$	$1.9 \times 10^{-12}$	$2.2 \times 10^{-22}$	$2.3 \times 10^{-12}$	$1.4 \times 10^{-10}$
300	$1.4 \times 10^{-10}$	$1.8 \times 10^{-12}$	$2.4 \times 10^{-22}$	$2.2 \times 10^{-12}$	$1.4 \times 10^{-10}$
320	$1.3 \times 10^{-10}$	$1.2 \times 10^{-12}$	$4.9 \times 10^{-22}$	$1.6 \times 10^{-12}$	$1.3 \times 10^{-10}$
340	$1.3 \times 10^{-10}$	$8.2 \times 10^{-13}$	$1.0 \times 10^{-21}$	$1.3 \times 10^{-12}$	$1.3 \times 10^{-10}$
360	$1.2 \times 10^{-10}$	$5.9 \times 10^{-13}$	$2.2 \times 10^{-21}$	$1.0 \times 10^{-12}$	$1.2 \times 10^{-10}$
380	$1.2 \times 10^{-10}$	$4.5 \times 10^{-13}$	$4.5 \times 10^{-21}$	$8.2 \times 10^{-13}$	$1.2 \times 10^{-10}$
400	$1.2 \times 10^{-10}$	$3.5 \times 10^{-13}$	$9.0 \times 10^{-21}$	$6.9 \times 10^{-13}$	$1.2 \times 10^{-10}$

**Table S4** Rate coefficients ( $\text{cm}^3 \text{ molecule}^{-1} \text{ s}^{-1}$ ) of each elementary pathway involved in the initiation reaction of *anti*- $\text{CH}_3\text{CHOO}$  with  $\text{HCOOH}$  computed at different temperatures

T/K	$k(\text{TS}_{\text{ent1-anti}})$	$k(\text{TS}_{\text{ent2-anti}})$	$k(\text{TS}_{\text{ent3-anti}})$	$k(\text{TS}_{\text{ent4-anti}})$	$k_{\text{tot-anti}}$
273	$5.9 \times 10^{-10}$	$4.2 \times 10^{-11}$	$5.5 \times 10^{-22}$	$6.1 \times 10^{-11}$	$6.9 \times 10^{-10}$
280	$5.7 \times 10^{-10}$	$3.8 \times 10^{-11}$	$6.7 \times 10^{-22}$	$4.9 \times 10^{-11}$	$6.6 \times 10^{-10}$
298	$5.4 \times 10^{-10}$	$2.3 \times 10^{-11}$	$1.2 \times 10^{-21}$	$3.0 \times 10^{-11}$	$5.9 \times 10^{-10}$
300	$5.3 \times 10^{-10}$	$2.0 \times 10^{-11}$	$1.3 \times 10^{-21}$	$2.8 \times 10^{-11}$	$5.8 \times 10^{-10}$
320	$5.0 \times 10^{-10}$	$1.5 \times 10^{-11}$	$2.6 \times 10^{-21}$	$1.7 \times 10^{-11}$	$5.3 \times 10^{-10}$
340	$4.7 \times 10^{-10}$	$9.4 \times 10^{-12}$	$5.4 \times 10^{-21}$	$1.1 \times 10^{-11}$	$4.9 \times 10^{-10}$
360	$4.5 \times 10^{-10}$	$7.0 \times 10^{-12}$	$1.1 \times 10^{-20}$	$7.8 \times 10^{-12}$	$4.7 \times 10^{-10}$
380	$4.4 \times 10^{-10}$	$3.6 \times 10^{-12}$	$2.1 \times 10^{-20}$	$5.6 \times 10^{-12}$	$4.5 \times 10^{-10}$
400	$4.3 \times 10^{-10}$	$2.0 \times 10^{-12}$	$4.0 \times 10^{-20}$	$4.2 \times 10^{-12}$	$4.4 \times 10^{-10}$

**Table S5** Rate coefficients ( $\text{cm}^3 \text{ molecule}^{-1} \text{ s}^{-1}$ ) of each elementary pathway involved in the initiation reaction of *syn*- $\text{CH}_3\text{CHOO}$  with  $\text{HCOOH}$  computed at different temperatures

T/K	$k(\text{TS}_{\text{ent1-syn}})$	$k(\text{TS}_{\text{ent2-syn}})$	$k(\text{TS}_{\text{ent3-syn}})$	$k(\text{TS}_{\text{ent4-syn}})$	$k_{\text{tot-syn}}$
-----	----------------------------------	----------------------------------	----------------------------------	----------------------------------	----------------------

273	$3.1 \times 10^{-10}$	$9.5 \times 10^{-13}$	$4.6 \times 10^{-27}$	$7.5 \times 10^{-16}$	$3.1 \times 10^{-10}$
280	$2.8 \times 10^{-10}$	$8.0 \times 10^{-13}$	$7.1 \times 10^{-27}$	$6.4 \times 10^{-16}$	$2.8 \times 10^{-10}$
298	$2.7 \times 10^{-10}$	$5.4 \times 10^{-13}$	$8.9 \times 10^{-26}$	$5.5 \times 10^{-16}$	$2.7 \times 10^{-10}$
300	$2.7 \times 10^{-10}$	$5.2 \times 10^{-13}$	$9.9 \times 10^{-26}$	$4.6 \times 10^{-16}$	$2.7 \times 10^{-10}$
320	$2.5 \times 10^{-10}$	$3.6 \times 10^{-13}$	$3.0 \times 10^{-25}$	$3.8 \times 10^{-16}$	$2.5 \times 10^{-10}$
340	$2.5 \times 10^{-10}$	$2.6 \times 10^{-13}$	$9.1 \times 10^{-25}$	$3.1 \times 10^{-16}$	$2.5 \times 10^{-10}$
360	$2.3 \times 10^{-10}$	$2.0 \times 10^{-13}$	$2.6 \times 10^{-24}$	$3.0 \times 10^{-16}$	$2.3 \times 10^{-10}$
380	$2.2 \times 10^{-10}$	$1.5 \times 10^{-13}$	$7.2 \times 10^{-24}$	$2.4 \times 10^{-16}$	$2.2 \times 10^{-10}$
400	$2.2 \times 10^{-10}$	$1.2 \times 10^{-13}$	$1.8 \times 10^{-23}$	$2.2 \times 10^{-16}$	$2.2 \times 10^{-10}$

**Table S6** Rate coefficients ( $\text{cm}^3 \text{ molecule}^{-1} \text{ s}^{-1}$ ) of each elementary pathway involved in the initiation reaction of  $(\text{CH}_3)_2\text{OO}$  with  $\text{HCOOH}$  computed at different temperatures

T/K	$k(\text{TS}_{\text{ent1-dim}})$	$k(\text{TS}_{\text{ent2-dim}})$	$k(\text{TS}_{\text{ent3-dim}})$	$k(\text{TS}_{\text{ent4-dim}})$	$k_{\text{tot-dim}}$
273	$5.3 \times 10^{-10}$	$6.8 \times 10^{-12}$	$1.4 \times 10^{-26}$	$4.4 \times 10^{-15}$	$5.4 \times 10^{-10}$
280	$5.1 \times 10^{-10}$	$5.2 \times 10^{-12}$	$2.2 \times 10^{-26}$	$4.2 \times 10^{-15}$	$5.2 \times 10^{-10}$
298	$4.8 \times 10^{-10}$	$2.8 \times 10^{-12}$	$8.0 \times 10^{-26}$	$4.0 \times 10^{-15}$	$4.8 \times 10^{-10}$
300	$4.7 \times 10^{-10}$	$2.6 \times 10^{-12}$	$9.2 \times 10^{-26}$	$3.9 \times 10^{-15}$	$4.7 \times 10^{-10}$
320	$4.5 \times 10^{-10}$	$1.4 \times 10^{-12}$	$3.6 \times 10^{-25}$	$3.7 \times 10^{-15}$	$4.5 \times 10^{-10}$
340	$4.2 \times 10^{-10}$	$8.6 \times 10^{-13}$	$1.3 \times 10^{-24}$	$3.6 \times 10^{-15}$	$4.2 \times 10^{-10}$
360	$3.9 \times 10^{-10}$	$5.5 \times 10^{-13}$	$4.5 \times 10^{-24}$	$3.5 \times 10^{-15}$	$3.9 \times 10^{-10}$
380	$3.7 \times 10^{-10}$	$3.7 \times 10^{-13}$	$1.4 \times 10^{-23}$	$3.4 \times 10^{-15}$	$3.7 \times 10^{-10}$
400	$3.7 \times 10^{-10}$	$2.6 \times 10^{-13}$	$3.9 \times 10^{-23}$	$3.4 \times 10^{-15}$	$3.7 \times 10^{-10}$

Corresponding descriptions have been added in the page 7 line 173-190, page 11 line 303-315, page 12 line 330-338 and page 13 line 346-351 of the revised manuscript:

*The rate coefficients for the barrierless reactions are determined by employing the inverse Laplace transformation (ILT) method. The ILT calculations are performed with the MESMER 6.0 program (Glowacki et al., 2012). In the ILT treatment, the rotational constants, vibrational frequencies, molecular weights, energies and other input parameters are obtained from the M06-2X/6-311+G(2df,2p) or M06-2X/ma-TZVP methods. For the barrierless reaction of 1,4 O-H insertion of SCIs into HCOOH, SCIs and HCOOH are assigned as the deficient and excess reactants,*

respectively. The concentration of HCOOH is given a value of  $5.0 \times 10^{10}$  molecules  $\text{cm}^{-3}$  in the simulation, which is taken from the typical concentration of HCOOH in the tropical forest environments (Vereecken et al., 2012).  $\text{N}_2$  is applied as the buffer gas. A single exponential down model is employed to simulate the collision transfer ( $\langle \Delta E \rangle_{\text{down}} = 200 \text{ cm}^{-1}$ ). The collisional Lennard-Jones parameters are estimated with the empirical formula described by Gilbert and Smith (1990).

The rate coefficients for the bimolecular reactions with the tight transition states are calculated by using the canonical transition state theory (CTST) along with one-dimensional asymmetric Eckart tunneling correction (Truhlar et al., 1996; Eckart, 1930). The CTST/Eckart calculations are performed with the KiSThelP 2019 program (Canneaux et al., 2013).

The rate coefficients of each elementary pathway included in the initiation reactions of distinct SCIs with HCOOH are calculated in the temperature range of 273-400 K, as listed in Table S3-S6. As shown in Table S3, the total rate coefficients  $k_{\text{tot-CH}_2\text{OO}}$  of  $\text{CH}_2\text{OO}$  reaction with HCOOH are in excess of  $1.0 \times 10^{-10} \text{ cm}^3 \text{ molecule}^{-1} \text{ s}^{-1}$ , and they exhibit a slightly negative temperature dependence in the temperature range studied.  $k_{\text{tot-CH}_2\text{OO}}$  is estimated to be  $1.4 \times 10^{-10} \text{ cm}^3 \text{ molecule}^{-1} \text{ s}^{-1}$  at 298 K, which is in good agreement with the experimental values reported by Welz et al. (2014) ( $[1.1 \pm 0.1] \times 10^{-10}$ ), Chung et al. (2019) ( $[1.4 \pm 0.3] \times 10^{-10}$ ), and Peltola et al. (2020) ( $[1.0 \pm 0.03] \times 10^{-10}$ ).  $k(\text{TS}_{\text{ent}1})$  is approximately equal to  $k_{\text{tot-CH}_2\text{OO}}$  in the whole temperature range, and it decreases in the range of  $1.7 \times 10^{-10}$  (273 K) to  $1.2 \times 10^{-10}$  (400 K)  $\text{cm}^3 \text{ molecule}^{-1} \text{ s}^{-1}$  with increasing temperature.  $k(\text{TS}_{\text{ent}1})$  is several orders of magnitude greater than  $k(\text{TS}_{\text{ent}2})$ ,  $k(\text{TS}_{\text{ent}3})$  and  $k(\text{TS}_{\text{ent}4})$  over the temperature range from 273 to 400 K. The result again shows that the barrierless 1,4 O-H insertion reaction is predominant.

Equivalent to the case of  $\text{CH}_2\text{OO}$  reaction with HCOOH, the rate coefficient of each elementary pathway involved in the anti- $\text{CH}_3\text{CHOO} + \text{HCOOH}$  reaction also decreases with the temperature increasing (Table S4). This table shows that Entry 1 is kinetically favored over Entry 2, 3 and 4, and Entry 2 is competitive with Entry 4 in the range 273-400 K. Similar conclusion is also obtained from the results of the rate coefficients for the reactions of syn- $\text{CH}_3\text{CHOO}$  and  $(\text{CH}_3)_2\text{COO}$  with HCOOH that Entry 1 is the dominant pathway (Table S5-S6). It deserves mentioning that the competition of Entry 2 is significantly greater than that of Entry 4 in the syn- $\text{CH}_3\text{CHOO} + \text{HCOOH}$  and  $(\text{CH}_3)_2\text{COO} + \text{HCOOH}$  systems. At ambient temperature, the total rate

coefficients of HCOOH reactions with *anti*-CH<sub>3</sub>CHOO, *syn*-CH<sub>3</sub>CHOO and (CH<sub>3</sub>)<sub>2</sub>COO are estimated to be 5.9, 2.7 and 4.8 × 10<sup>-10</sup> cm<sup>3</sup> molecule<sup>-1</sup> s<sup>-1</sup>, respectively, which are consistent with the prior experimental measurements of 5 ± 3, 2.5 ± 0.3 and 4.5 × 10<sup>-10</sup> cm<sup>3</sup> molecule<sup>-1</sup> s<sup>-1</sup> (Welz et al., 2014; Chung et al., 2019; Sipilä et al., 2014).

2. The trend in exothermicity with substitution pattern (p.8-9) should be explained.

**Response:** Based on the Reviewer's suggestion, the relevance explanations on the trend in exothermicity have been added in the revised manuscript. The exothermicity of 1,4 O-H insertion reactions of distinct SCIs with HCOOH is assessed by the reaction enthalpy ( $\Delta_r H_{298}^\circ$ ), which is defined as the difference between the enthalpies of formation ( $\Delta_f H_{298}^\circ$ ) of the products and reactants ( $\Delta_r H_{298}^\circ = \sum_{\text{products}} \Delta_f H_{298}^\circ - \sum_{\text{reactants}} \Delta_f H_{298}^\circ$ ). To the best of our knowledge, there are no literature values available on the enthalpies of formation of carbonyl oxides and hydroperoxide esters except the simplest carbonyl oxide CH<sub>2</sub>OO. Therefore, the isodesmic reaction method is adopted to obtain the enthalpies of formation, and the results are listed in Table S2. An isodesmic reaction is a hypothetical reaction, in which the type of chemical bonds in the reactants is the similar as that of chemical bonds in the products. The following isodesmic reaction is constructed because the experimental values of H<sub>2</sub>, CH<sub>4</sub> and H<sub>2</sub>O are available ( $\Delta_f H_{298}^\circ$  (H<sub>2</sub>) = 0.00 kcal·mol<sup>-1</sup>;  $\Delta_f H_{298}^\circ$  (CH<sub>4</sub>) = -17.82 kcal·mol<sup>-1</sup>;  $\Delta_f H_{298}^\circ$  (H<sub>2</sub>O) = -57.79 kcal·mol<sup>-1</sup>).



As seen in Table S2, the enthalpy of formation of CH<sub>2</sub>OO is calculated to be 23.23 kcal·mol<sup>-1</sup>, which is in good agreement with the available literature values (Karton et al., 2013; Chen et al., 2016). This result implies that the theoretical method employed herein is reasonable to predict the thermochemical parameters. The enthalpies of formation of carbonyl oxides and hydroperoxide esters significantly decrease with increasing the number of methyl groups. Notably, the decreased values in the enthalpies of formation of carbonyl oxides are greater than those of hydroperoxide esters under the condition of the same number of methyl groups. For example, the enthalpy of formation of *anti*-CH<sub>3</sub>CHOO decreases by 12.95 kcal·mol<sup>-1</sup> compared to the enthalpy of formation of CH<sub>2</sub>OO, and the enthalpy of formation of Pent1b decreases by 12.12 kcal·mol<sup>-1</sup> compared to the

enthalpy of formation of Pent1a. The reaction enthalpies decrease in the order of  $-44.69$  ( $\text{CH}_2\text{OO} + \text{HCOOH} \rightarrow \text{Pent1a}$ )  $< -43.86$  (*anti*- $\text{CH}_3\text{CHOO} + \text{HCOOH} \rightarrow \text{Pent1b}$ )  $< -38.13$  (*syn*- $\text{CH}_3\text{CHOO} + \text{HCOOH} \rightarrow \text{Pent1c}$ )  $< -37.12$   $\text{kcal}\cdot\text{mol}^{-1}$  ( $(\text{CH}_3)_2\text{COO} + \text{HCOOH} \rightarrow \text{Pent1d}$ ), indicating that the reaction enthalpies are highly dependent on the number and location of methyl groups. The trend in reaction enthalpies is consistent with the trend in the enthalpies of formation of carbonyl oxides. The reason might be attributed to the decreased values in the enthalpies of formation of carbonyl oxides greater than those of hydroperoxide esters under the condition of the same number of methyl groups.

**Table S2** Enthalpies of formation ( $\Delta_f H_{298}^{\circ}$ ) for the various carbonyl oxides and hydroperoxide esters computed at the CCSD(T)//M06-2X/6-311+G(2df,2p) level of theory

Species	Cal (kcal·mol <sup>-1</sup> )	Refs. (kcal·mol <sup>-1</sup> )
CH <sub>2</sub> OO	23.23	22.92 <sup>a</sup> 24.59 <sup>b</sup>
<i>anti</i> -CH <sub>3</sub> OO	10.28	
<i>syn</i> -CH <sub>3</sub> CHOO	6.73	
(CH <sub>3</sub> ) <sub>2</sub> COO	-6.77	
HCOOH		-90.62 (exp)
HC(O)OCH <sub>2</sub> OOH (Pent1a)	-112.08	
HC(O)OCH(CH <sub>3</sub> )OOH (Pent1b)	-124.20	
HC(O)OCH(CH <sub>3</sub> )OOH (Pent1c)	-122.02	
HC(O)OC(CH <sub>3</sub> ) <sub>2</sub> OOH (Pent1d)	-134.51	

Exp is taken from NIST Chemistry Webbook

<sup>a</sup> the value is obtained at the G4 level of theory (Chen et al., 2016)

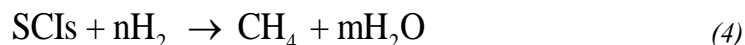
<sup>b</sup> the value is obtained at the W3-F12 level of theory (Karton et al., 2013)

Corresponding descriptions have been added in the page 9 line 240-247 and page 10 line 248-271 of the revised manuscript:

*The exothermicity of 1,4 O-H insertion reactions of distinct SCIs with HCOOH is assessed by the reaction enthalpy ( $\Delta_r H_{298}^{\circ}$ ), which is defined as the difference between the enthalpies of formation ( $\Delta_f H_{298}^{\circ}$ ) of the products and reactants ( $\Delta_r H_{298}^{\circ} = \sum_{\text{products}} \Delta_f H_{298}^{\circ} - \sum_{\text{reactants}} \Delta_f H_{298}^{\circ}$ ). To the best of our knowledge, there are no literature values available on the enthalpies of formation of carbonyl oxides and hydroperoxide esters except the simplest carbonyl oxide CH<sub>2</sub>OO. Therefore, the isodesmic reaction method is adopted to obtain the enthalpies of formation, and the results are listed*



in Table S2. An isodesmic reaction is a hypothetical reaction, in which the type of chemical bonds in the reactants is the similar as that of chemical bonds in the products. The following isodesmic reaction is constructed because the experimental values of  $H_2$ ,  $CH_4$  and  $H_2O$  are available ( $\Delta_f H_{298}^0(H_2) = 0.00 \text{ kcal}\cdot\text{mol}^{-1}$ ;  $\Delta_f H_{298}^0(CH_4) = -17.82 \text{ kcal}\cdot\text{mol}^{-1}$ ;  $\Delta_f H_{298}^0(H_2O) = -57.79 \text{ kcal}\cdot\text{mol}^{-1}$ ).

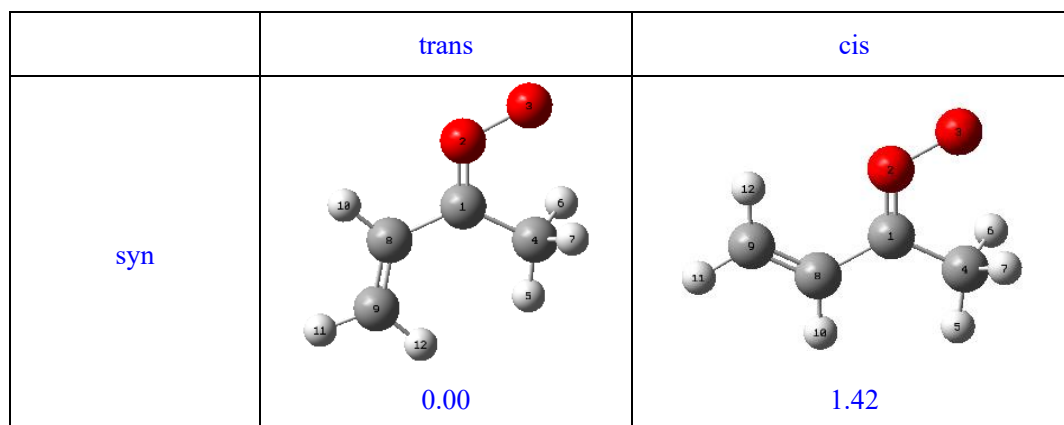


As seen in Table S2, the enthalpy of formation of  $CH_2OO$  is calculated to be  $23.23 \text{ kcal}\cdot\text{mol}^{-1}$ , which is in good agreement with the available literature values (Chen et al., 2016; Karton et al., 2013). This result implies that the theoretical method employed herein is reasonable to predict the thermochemical parameters. The enthalpies of formation of carbonyl oxides and hydroperoxide esters significantly decrease with increasing the number of methyl groups. Notably, the decreased values in the enthalpies of formation of carbonyl oxides are greater than those of hydroperoxide esters under the condition of the same number of methyl groups. For example, the enthalpy of formation of anti- $CH_3CHOO$  decreases by  $12.95 \text{ kcal}\cdot\text{mol}^{-1}$  compared to the enthalpy of formation of  $CH_2OO$ , and the enthalpy of formation of Pent1b decreases by  $12.12 \text{ kcal}\cdot\text{mol}^{-1}$  compared to the enthalpy of formation of Pent1a. The reaction enthalpies decrease in the order of  $-44.69$  ( $CH_2OO + HCOOH \rightarrow Pent1a$ )  $< -43.86$  (anti- $CH_3CHOO + HCOOH \rightarrow Pent1b$ )  $< -38.13$  (syn- $CH_3CHOO + HCOOH \rightarrow Pent1c$ )  $< -37.12 \text{ kcal}\cdot\text{mol}^{-1}$  ( $(CH_3)_2COO + HCOOH \rightarrow Pent1d$ ), indicating that the reaction enthalpies are highly dependent on the number and location of methyl groups. The trend in reaction enthalpies is consistent with the trend in the enthalpies of formation of carbonyl oxides. The reason might be attributed to the decreased values in the enthalpies of formation of carbonyl oxides greater than those of hydroperoxide esters under the condition of the same number of methyl groups.

3. The analysis of possible bimolecular CI reactions (p.21) should be extended to the three substituted CIs.

**Response:** Kalinowski et al. has confirmed that the central CO bond of carbonyl oxides is a double bond, while the terminal OO bond is a single bond (Kalinowski et al., 2014). It is therefore that the maximum degree of substitution of carbonyl oxides is two. To further evaluate the relative importance of the complex SCIs reactions with coreactant, the bimolecular reactions of methyl vinyl ketone

oxide (MVK-OO) with H<sub>2</sub>O, HCOOH, SO<sub>2</sub> and HPMF have been considered in the revised manuscript. MVK-OO, formed with 21 to 23% yield from the ozonolysis of isoprene, is a four carbon, asymmetric, resonance-stabilized Criegee intermediate (Barber et al., 2018). MVK-OO has four conformers, *syn-trans*-, *syn-cis*-, *anti-trans*-, and *anti-cis*- as shown in Fig. S10. Herein, *syn* and *anti* refer to the orientation of the -CH<sub>3</sub> group relative to the terminal oxygen of MVK-OO, whereas *cis* and *trans* refer to the orientation of the C<sub>8</sub>=C<sub>9</sub> bond relative to the C<sub>1</sub>=O<sub>2</sub> bond. According to the results shown in the Fig. S10, the lowest-energy conformer is *syn-trans*-MVK-OO, which is lower than *syn-cis*-, *anti-trans*-, and *anti-cis*-MVK-OO by 1.42, 2.43 and 2.69 kcal·mol<sup>-1</sup>, respectively. Therefore, the lowest-energy conformer *syn-trans*-MVK-OO is selected as the model compound to study its bimolecular reactions. As shown in Table 2, the rate coefficient of H<sub>2</sub>O reaction with *syn-trans*-MVK-OO is lower than with other SCIs by 2 to 3 orders of magnitude. The reason is likely to be that the existence of methyl and vinyl groups hinders the occurrence of bimolecular reaction with water vapour. Consequently, a fraction of *syn-trans*-MVK-OO may survive in the presence of water vapour and react with other species.  $k_{\text{eff(MVK-OO+H}_2\text{O)}}$  is nearly identical to  $k_{\text{eff(MVK-OO+HCOOH)}}$ , which is greater than  $k_{\text{eff(MVK-OO+SO}_2)}$  and  $k_{\text{eff(MVK-OO+HPMF)}}$  when the concentration of HPMF is the same as that of HCOOH.  $k_{\text{eff(MVK-OO+H}_2\text{O)}}$  and  $k_{\text{eff(MVK-OO+HCOOH)}}$  are greater than  $k_{\text{eff(MVK-OO+SO}_2)}$ , which, in turn, are greater than  $k_{\text{eff(MVK-OO+HPMF)}}$  when the concentration of HPMF is equal to that of SCIs. Based on the above discussions, it can be concluded that the relative importance of carbonyl oxides reactions with hydroperoxide esters is significantly dependent on the concentrations of hydroperoxide esters. These reactions may play a certain role in the formation of organic new particle in some regions where low concentration of water vapour and high concentration of hydroperoxide esters occur.



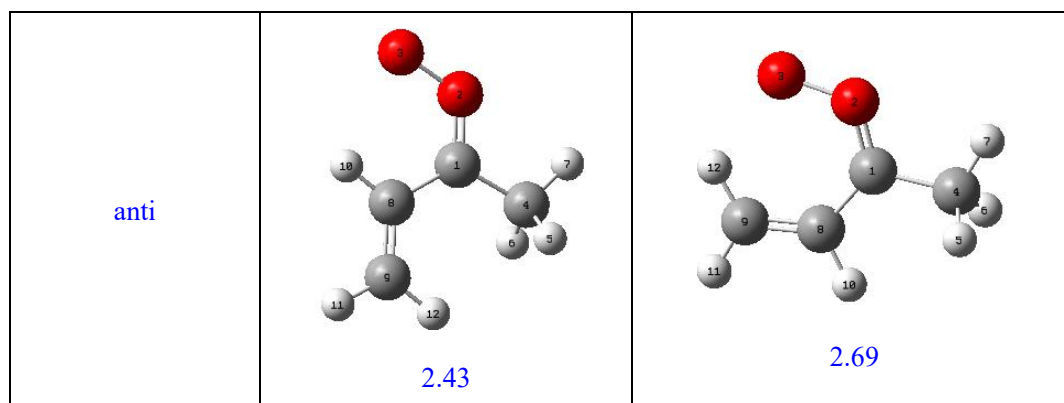


**Figure S10.** The optimized geometries and relative energies ( $\text{kcal}\cdot\text{mol}^{-1}$ ) computed for the four conformers of MVK-oxide. Geometries are optimized at the M06-2X/6-311+g(2df,2p) level of theory. Single point energies are calculated at the CCSD(T)/6-311+g(2df,2p) level of theory.

Corresponding descriptions have been added in the page 24 line 611-619 and page 25 line 620-636 of the revised manuscript:

To further evaluate the relative importance of the complex SCIs reactions with coreactant, the bimolecular reactions of methyl vinyl ketone oxide (MVK-OO) with  $\text{H}_2\text{O}$ ,  $\text{HCOOH}$ ,  $\text{SO}_2$ , and HPMF are considered. MVK-OO, formed with 21 to 23% yield from the ozonolysis of isoprene, is a four carbon, asymmetric, resonance-stabilized Criegee intermediate (Barber et al., 2018). MVK-OO has four conformers, syn-trans-, syn-cis-, anti-trans-, and anti-cis- as shown in Fig. S10. Herein, syn and anti refer to the orientation of the  $-\text{CH}_3$  group relative to the terminal oxygen of MVK-OO, whereas cis and trans refer to the orientation of the  $\text{C}_8=\text{C}_9$  bond relative to the  $\text{C}_1=\text{O}_2$  bond. According to the results shown in the Fig. S10, the lowest-energy conformer is syn-trans-MVK-OO, which is lower than syn-cis-, anti-trans-, and anti-cis-MVK-OO by 1.42, 2.43 and 2.69  $\text{kcal}\cdot\text{mol}^{-1}$ , respectively. Therefore, the lowest-energy conformer syn-trans-MVK-OO is selected as the model compound to study its bimolecular reactions. As shown in Table 2, the rate coefficient of  $\text{H}_2\text{O}$  reaction with syn-trans-MVK-OO is lower than with other SCIs by 2 to 3 orders of magnitude. The reason is likely to be that the existence of methyl and vinyl groups hinders the occurrence of bimolecular reaction with water vapour. Consequently, a fraction of syn-trans-MVK-OO may survive in the presence of water vapour and react with other species.  $k_{\text{eff}}(\text{MVK-OO}+\text{H}_2\text{O})$  is nearly identical to  $k_{\text{eff}}(\text{MVK-OO}+\text{HCOOH})$ , which is greater than  $k_{\text{eff}}(\text{MVK-OO}+\text{SO}_2)$  and  $k_{\text{eff}}(\text{MVK-OO}+\text{HPMF})$  when the concentration of HPMF is the same as that of HCOOH.  $k_{\text{eff}}(\text{MVK-OO}+\text{H}_2\text{O})$  and  $k_{\text{eff}}(\text{MVK-OO}+\text{HCOOH})$  are greater than  $k_{\text{eff}}(\text{MVK-OO}+\text{SO}_2)$ , which, in turn, are greater than  $k_{\text{eff}}(\text{MVK-OO}+\text{HPMF})$  when the concentration of HPMF is equal to that of SCIs. Based on the above discussions, it can be concluded

*that the relative importance of carbonyl oxides reactions with hydroperoxide esters is significantly dependent on the concentrations of hydroperoxide esters. These reactions may play a certain role in the formation of organic new particle in some regions where low concentration of water vapour and high concentration of hydroperoxide esters occur.*

4. Since the CI is clearly the limiting reactant in the CI + HCOOH reaction, the atmospheric concentration of HPMF (and the other hydroperoxy esters) is much better estimated to be the CI concentration. (This, of course, will greatly lower the predicted pseudo-first-order rate constants for the CI + HPMF reaction.)

**Response:** Based on the Reviewer's suggestion, the relevance explanations on the predicted pseudo-first-order rate constants have been added in the revised manuscript. It is of interest to assess whether the reactions of distinct SCIs with HPMF can compete well with the losses to reactions with trace species (e.g., H<sub>2</sub>O, HCOOH and SO<sub>2</sub>), because it is well known that the reactions with trace species are expected to be the dominant chemical sinks for SCIs in the atmosphere (Taatjes et al., 2013; Long et al., 2016). The reported concentrations of coreactant, the rate coefficients  $k$ , and the effective pseudo-first-order rate constants ( $k_{\text{eff}} = k[\text{coreactant}]$ ) for distinct SCI reactions with H<sub>2</sub>O, HCOOH, SO<sub>2</sub> and HPMF are summarized in Table 2. As seen in Table 2, the rate coefficient of a particular SCI reaction with trace species is strongly dependent on its structure. The methyl group substitution may alter the rate coefficient by several to tens of times. The atmospheric concentrations of H<sub>2</sub>O, HCOOH and SO<sub>2</sub> in the tropical forest environments are measured to be  $3.9\text{--}6.1 \times 10^{17}$ ,  $5.0\text{--}10 \times 10^{10}$ , and  $1.7\text{--}9.0 \times 10^{10}$  molecules cm<sup>-3</sup>, respectively (Vereecken, 2012). For the reactions of CH<sub>2</sub>OO with H<sub>2</sub>O, HCOOH, and SO<sub>2</sub>, the experimental rate coefficients are determined to be  $< 1.5 \times 10^{-15}$ ,  $[1.1 \pm 0.1] \times 10^{-10}$ , and  $[3.9 \pm 0.7] \times 10^{-11}$  cm<sup>3</sup> molecule<sup>-1</sup> s<sup>-1</sup>, respectively (Welz et al., 2012 and 2014; Chao et al., 2015), which translate into  $k_{\text{eff(CH}_2\text{OO+H}_2\text{O)}}$ ,  $k_{\text{eff(CH}_2\text{OO+HCOOH)}}$  and  $k_{\text{eff(CH}_2\text{OO+SO}_2)}$  of  $5.9\text{--}9.2 \times 10^2$ ,  $5.5\text{--}11$ , and  $0.7\text{--}3.5$  s<sup>-1</sup>, respectively. The result reveals that the reaction of CH<sub>2</sub>OO with H<sub>2</sub>O is the most important bimolecular reaction.  $k_{\text{eff(CH}_2\text{OO+HCOOH)}}$  is greater by a factor of 3-8 than  $k_{\text{eff(CH}_2\text{OO+SO}_2)}$ , indicating that the reaction of CH<sub>2</sub>OO with HCOOH is favored over reaction with SO<sub>2</sub>. Similar conclusion is also obtained from the results of  $k_{\text{eff}}$  for the reactions of *anti*-CH<sub>3</sub>CHOO, *syn*-CH<sub>3</sub>CHOO and (CH<sub>3</sub>)<sub>2</sub>COO with H<sub>2</sub>O, HCOOH and SO<sub>2</sub> that SCIs reactions with H<sub>2</sub>O are faster than with HCOOH, which, in turn, are

faster than with SO<sub>2</sub>.

According to the results shown in the Table 2, the room temperature rate coefficient for the reaction of CH<sub>2</sub>OO with HPMF is calculated to be  $2.7 \times 10^{-11} \text{ cm}^3 \text{ molecule}^{-1} \text{ s}^{-1}$ . However, to the best of our knowledge, the atmospheric concentration of HPMF has not been reported up to now. If we assume that the concentration of HPMF is the same as that of HCOOH,  $k_{\text{eff}}(\text{CH}_2\text{OO}+\text{HPMF})$  is estimated to be 1.4-2.7 s<sup>-1</sup>, which is significantly lower than  $k_{\text{eff}}(\text{CH}_2\text{OO}+\text{H}_2\text{O})$  and  $k_{\text{eff}}(\text{CH}_2\text{OO}+\text{HCOOH})$ .  $k_{\text{eff}}(\text{CH}_2\text{OO}+\text{HPMF})$  is nearly identical to  $k_{\text{eff}}(\text{CH}_2\text{OO}+\text{SO}_2)$ , indicating that the CH<sub>2</sub>OO + HPMF reaction is competitive with the CH<sub>2</sub>OO + SO<sub>2</sub> system. Previous model-measurement studies have estimated the surface-level SCIs concentrations in the range of  $1.0 \times 10^4$  to  $1.0 \times 10^5 \text{ molecules cm}^{-3}$  (Khan et al., 2018; Novelli et al., 2017). If we assume that the concentration of HPMF is equal to that of SCIs,  $k_{\text{eff}}(\text{CH}_2\text{OO}+\text{HPMF})$  is calculated to be  $2.7\text{-}27 \times 10^{-7} \text{ s}^{-1}$ , which is several orders of magnitude lower than  $k_{\text{eff}}(\text{CH}_2\text{OO}+\text{H}_2\text{O})$ ,  $k_{\text{eff}}(\text{CH}_2\text{OO}+\text{HCOOH})$  and  $k_{\text{eff}}(\text{CH}_2\text{OO}+\text{SO}_2)$ . This result indicates that the reaction of CH<sub>2</sub>OO with HPMF is of less importance. Similar conclusion is also obtained from the reactions of *anti*-CH<sub>3</sub>CHOO, *syn*-CH<sub>3</sub>CHOO and (CH<sub>3</sub>)<sub>2</sub>COO with HPMF. Based on the above discussions, it can be concluded that the relative importance of carbonyl oxides reactions with hydroperoxide esters is significantly dependent on the concentrations of hydroperoxide esters.

**Table 2** The reported concentrations of coreactant, the rate coefficients  $k$ , and the effective pseudo-first-order rate constants ( $k_{\text{eff}} = k[\text{coreactant}]$ ) for distinct SCI reactions with HPMF, H<sub>2</sub>O, HCOOH and SO<sub>2</sub> at the tropical forest environments

SCIs	Coreactant	[Coreactant] (molecules cm <sup>-3</sup> )	$k$ (cm <sup>3</sup> molecule <sup>-1</sup> s <sup>-1</sup> )	$k_{\text{eff}}$ (s <sup>-1</sup> )	Reference
CH <sub>2</sub> OO	H <sub>2</sub> O	$3.9\text{-}6.1 \times 10^{17}$	$< 1.5 \times 10^{-15}$	$5.9\text{-}9.2 \times 10^2$	Chao et al., (2015)
	HCOOH	$5.0\text{-}10.0 \times 10^{10}$	$[1.1 \pm 0.1] \times 10^{-10}$	5.5-11	Welz et al., (2014)
	SO <sub>2</sub>	$1.7\text{-}9.0 \times 10^{10}$	$[3.9 \pm 0.7] \times 10^{-11}$	0.7-3.5	Welz et al., (2012)
	HPMF	-	$2.7 \times 10^{-11}$	-	This work
<i>anti</i> -CH <sub>3</sub> CHOO	H <sub>2</sub> O	$3.9\text{-}6.1 \times 10^{17}$	$[1.0 \pm 0.4] \times 10^{-14}$	$3.9\text{-}6.1 \times 10^3$	Taatjes et al., (2013)
	HCOOH	$5.0\text{-}10.0 \times 10^{10}$	$[5 \pm 3] \times 10^{-10}$	25.0-50.0	Welz et al., (2014)
	SO <sub>2</sub>	$1.7\text{-}9.0 \times 10^{10}$	$[6.7 \pm 1.0] \times 10^{-11}$	1.1-6.0	Taatjes et al., (2013)

	HPMF	-	$3.3 \times 10^{-10}$	-	This work
	H <sub>2</sub> O	$3.9\text{-}6.1 \times 10^{17}$	$< 4.0 \times 10^{-15}$	$1.6\text{-}2.4 \times 10^3$	Taatjes et al., (2013)
<i>syn</i> -CH <sub>3</sub> CHOO	HCOOH	$5.0\text{-}10.0 \times 10^{10}$	$[2.5 \pm 0.3] \times 10^{-10}$	12.5-25.0	Welz et al., (2014)
	SO <sub>2</sub>	$1.7\text{-}9.0 \times 10^{10}$	$[2.4 \pm 0.3] \times 10^{-11}$	0.4-2.2	Taatjes et al., (2013)
	HPMF	-	$1.7 \times 10^{-13}$	-	This work
	H <sub>2</sub> O	$3.9\text{-}6.1 \times 10^{17}$	$< 1.5 \times 10^{-16}$	58.5-91.5	Huang et al., (2015)
(CH <sub>3</sub> ) <sub>2</sub> COO	HCOOH	$5.0\text{-}10.0 \times 10^{10}$	$4.5 \times 10^{-10}$	22.5-45.0	Sipilä et al., (2014)
	SO <sub>2</sub>	$1.7\text{-}9.0 \times 10^{10}$	$1.3 \times 10^{-10}$	2.2-11.7	Huang et al., (2015)
	HPMF	-	$2.2 \times 10^{-11}$	-	This work
	H <sub>2</sub> O	$3.9\text{-}6.1 \times 10^{17}$	$< 4.0 \times 10^{-17}$	15.6-24.4	Caravan et al., (2020)
<i>syn-trans</i> -MVK-OO	HCOOH	$5.0\text{-}10.0 \times 10^{10}$	$[3.0 \pm 0.1] \times 10^{-10}$	15.0-30.0	Caravan et al., (2020)
	SO <sub>2</sub>	$1.7\text{-}9.0 \times 10^{10}$	$[4.2 \pm 0.6] \times 10^{-11}$	0.7-3.8	Caravan et al., (2020)
	HPMF	-	$3.0 \times 10^{-11}$	-	This work

Corresponding descriptions have been added in the page 23 line 573-590 and page 24 line 591-610 of the revised manuscript:

*It is of interest to assess whether the reactions of distinct SCIs with HPMF can compete well with the losses to reactions with trace species (e.g., H<sub>2</sub>O, HCOOH and SO<sub>2</sub>), because it is well known that the reactions with trace species are expected to be the dominant chemical sinks for SCIs in the atmosphere (Taatjes et al., 2013; Long et al., 2016). The reported concentrations of coreactant, the rate coefficients  $k$ , and the effective pseudo-first-order rate constants ( $k_{\text{eff}} = k[\text{coreactant}]$ ) for distinct SCI reactions with H<sub>2</sub>O, HCOOH, SO<sub>2</sub>, and HPMF are summarized in Table 2. As seen in Table 2, the rate coefficient of a particular SCI reaction with trace species is strongly dependent on its structure. The methyl group substitution may alter the rate coefficient by several to tens of times. The atmospheric concentrations of H<sub>2</sub>O, HCOOH and SO<sub>2</sub> in the tropical forest environments are*

measured to be  $3.9\text{-}6.1 \times 10^{17}$ ,  $5.0\text{-}10 \times 10^{10}$ , and  $1.7\text{-}9.0 \times 10^{10}$  molecules  $\text{cm}^{-3}$ , respectively (Vereecken, 2012). For the reactions of  $\text{CH}_2\text{OO}$  with  $\text{H}_2\text{O}$ ,  $\text{HCOOH}$ , and  $\text{SO}_2$ , the experimental rate coefficients are determined to be  $< 1.5 \times 10^{-15}$ ,  $[1.1 \pm 0.1] \times 10^{-10}$ , and  $[3.9 \pm 0.7] \times 10^{-11}$   $\text{cm}^3$  molecule $^{-1}$   $\text{s}^{-1}$ , respectively (Welz et al., 2012 and 2014; Chao et al., 2015), which translate into  $k_{\text{eff}(\text{CH}_2\text{OO}+\text{H}_2\text{O})}$ ,  $k_{\text{eff}(\text{CH}_2\text{OO}+\text{HCOOH})}$  and  $k_{\text{eff}(\text{CH}_2\text{OO}+\text{SO}_2)}$  of  $5.9\text{-}9.2 \times 10^2$ ,  $5.5\text{-}11$ , and  $0.7\text{-}3.5$   $\text{s}^{-1}$ , respectively. The result reveals that the reaction of  $\text{CH}_2\text{OO}$  with  $\text{H}_2\text{O}$  is the most important bimolecular reaction.  $k_{\text{eff}(\text{CH}_2\text{OO}+\text{HCOOH})}$  is greater by a factor of 3-8 than  $k_{\text{eff}(\text{CH}_2\text{OO}+\text{SO}_2)}$ , indicating that the reaction of  $\text{CH}_2\text{OO}$  with  $\text{HCOOH}$  is favored over reaction with  $\text{SO}_2$ . Similar conclusion is also obtained from the results of  $k_{\text{eff}}$  for the reactions of anti- $\text{CH}_3\text{CHOO}$ , syn- $\text{CH}_3\text{CHOO}$  and  $(\text{CH}_3)_2\text{COO}$  with  $\text{H}_2\text{O}$ ,  $\text{HCOOH}$  and  $\text{SO}_2$  that SCIs reactions with  $\text{H}_2\text{O}$  are faster than with  $\text{HCOOH}$ , which, in turn, are faster than with  $\text{SO}_2$ .

According to the results shown in the Table 2, the room temperature rate coefficient for the reaction of  $\text{CH}_2\text{OO}$  with HPMF is calculated to be  $2.7 \times 10^{-11}$   $\text{cm}^3$  molecule $^{-1}$   $\text{s}^{-1}$ . However, to the best of our knowledge, the atmospheric concentration of HPMF has not been reported up to now. If we assume that the concentration of HPMF is the same as that of  $\text{HCOOH}$ ,  $k_{\text{eff}(\text{CH}_2\text{OO}+\text{HPMF})}$  is estimated to be  $1.4\text{-}2.7$   $\text{s}^{-1}$ , which is significantly lower than  $k_{\text{eff}(\text{CH}_2\text{OO}+\text{H}_2\text{O})}$  and  $k_{\text{eff}(\text{CH}_2\text{OO}+\text{HCOOH})}$ .  $k_{\text{eff}(\text{CH}_2\text{OO}+\text{HPMF})}$  is nearly identical to  $k_{\text{eff}(\text{CH}_2\text{OO}+\text{SO}_2)}$ , indicating that the  $\text{CH}_2\text{OO} + \text{HPMF}$  reaction is competitive with the  $\text{CH}_2\text{OO} + \text{SO}_2$  system. Previous model-measurement studies have estimated the surface-level SCIs concentrations in the range of  $1.0 \times 10^4$  to  $1.0 \times 10^5$  molecules  $\text{cm}^{-3}$  (Khan et al., 2018; Novelli et al., 2017). If we assume that the concentration of HPMF is equal to that of SCIs,  $k_{\text{eff}(\text{CH}_2\text{OO}+\text{HPMF})}$  is calculated to be  $2.7\text{-}27 \times 10^{-7}$   $\text{s}^{-1}$ , which is several orders of magnitude lower than  $k_{\text{eff}(\text{CH}_2\text{OO}+\text{H}_2\text{O})}$ ,  $k_{\text{eff}(\text{CH}_2\text{OO}+\text{HCOOH})}$  and  $k_{\text{eff}(\text{CH}_2\text{OO}+\text{SO}_2)}$ . This result indicates that the reaction of  $\text{CH}_2\text{OO}$  with HPMF is of less importance. Similar conclusion is also obtained from the reactions of anti- $\text{CH}_3\text{CHOO}$ , syn- $\text{CH}_3\text{CHOO}$  and  $(\text{CH}_3)_2\text{COO}$  with HPMF. Based on the above discussions, it can be concluded that the relative importance of carbonyl oxides reactions with hydroperoxide esters is significantly dependent on the concentrations of hydroperoxide esters.

5. Since a big motivation for the computations is the potential for CI + hydroperoxy ester reactions to lead to SOA, there should be some specific discussion, perhaps buttressed by rough calculations, of how many cycles of CI addition are required before a given adduct is expected to have low

volatility. The approach of Chhantyal-Pun et al. (ACS Earth Space Chem. 2018, 2, 8, 833-842) is an example of the approach the authors should take.

**Response:** Based on the Reviewer's suggestion, the vapour pressure and volatility of adduct products formed from the successive reactions of SCIs with hydroperoxide esters have been added in the revised manuscript. The assessment of Barley and McFiggans (2010) and O'Meara et al. (2014) found that the combination of boiling point estimation from Nannoolal et al. (2004) and vapour pressure estimation from Nannoolal et al. (2008) gives the lowest mean bias error of vapour pressure for atmospherically relevant compounds. Therefore, the saturated vapour pressure ( $P^0$ ) of adduct products at room temperature is estimated by using the Nannoolal-Nannoolal method, and the results are listed in Table S10.

From Table S10, it can be seen that the  $P^0$  of adduct products involved in the successive reactions of  $\text{CH}_2\text{OO}$  with  $\text{HCOOH}$  increases first and then decreases with increasing the number of  $\text{CH}_2\text{OO}$ . The  $P^0$  of the adduct product  $\text{HC(O)O(CH}_2\text{OO)}_3\text{H}$  is maximum when the number of  $\text{CH}_2\text{OO}$  is equal to three. The  $P^0$  of adduct products included in the successive reactions of *anti*- $\text{CH}_3\text{CHOO}$  with  $\text{HCOOH}$  decreases significantly as the number of *anti*- $\text{CH}_3\text{CHOO}$  is increased. Similar phenomenon is also observed from the successive reactions of *syn*- $\text{CH}_3\text{CHOO}$  and  $(\text{CH}_3)_2\text{COO}$  with  $\text{HCOOH}$ . Notably, the  $P^0$  of adduct products decreases obviously when the size of SCIs increases. For example, the  $P^0$  of the adduct product  $\text{HC(O)O(CH}_2\text{OO)}_3\text{H}$  in the  $n\text{CH}_2\text{OO} + \text{HCOOH}$  reaction is estimated to be  $4.43 \times 10^{-3}$  atm, which is greater than those of the corresponding adduct products in the *nanti*- $\text{CH}_3\text{CHOO} + \text{HCOOH}$  ( $7.12 \times 10^{-4}$ ), *nsyn*- $\text{CH}_3\text{CHOO} + \text{HCOOH}$  ( $7.12 \times 10^{-4}$ ), and  $n(\text{CH}_3)_2\text{COO} + \text{HCOOH}$  ( $1.27 \times 10^{-4}$ ) reactions by 6.22, 6.22 and 34.88 times, respectively.

A classify scheme of various organic compounds is based on their volatility, as presented by Donahue et al. (2012) The volatility of organic compounds is described by their effective saturation concentration. The saturated concentrations ( $c^0$ ) of adduct products formed from the successive reactions of SCIs with  $\text{HCOOH}$  are predicted by using the SIMPOL.1 method proposed by Pankow and Asher (2008), and the results are listed in Table S10. As shown in Table S10, the  $c^0$  of adduct products involved in the  $n\text{CH}_2\text{OO} + \text{HCOOH}$  reaction decreases with increasing the number of  $\text{CH}_2\text{OO}$ . According to the Volatility Basis Set (VBS) of organic compounds (Donahue et al., 2012), these adduct products belong to volatile organic compounds (VOC,  $c^0 > 3 \times 10^6$   $\mu\text{g}/\text{m}^3$ ). Similarly,



the  $c^0$  of adduct products included in the *nanti*-CH<sub>3</sub>CHOO + HCOOH, *nsyn*-CH<sub>3</sub>CHOO + HCOOH, and n(CH<sub>3</sub>)<sub>2</sub>COO + HCOOH reactions decreases when the number of SCIs increases. It deserves mentioning that the adduct products in the *nanti*-CH<sub>3</sub>CHOO + HCOOH and *nsyn*-CH<sub>3</sub>CHOO + HCOOH reactions belong to intermediate volatility organic compounds (IVOC,  $300 < c^0 < 3 \times 10^6$  ug/m<sup>3</sup>) when the number of SCIs is equal to five. However, the adduct products in the n(CH<sub>3</sub>)<sub>2</sub>COO + HCOOH reaction become IVOC when the number of (CH<sub>3</sub>)<sub>2</sub>COO is greater than or equal to two. Based on the above discussions, it can be concluded that the volatility of adduct products is significantly affected by the number and size of SCIs in the successive reaction of SCIs with HCOOH.

**Table S10** Predicted saturated vapour pressure ( $P^0$ ) and saturated concentrations ( $c^0$ ) for the adduct products of the successive reactions of SCIs with HCOOH

	formula	$P^0$ (atm)	$c^0$ (ug/m <sup>3</sup> )
n CH <sub>2</sub> OO + HCOOH			
n = 1	HC(O)OCH <sub>2</sub> OOH	$2.12 \times 10^{-3}$	$7.86 \times 10^7$
n = 2	HC(O)O(CH <sub>2</sub> OO) <sub>2</sub> H	$3.80 \times 10^{-3}$	$3.99 \times 10^7$
n = 3	HC(O)O(CH <sub>2</sub> OO) <sub>3</sub> H	$4.43 \times 10^{-3}$	$3.91 \times 10^7$
n = 4	HC(O)O(CH <sub>2</sub> OO) <sub>4</sub> H	$4.21 \times 10^{-3}$	$3.29 \times 10^7$
n = 5	HC(O)O(CH <sub>2</sub> OO) <sub>5</sub> H	$3.59 \times 10^{-3}$	$2.12 \times 10^7$
n <i>anti</i> -CH <sub>3</sub> CHOO + HCOOH			
n = 1	HC(O)OCH(CH <sub>3</sub> )OOH	$1.25 \times 10^{-3}$	$8.32 \times 10^6$
n = 2	HC(O)O(CH(CH <sub>3</sub> )OO) <sub>2</sub> H	$1.13 \times 10^{-3}$	$7.57 \times 10^6$
n = 3	HC(O)O(CH(CH <sub>3</sub> )OO) <sub>3</sub> H	$7.12 \times 10^{-4}$	$6.49 \times 10^6$
n = 4	HC(O)O(CH(CH <sub>3</sub> )OO) <sub>4</sub> H	$3.90 \times 10^{-4}$	$4.50 \times 10^6$
n = 5	HC(O)O(CH(CH <sub>3</sub> )OO) <sub>5</sub> H	$2.01 \times 10^{-4}$	$2.81 \times 10^6$
n <i>syn</i> -CH <sub>3</sub> CHOO + HCOOH			
n = 1	HC(O)OCH(CH <sub>3</sub> )OOH	$1.25 \times 10^{-3}$	$8.32 \times 10^6$
n = 2	HC(O)O(CH(CH <sub>3</sub> )OO) <sub>2</sub> H	$1.13 \times 10^{-3}$	$7.57 \times 10^6$
n = 3	HC(O)O(CH(CH <sub>3</sub> )OO) <sub>3</sub> H	$7.12 \times 10^{-4}$	$6.49 \times 10^6$
n = 4	HC(O)O(CH(CH <sub>3</sub> )OO) <sub>4</sub> H	$3.90 \times 10^{-4}$	$4.50 \times 10^6$
n = 5	HC(O)O(CH(CH <sub>3</sub> )OO) <sub>5</sub> H	$2.01 \times 10^{-4}$	$2.81 \times 10^6$
n (CH <sub>3</sub> ) <sub>2</sub> COO + HCOOH			
n = 1	HC(O)OC(CH <sub>3</sub> ) <sub>2</sub> OOH	$7.23 \times 10^{-4}$	$3.50 \times 10^6$
n = 2	HC(O)O(C(CH <sub>3</sub> ) <sub>2</sub> OO) <sub>2</sub> H	$3.50 \times 10^{-4}$	$2.74 \times 10^6$
n = 3	HC(O)O(C(CH <sub>3</sub> ) <sub>2</sub> OO) <sub>3</sub> H	$1.27 \times 10^{-4}$	$1.38 \times 10^6$
n = 4	HC(O)O(C(CH <sub>3</sub> ) <sub>2</sub> OO) <sub>4</sub> H	$4.27 \times 10^{-5}$	$5.90 \times 10^5$
n = 5	HC(O)O(C(CH <sub>3</sub> ) <sub>2</sub> OO) <sub>5</sub> H	$1.40 \times 10^{-5}$	$2.36 \times 10^5$

Corresponding descriptions have been added in the page 27 line 644-671 and page 28 line 672-682 of the revised manuscript:

*The assessment of Barley and McFiggans (2010) and O'Meara et al. (2014) found that the combination of boiling point estimation from Nannoolal et al. (2004) and vapour pressure estimation from Nannoolal et al. (2008) gives the lowest mean bias error of vapour pressure for atmospherically relevant compounds. Therefore, the saturated vapour pressure ( $P^0$ ) of adduct products at room temperature is estimated by using the Nannoolal-Nannoolal method, and the results are listed in Table S10. From Table S10, it can be seen that the  $P^0$  of adduct products involved in the successive reactions of  $\text{CH}_2\text{OO}$  with  $\text{HCOOH}$  increases first and then decreases with increasing the number of  $\text{CH}_2\text{OO}$ . The  $P^0$  of the adduct product  $\text{HC(O)O(CH}_2\text{OO)}_3\text{H}$  is maximum when the number of  $\text{CH}_2\text{OO}$  is equal to three. The  $P^0$  of adduct products included in the successive reactions of anti- $\text{CH}_3\text{CHOO}$  with  $\text{HCOOH}$  decreases significantly as the number of anti- $\text{CH}_3\text{CHOO}$  is increased. Similar phenomenon is also observed from the successive reactions of syn- $\text{CH}_3\text{CHOO}$  and  $(\text{CH}_3)_2\text{COO}$  with  $\text{HCOOH}$ . Notably, the  $P^0$  of adduct products decreases obviously when the size of SCIs increases. For example, the  $P^0$  of the adduct product  $\text{HC(O)O(CH}_2\text{OO)}_3\text{H}$  in the  $n\text{CH}_2\text{OO} + \text{HCOOH}$  reaction is estimated to be  $4.43 \times 10^{-3}$  atm, which is greater than those of the corresponding adduct products in the nanti- $\text{CH}_3\text{CHOO} + \text{HCOOH}$  ( $7.12 \times 10^{-4}$ ), nsyn- $\text{CH}_3\text{CHOO} + \text{HCOOH}$  ( $7.12 \times 10^{-4}$ ), and  $n(\text{CH}_3)_2\text{COO} + \text{HCOOH}$  ( $1.27 \times 10^{-4}$ ) reactions by 6.22, 6.22 and 34.88 times, respectively.*

*A classify scheme of various organic compounds is based on their volatility, as presented by Donahue et al. (2012) The volatility of organic compounds is described by their effective saturation concentration. The saturated concentrations ( $c^0$ ) of adduct products formed from the successive reactions of SCIs with  $\text{HCOOH}$  are predicted by using the SIMPOL.1 method proposed by Pankow and Asher (2008), and the results are listed in Table S10. As shown in Table S10, the  $c^0$  of adduct products involved in the  $n\text{CH}_2\text{OO} + \text{HCOOH}$  reaction decreases with increasing the number of  $\text{CH}_2\text{OO}$ . According to the Volatility Basis Set (VBS) of organic compounds (Donahue et al., 2012), these adduct products belong to VOC ( $c^0 > 3 \times 10^6$  ug/m<sup>3</sup>). Similarly, the  $c^0$  of adduct products included in the nanti- $\text{CH}_3\text{CHOO} + \text{HCOOH}$ , nsyn- $\text{CH}_3\text{CHOO} + \text{HCOOH}$ , and  $n(\text{CH}_3)_2\text{COO} + \text{HCOOH}$  reactions decreases when the number of SCIs increases. It deserves mentioning that the adduct products in the nanti- $\text{CH}_3\text{CHOO} + \text{HCOOH}$  and nsyn- $\text{CH}_3\text{CHOO} + \text{HCOOH}$  reactions*

*belong to intermediate volatility organic compounds (IVOC,  $300 < c^0 < 3 \times 10^6 \text{ ug/m}^3$ ) when the number of SCIs is equal to five. However, the adduct products in the  $n(\text{CH}_3)_2\text{COO} + \text{HCOOH}$  reaction become IVOC when the number of  $(\text{CH}_3)_2\text{COO}$  is greater than or equal to two. Based on the above discussions, it can be concluded that the volatility of adduct products is significantly affected by the number and size of SCIs in the successive reaction of SCIs with HCOOH.*

6. On p. 6, line 145: "saddle point" should be "minimum".

**Response:** The word “saddle point” has been replaced by “minimum” in the revised manuscript.

7. On p. 6, line 162: "precision" should be "accuracy".

**Response:** The word “precision” has been replaced by “accuracy” in the revised manuscript.

8. On p. 7, line 182: "decomposes" should be "rearranges".

**Response:** The word “decomposes” has been replaced by “rearranges” in the revised manuscript.

9. On p. 14, lines 341-342, use a non-breaking hyphen.

**Response:** A non-breaking hyphen has been used in the revised manuscript.

10. On p. 15, line 372, "intermolecular" should be "intramolecular".

**Response:** The word “intermolecular” has been replaced by “intramolecular” in the revised manuscript.

11. On p. 17, lines 413-414, use a non-breaking hyphen.

**Response:** A non-breaking hyphen has been used in the revised manuscript.

## References

- Barber, V. P., Pandit, S., Green, A. M., Trongsiwat, N., Walsh, P. J., Klippenstein, S. J., and Lester, M. I.: Four-carbon Criegee intermediate from isoprene ozonolysis: methyl vinyl ketone oxide synthesis, infrared spectrum, and OH production, *J. Am. Chem. Soc.*, 140, 10866-10880, <https://doi.org/10.1021/jacs.8b06010>, 2018.
- Barley, M. H., and McFiggans, G.: The critical assessment of vapour pressure estimation methods for use in modelling the formation of atmospheric organic aerosol, *Atmos. Chem. Phys.*, 10, 749-767, <https://doi.org/10.5194/acp-10-749-2010>, 2010.
- Canneaux, S., Bohr, F., and Henon, E.: KiSThelP: a program to predict thermodynamic properties and rate constants from quantum chemistry results, *J. Comput. Chem.*, 35, 82-93, <https://doi.org/10.1002/jcc.23470>, 2013.
- Caravan, R. L., Vansco, M. F., Au, K., Khan, M. A. H., Li, Y. L., Winiberg, F. A. F., Zuraski, K., Lin, Y. H., Chao, W., Trongsiwat, N., Walsh, P. J., Osborn, D. L., Percival, C. J., Lin, J. J. M., Shallcross, D. E., Sheps, L., Klippenstein, S. J., Taatjes, C. A., and Lester, M. I.: Direct kinetic measurements and theoretical predictions of an isoprene-derived Criegee intermediate, *Proc. Natl. Acad. Sci. U.S.A.*, 117, 9733-9740, <https://doi.org/10.1073/pnas.1916711117>, 2020.
- Chao, W., Hsieh, J. T., Chang, C. H., and Lin, J. J. M.: Direct kinetic measurement of the reaction of the simplest Criegee intermediate with water vapor, *Science*, 347, 751-754, <https://doi.org/10.1126/science.1261549>, 2015.
- Chen, L., Wang, W., Wang, W., Liu, Y., Liu, F., Liu, N., and Wang, B.: Water-catalyzed decomposition of the simplest Criegee intermediate CH<sub>2</sub>OO, *Theor. Chem. Acc.*, 135, 131-143, <https://doi.org/10.1007/s00214-016-1894-9>, 2016.
- Chung, C. A., Su, J. W., and Lee, Y. P.: Detailed mechanism and kinetics of the reaction of Criegee intermediate CH<sub>2</sub>OO with HCOOH investigated via infrared identification of conformers of hydroperoxymethyl formate and formic acid anhydride, *Phys. Chem. Chem. Phys.*, 21, 21445-21455, <https://doi.org/10.1039/c9cp04168k>, 2019.
- Donahue, N. M., Kroll, J. H., Pandis, S. N., and Robinson, A. L.: A two-dimensional volatility basis set – Part 2: Diagnostics of organic-aerosol evolution, *Atmos. Chem. Phys.*, 12, 615-634, <https://doi.org/10.5194/acp-12-615-2012>, 2012.
- Gilbert, R. G., and Smith, S. C.: *Theory of unimolecular and recombination reactions*; Blackwell Scientific: Carlton, Australia, 1990.
- Glowacki, D. R., Liang, C. H., Morley, C., Pilling, M. J., and Robertson, S. H.: MESMER: an open-source master equation solver for multi-energy well reactions, *J. Phys. Chem. A*, 116, 9545-9560, <https://doi.org/10.1021/jp3051033>, 2012.
- Huang, H. L., Chao, W., and Lin, J. J. M.: Kinetics of a Criegee intermediate that would survive high humidity and may oxidize atmospheric SO<sub>2</sub>, *Proc. Natl. Acad. Sci. U.S.A.*, 112, 10857-10862, <https://doi.org/10.1073/pnas.1513149112>, 2015.
- Kalinowski, J., Räsänen, M., Heinonen, P., Kilpeläinen, I., and Gerber, R. B.: Isomerization and decomposition of a Criegee intermediate in the ozonolysis of alkenes: dynamics using a multireference potential, *Angew. Chem.*, 126, 269-272, <https://doi.org/10.1002/ange.201307286>, 2014.
- Karton, A., Kettner, M., and Wild, D. A.: Sneaking up on the Criegee intermediate from below: Predicted photoelectron spectrum of the CH<sub>2</sub>OO<sup>-</sup> anion and W3-F12 electron affinity of CH<sub>2</sub>OO, *Chem. Phys. Lett.*, 585, 15-20, <https://doi.org/10.1016/j.cplett.2013.08.075>, 2013.

- Khan, M. A. H., Percival, C. J., Caravan, R. L., Taatjes, C. A., and Shallcross, D. E.: Criegee intermediates and their impacts on the troposphere, *Environ. Sci.: Processes Impacts*, 20, 437-453, <https://doi.org/10.1039/C7EM00585G>, 2018.
- Long, B., Bao, J. L., and Truhlar, D. G.: Atmospheric chemistry of Criegee intermediates: unimolecular reactions and reactions with water, *J. Am. Chem. Soc.*, 138, 14409-14422, <https://doi.org/10.1021/jacs.6b08655>, 2016.
- Nannoolal, Y., Rarey, J., and Ramjugernatha, D.: Estimation of pure component properties Part 3. Estimation of the vapor pressure of non-electrolyte organic compounds via group contributions and group interactions, *Fluid Phase Equilibria*, 269, 117-133, <https://doi.org/10.1016/j.fluid.2008.04.020>, 2008.
- Nannoolal, Y., Rarey, J., Ramjugernatha, D., and Cordesb, W.: Estimation of pure component properties Part 1. Estimation of the normal boiling point of non-electrolyte organic compounds via group contributions and group interactions, *Fluid Phase Equilibria*, 226, 45-63, <https://doi.org/10.1016/j.fluid.2004.09.001>, 2004.
- Novelli, A., Hens, K., Ernest, C. T., Martinez, M., Nölscher, A. C., Sinha, V., Paasonen, P., Petäjä, T., Sipilä, M., Elste, T., Plass-Dülmer, C., Phillips, G. J., Kubistin, D., Williams, J., Vereecken, L., Lelieveld, J., and Harder, H.: Estimating the atmospheric concentration of Criegee intermediates and their possible interference in a FAGE-LIF instrument, *Atmos. Chem. Phys.*, 17, 7807-7826, <https://doi.org/10.5194/acp-17-7807-2017>, 2017.
- O'Meara, S., Booth, A. M., Barley, M. H., Topping, D., and McFiggans, G.: An assessment of vapour pressure estimation methods, *Phys. Chem. Chem. Phys.*, 16, 19453-19469, <https://doi.org/10.1039/C4CP00857J>, 2014.
- Pankow, J. F., and Asher, W. E.: SIMPOL.1: a simple group contribution method for predicting vapor pressures and enthalpies of vaporization of multifunctional organic compounds, *Atmos. Chem. Phys.*, 8, 2773-2796, <https://doi.org/10.5194/acp-8-2773-2008>, 2008.
- Peltola, J., Seal, P., Inkilä, A., and Eskola, A.: Time-resolved, broadband UV-absorption spectrometry measurements of Criegee intermediate kinetics using a new photolytic precursor: unimolecular decomposition of CH<sub>2</sub>OO and its reaction with formic acid, *Phys. Chem. Chem. Phys.*, 22, 11797-11808, <https://doi.org/10.1039/d0cp00302f>, 2020.
- Raghunath, P., Lee, Y. P., and Lin, M. C.: Computational chemical kinetics for the reaction of Criegee intermediate CH<sub>2</sub>OO with HNO<sub>3</sub> and its catalytic conversion to OH and HCO, *J. Phys. Chem. A*, 121, 3871-3878, <https://doi.org/10.1021/acs.jpca.7b02196>, 2017.
- Sipilä, M., Jokinen, T., Berndt, T., Richters, S., Makkonen, R., Donahue, N. M., Mauldin Iii, R. L., Kurtén, T., Paasonen, P., Sarnela, N., Ehn, M., Junninen, H., Rissanen, M. P., Thornton, J., Stratmann, F., Herrmann, H., Worsnop, D. R., Kulmala, M., Kerminen, V. M., and Petäjä, T.: Reactivity of stabilized Criegee intermediates (sCIs) from isoprene and monoterpene ozonolysis toward SO<sub>2</sub> and organic acids, *Atmos. Chem. Phys.*, 14, 12143-12153, <https://doi.org/10.5194/acp-14-12143-2014>, 2014.
- Taatjes, C. A., Welz, O., Eskola, A. J., Savee, J. D., Scheer, A. M., Shallcross, D. E., Rotavera, B., Lee, E. P. F., Dyke, J. M., Mok, D. K. W., Osborn, D. L., and Percival, C. J.: Direct measurements of conformer-dependent reactivity of the Criegee intermediate CH<sub>3</sub>CHOO, *Science*, 340, 177-180, <https://doi.org/10.1126/science.1234689>, 2013.
- Vereecken, L., Harder, H., and Novelli, A.: The reaction of Criegee intermediates with NO, RO<sub>2</sub>, and SO<sub>2</sub>, and their fate in the atmosphere, *Phys. Chem. Chem. Phys.*, 14, 14682-14695,

<https://doi.org/10.1039/c2cp42300f>, 2012.

Welz, O., Eskola, A. J., Sheps, L., Rotavera, B., Savee, J. D., Scheer, A. M., Osborn, D. L., Lowe, D., Booth, A. M., Xiao, P., Khan, M. A. H., Percival, C. J., Shallcross, D. E., and Taatjes, C. A.: Rate coefficients of C(1) and C(2) Criegee intermediate reactions with formic and acetic Acid near the collision limit: direct kinetics measurements and atmospheric implications, *Angew. Chem. Int. Ed.*, 53, 4547-4550, <https://doi.org/10.1002/anie.201400964>, 2014.

Welz, O., Savee, J. D., Osborn, D. L., Vasu, S. S., Percival, C. J., Shallcross, D. E., and Taatjes, C. A.: Direct kinetic measurements of Criegee intermediate ( $\text{CH}_2\text{OO}$ ) formed by reaction of  $\text{CH}_2\text{I}$  with  $\text{O}_2$ , *Science*, 335, 204-207, <https://doi.org/10.1126/science.1213229>, 2012.

## Comments of reviewer #2

1. However, a deeper discussion is required for the data in this paper. For example, in lines 263-266 “At room temperature,  $k_{\text{tot}}$  is estimated to be  $3.6 \times 10^{-10} \text{ cm}^3 \text{ molecule}^{-1} \text{ s}^{-1}$ , which is greater by a factor of  $\sim 3$  than that reported by Welz et al. (2014) ( $[1.1 \pm 0.1] \times 10^{-10} \text{ cm}^3 \text{ molecule}^{-1} \text{ s}^{-1}$ ), Chung et al. (2019) ( $[1.4 \pm 0.3] \times 10^{-10} \text{ cm}^3 \text{ molecule}^{-1} \text{ s}^{-1}$ ), and Peltola et al. (2020) ( $[1.0 \pm 0.03] \times 10^{-10} \text{ cm}^3 \text{ molecule}^{-1} \text{ s}^{-1}$ )”. What is the reason for the difference of the  $k$  value about three times?

**Response:** In the original manuscript, the rate coefficients for the barrierless reactions are calculated by employing the variational transition state theory (VTST), and the rate coefficients for the bimolecular reactions with the tight transition states are computed by using the canonical transition state theory (CTST) along with one-dimensional asymmetric Eckart tunneling correction. For the initiation reactions of distinct stabilized Criegee intermediates (SCIs) with HCOOH, there are four possible pathways, namely (1) 1,4 O-H insertion (Entry 1), (2) 1,2 O-H insertion (Entry 2), (3) C-H insertion (Entry 3), and (4) C=O cycloaddition (Entry 4), in which Entry 1 is barrierless and Entry 2-4 have the tight transition states. The total rate coefficient for the reaction of SCIs with HCOOH is equal to the sum of the rate coefficient of each pathway. For the barrierless 1,4 O-H insertion reaction, the VTST is approximated with a Morse potential function,  $V(R) = D_e\{1 - \exp[-\beta(R - R_e)]\}^2$ , along with an anisotropy potential function to stand for the minimum energy path, which is used to calculate the rate coefficients (Raghunath et al., 2017). Here,  $D_e$  is the bond energy excluding the zero-point energy,  $R$  is the reaction coordinate, and  $R_e$  is the equilibrium value of  $R$ . It is assumed that the stretching potential in an anisotropy potential is used in conjunction with a potential form of  $V_{\text{anisotropy}} = V_0[1 - \cos^2(\theta_1 - \theta_{1e}) \times \cos^2(\theta_2 - \theta_{2e})]$  (Raghunath et al., 2017). Here,  $V_0$  is the stretching potential, which stands for by a Morse potential,  $\theta_1$  and  $\theta_{1e}$  represent the rotational angle between fragment 1 and the reference axis and the equilibrium bond angle of fragment 1,  $\theta_2$  and  $\theta_{2e}$  stand for the rotational angle between fragment 2 and the reference axis and the equilibrium bond angle of fragment 2. The association curve for the reaction of 1,4 O-H insertion of SCIs into HCOOH is computed at the M06-2X/6-311+G(2df,2p) level of theory to cover a range from 0.97 to 1.97 Å at step size 0.1 Å for O-H bond and from 1.44 to 2.44 Å at step size 0.1 Å for C-O bond, while other structural parameters are fully optimized. The computed potential energies are fitted to the Morse potential function. However, the calculated rate coefficients for the reactions of SCIs with HCOOH are higher than the prior experimental measurements. The reason is ascribed to the fact

that the approximation of VTST using a Morse potential function in conjunction with an anisotropy potential function is unsuitable to predict the rate coefficients for the barrierless 1,4 O-H insertion reaction.

In the revised manuscript, the rate coefficients for the barrierless reactions are computed by employing the inverse Laplace transformation (ILT) method, and the rate coefficients for the bimolecular reactions with the tight transition states are calculated by utilizing CTST in conjunction with Eckart tunneling correction. The ILT and CTST/Eckart calculations are performed by using the MESMER 6.0 and KiSTheLP 2019 programs, respectively (Glowacki et al., 2012; Canneaux et al., 2013). In the ILT treatment, the rotational constants, vibrational frequencies, molecular weights, energies and other input parameters are obtained from the M06-2X/6-311+G(2df,2p) or M06-2X/ma-TZVP methods. For the barrierless reaction of 1,4 O-H insertion of SCIs into HCOOH, SCIs and HCOOH are assigned as the deficient and excess reactants, respectively. The concentration of HCOOH is given a value of  $5.0 \times 10^{10}$  molecules  $\text{cm}^{-3}$  in the simulation, which is taken from the typical concentration of HCOOH in the tropical forest environments (Vereecken, 2012).  $\text{N}_2$  is applied as the buffer gas. A single exponential down model is employed to simulate the collision transfer ( $\langle \Delta E \rangle_{\text{down}} = 200 \text{ cm}^{-1}$ ). The collisional Lennard-Jones parameters are estimated with the empirical formula described by Gilbert and Smith (1990).

The rate coefficients of each elementary pathway included in the initiation reactions of distinct SCIs with HCOOH are calculated in the temperature range of 273-400 K, as listed in Table S3-S6. As shown in Table S3, the total rate coefficients  $k_{\text{tot-CH}_2\text{OO}}$  of  $\text{CH}_2\text{OO}$  reaction with HCOOH are in excess of  $1.0 \times 10^{-10} \text{ cm}^3 \text{ molecule}^{-1} \text{ s}^{-1}$ , and they exhibit a slightly negative temperature dependence in the temperature range studied.  $k_{\text{tot-CH}_2\text{OO}}$  is estimated to be  $1.4 \times 10^{-10} \text{ cm}^3 \text{ molecule}^{-1} \text{ s}^{-1}$  at 298 K, which is in good agreement with the experimental values reported by Welz et al. (2014) ( $[1.1 \pm 0.1] \times 10^{-10}$ ), Chung et al. (2019) ( $[1.4 \pm 0.3] \times 10^{-10}$ ), and Peltola et al. (2020) ( $[1.0 \pm 0.03] \times 10^{-10}$ ).  $k(\text{TS}_{\text{ent1}})$  is approximately equal to  $k_{\text{tot-CH}_2\text{OO}}$  in the whole temperature range, and it decreases in the range of  $1.7 \times 10^{-10}$  (273 K) to  $1.2 \times 10^{-10}$  (400 K)  $\text{cm}^3 \text{ molecule}^{-1} \text{ s}^{-1}$  with increasing temperature.  $k(\text{TS}_{\text{ent1}})$  is several orders of magnitude greater than  $k(\text{TS}_{\text{ent2}})$ ,  $k(\text{TS}_{\text{ent3}})$  and  $k(\text{TS}_{\text{ent4}})$  over the temperature range from 273 to 400 K. The result again shows that the barrierless 1,4 O-H insertion reaction is predominant. Similar conclusion is also obtained from the results of the rate coefficients for the reactions of HCOOH with *anti*- $\text{CH}_3\text{CHOO}$ , *syn*- $\text{CH}_3\text{CHOO}$  and  $(\text{CH}_3)_2\text{COO}$  (Table S4-S6).



At ambient temperature, the total rate coefficients of HCOOH reactions with *anti*-CH<sub>3</sub>CHOO, *syn*-CH<sub>3</sub>CHOO and (CH<sub>3</sub>)<sub>2</sub>COO are estimated to be 5.9, 2.7 and 4.8 × 10<sup>-10</sup> cm<sup>3</sup> molecule<sup>-1</sup> s<sup>-1</sup>, respectively, which are consistent with the prior experimental measurements of 5 ± 3, 2.5 ± 0.3 and 4.5 × 10<sup>-10</sup> cm<sup>3</sup> molecule<sup>-1</sup> s<sup>-1</sup> (Welz et al., 2014; Chung et al., 2019; Sipilä et al., 2014).

**Table S3** Rate coefficients (cm<sup>3</sup> molecule<sup>-1</sup> s<sup>-1</sup>) of each elementary pathway involved in the initiation reaction of CH<sub>2</sub>OO with HCOOH computed at different temperatures

T/K	$k$ (TS <sub>ent1</sub> )	$k$ (TS <sub>ent2</sub> )	$k$ (TS <sub>ent3</sub> )	$k$ (TS <sub>ent4</sub> )	$k_{\text{tot-CH2OO}}$
273	1.7 × 10 <sup>-10</sup>	3.6 × 10 <sup>-12</sup>	1.0 × 10 <sup>-22</sup>	3.6 × 10 <sup>-12</sup>	1.8 × 10 <sup>-10</sup>
280	1.6 × 10 <sup>-10</sup>	2.9 × 10 <sup>-12</sup>	1.2 × 10 <sup>-22</sup>	3.1 × 10 <sup>-12</sup>	1.7 × 10 <sup>-10</sup>
298	1.4 × 10 <sup>-10</sup>	1.9 × 10 <sup>-12</sup>	2.2 × 10 <sup>-22</sup>	2.3 × 10 <sup>-12</sup>	1.4 × 10 <sup>-10</sup>
300	1.4 × 10 <sup>-10</sup>	1.8 × 10 <sup>-12</sup>	2.4 × 10 <sup>-22</sup>	2.2 × 10 <sup>-12</sup>	1.4 × 10 <sup>-10</sup>
320	1.3 × 10 <sup>-10</sup>	1.2 × 10 <sup>-12</sup>	4.9 × 10 <sup>-22</sup>	1.6 × 10 <sup>-12</sup>	1.3 × 10 <sup>-10</sup>
340	1.3 × 10 <sup>-10</sup>	8.2 × 10 <sup>-13</sup>	1.0 × 10 <sup>-21</sup>	1.3 × 10 <sup>-12</sup>	1.3 × 10 <sup>-10</sup>
360	1.2 × 10 <sup>-10</sup>	5.9 × 10 <sup>-13</sup>	2.2 × 10 <sup>-21</sup>	1.0 × 10 <sup>-12</sup>	1.2 × 10 <sup>-10</sup>
380	1.2 × 10 <sup>-10</sup>	4.5 × 10 <sup>-13</sup>	4.5 × 10 <sup>-21</sup>	8.2 × 10 <sup>-13</sup>	1.2 × 10 <sup>-10</sup>
400	1.2 × 10 <sup>-10</sup>	3.5 × 10 <sup>-13</sup>	9.0 × 10 <sup>-21</sup>	6.9 × 10 <sup>-13</sup>	1.2 × 10 <sup>-10</sup>

**Table S4** Rate coefficients (cm<sup>3</sup> molecule<sup>-1</sup> s<sup>-1</sup>) of each elementary pathway involved in the initiation reaction of *anti*-CH<sub>3</sub>CHOO with HCOOH computed at different temperatures

T/K	$k$ (TS <sub>ent1-anti</sub> )	$k$ (TS <sub>ent2-anti</sub> )	$k$ (TS <sub>ent3-anti</sub> )	$k$ (TS <sub>ent4-anti</sub> )	$k_{\text{tot-anti}}$
273	5.9 × 10 <sup>-10</sup>	4.2 × 10 <sup>-11</sup>	5.5 × 10 <sup>-22</sup>	6.1 × 10 <sup>-11</sup>	6.9 × 10 <sup>-10</sup>
280	5.7 × 10 <sup>-10</sup>	3.8 × 10 <sup>-11</sup>	6.7 × 10 <sup>-22</sup>	4.9 × 10 <sup>-11</sup>	6.6 × 10 <sup>-10</sup>
298	5.4 × 10 <sup>-10</sup>	2.3 × 10 <sup>-11</sup>	1.2 × 10 <sup>-21</sup>	3.0 × 10 <sup>-11</sup>	5.9 × 10 <sup>-10</sup>
300	5.3 × 10 <sup>-10</sup>	2.0 × 10 <sup>-11</sup>	1.3 × 10 <sup>-21</sup>	2.8 × 10 <sup>-11</sup>	5.8 × 10 <sup>-10</sup>
320	5.0 × 10 <sup>-10</sup>	1.5 × 10 <sup>-11</sup>	2.6 × 10 <sup>-21</sup>	1.7 × 10 <sup>-11</sup>	5.3 × 10 <sup>-10</sup>
340	4.7 × 10 <sup>-10</sup>	9.4 × 10 <sup>-12</sup>	5.4 × 10 <sup>-21</sup>	1.1 × 10 <sup>-11</sup>	4.9 × 10 <sup>-10</sup>
360	4.5 × 10 <sup>-10</sup>	7.0 × 10 <sup>-12</sup>	1.1 × 10 <sup>-20</sup>	7.8 × 10 <sup>-12</sup>	4.7 × 10 <sup>-10</sup>
380	4.4 × 10 <sup>-10</sup>	3.6 × 10 <sup>-12</sup>	2.1 × 10 <sup>-20</sup>	5.6 × 10 <sup>-12</sup>	4.5 × 10 <sup>-10</sup>
400	4.3 × 10 <sup>-10</sup>	2.0 × 10 <sup>-12</sup>	4.0 × 10 <sup>-20</sup>	4.2 × 10 <sup>-12</sup>	4.4 × 10 <sup>-10</sup>

**Table S5** Rate coefficients (cm<sup>3</sup> molecule<sup>-1</sup> s<sup>-1</sup>) of each elementary pathway involved in the initiation reaction of *syn*-CH<sub>3</sub>CHOO with HCOOH computed at different temperatures

T/K	$k$ (TS <sub>ent1-syn</sub> )	$k$ (TS <sub>ent2-syn</sub> )	$k$ (TS <sub>ent3-syn</sub> )	$k$ (TS <sub>ent4-syn</sub> )	$k_{\text{tot-syn}}$
273	$3.1 \times 10^{-10}$	$9.5 \times 10^{-13}$	$4.6 \times 10^{-27}$	$7.5 \times 10^{-16}$	$3.1 \times 10^{-10}$
280	$2.8 \times 10^{-10}$	$8.0 \times 10^{-13}$	$7.1 \times 10^{-27}$	$6.4 \times 10^{-16}$	$2.8 \times 10^{-10}$
298	$2.7 \times 10^{-10}$	$5.4 \times 10^{-13}$	$8.9 \times 10^{-26}$	$5.5 \times 10^{-16}$	$2.7 \times 10^{-10}$
300	$2.7 \times 10^{-10}$	$5.2 \times 10^{-13}$	$9.9 \times 10^{-26}$	$4.6 \times 10^{-16}$	$2.7 \times 10^{-10}$
320	$2.5 \times 10^{-10}$	$3.6 \times 10^{-13}$	$3.0 \times 10^{-25}$	$3.8 \times 10^{-16}$	$2.5 \times 10^{-10}$
340	$2.5 \times 10^{-10}$	$2.6 \times 10^{-13}$	$9.1 \times 10^{-25}$	$3.1 \times 10^{-16}$	$2.5 \times 10^{-10}$
360	$2.3 \times 10^{-10}$	$2.0 \times 10^{-13}$	$2.6 \times 10^{-24}$	$3.0 \times 10^{-16}$	$2.3 \times 10^{-10}$
380	$2.2 \times 10^{-10}$	$1.5 \times 10^{-13}$	$7.2 \times 10^{-24}$	$2.4 \times 10^{-16}$	$2.2 \times 10^{-10}$
400	$2.2 \times 10^{-10}$	$1.2 \times 10^{-13}$	$1.8 \times 10^{-23}$	$2.2 \times 10^{-16}$	$2.2 \times 10^{-10}$

**Table S6** Rate coefficients ( $\text{cm}^3 \text{ molecule}^{-1} \text{ s}^{-1}$ ) of each elementary pathway involved in the initiation reaction of  $(\text{CH}_3)_2\text{OO}$  with  $\text{HCOOH}$  computed at different temperatures

T/K	$k$ (TS <sub>ent1-dim</sub> )	$k$ (TS <sub>ent2-dim</sub> )	$k$ (TS <sub>ent3-dim</sub> )	$k$ (TS <sub>ent4-dim</sub> )	$k_{\text{tot-dim}}$
273	$5.3 \times 10^{-10}$	$6.8 \times 10^{-12}$	$1.4 \times 10^{-26}$	$4.4 \times 10^{-15}$	$5.4 \times 10^{-10}$
280	$5.1 \times 10^{-10}$	$5.2 \times 10^{-12}$	$2.2 \times 10^{-26}$	$4.2 \times 10^{-15}$	$5.2 \times 10^{-10}$
298	$4.8 \times 10^{-10}$	$2.8 \times 10^{-12}$	$8.0 \times 10^{-26}$	$4.0 \times 10^{-15}$	$4.8 \times 10^{-10}$
300	$4.7 \times 10^{-10}$	$2.6 \times 10^{-12}$	$9.2 \times 10^{-26}$	$3.9 \times 10^{-15}$	$4.7 \times 10^{-10}$
320	$4.5 \times 10^{-10}$	$1.4 \times 10^{-12}$	$3.6 \times 10^{-25}$	$3.7 \times 10^{-15}$	$4.5 \times 10^{-10}$
340	$4.2 \times 10^{-10}$	$8.6 \times 10^{-13}$	$1.3 \times 10^{-24}$	$3.6 \times 10^{-15}$	$4.2 \times 10^{-10}$
360	$3.9 \times 10^{-10}$	$5.5 \times 10^{-13}$	$4.5 \times 10^{-24}$	$3.5 \times 10^{-15}$	$3.9 \times 10^{-10}$
380	$3.7 \times 10^{-10}$	$3.7 \times 10^{-13}$	$1.4 \times 10^{-23}$	$3.4 \times 10^{-15}$	$3.7 \times 10^{-10}$
400	$3.7 \times 10^{-10}$	$2.6 \times 10^{-13}$	$3.9 \times 10^{-23}$	$3.4 \times 10^{-15}$	$3.7 \times 10^{-10}$

Corresponding descriptions have been added in the page 7 line 173-190, page 11 line 303-315, page 12 line 330-338 and page 13 line 346-351 of the revised manuscript:

*The rate coefficients for the barrierless reactions are determined by employing the inverse Laplace transformation (ILT) method. The ILT calculations are performed with the MESMER 6.0 program (Glowacki et al., 2012). In the ILT treatment, the rotational constants, vibrational frequencies, molecular weights, energies and other input parameters are obtained from the M06-2X/6-311+G(2df,2p) or M06-2X/ma-TZVP methods. For the barrierless reaction of 1,4 O-H*

insertion of SCIs into HCOOH, SCIs and HCOOH are assigned as the deficient and excess reactants, respectively. The concentration of HCOOH is given a value of  $5.0 \times 10^{10}$  molecules  $\text{cm}^{-3}$  in the simulation, which is taken from the typical concentration of HCOOH in the tropical forest environments (Vereecken et al., 2012).  $\text{N}_2$  is applied as the buffer gas. A single exponential down model is employed to simulate the collision transfer ( $\langle \Delta E \rangle_{\text{down}} = 200 \text{ cm}^{-1}$ ). The collisional Lennard-Jones parameters are estimated with the empirical formula described by Gilbert and Smith (1990).

The rate coefficients for the bimolecular reactions with the tight transition states are calculated by using the canonical transition state theory (CTST) along with one-dimensional asymmetric Eckart tunneling correction (Truhlar et al., 1996; Eckart, 1930). The CTST/Eckart calculations are performed with the KiSThelP 2019 program (Canneaux et al., 2013).

The rate coefficients of each elementary pathway included in the initiation reactions of distinct SCIs with HCOOH are calculated in the temperature range of 273-400 K, as listed in Table S3-S6. As shown in Table S3, the total rate coefficients  $k_{\text{tot-CH}_2\text{OO}}$  of  $\text{CH}_2\text{OO}$  reaction with HCOOH are in excess of  $1.0 \times 10^{-10} \text{ cm}^3 \text{ molecule}^{-1} \text{ s}^{-1}$ , and they exhibit a slightly negative temperature dependence in the temperature range studied.  $k_{\text{tot-CH}_2\text{OO}}$  is estimated to be  $1.4 \times 10^{-10} \text{ cm}^3 \text{ molecule}^{-1} \text{ s}^{-1}$  at 298 K, which is in good agreement with the experimental values reported by Welz et al. (2014) ( $[1.1 \pm 0.1] \times 10^{-10}$ ), Chung et al. (2019) ( $[1.4 \pm 0.3] \times 10^{-10}$ ), and Peltola et al. (2020) ( $[1.0 \pm 0.03] \times 10^{-10}$ ).  $k(\text{TS}_{\text{ent}1})$  is approximately equal to  $k_{\text{tot-CH}_2\text{OO}}$  in the whole temperature range, and it decreases in the range of  $1.7 \times 10^{-10}$  (273 K) to  $1.2 \times 10^{-10}$  (400 K)  $\text{cm}^3 \text{ molecule}^{-1} \text{ s}^{-1}$  with increasing temperature.  $k(\text{TS}_{\text{ent}1})$  is several orders of magnitude greater than  $k(\text{TS}_{\text{ent}2})$ ,  $k(\text{TS}_{\text{ent}3})$  and  $k(\text{TS}_{\text{ent}4})$  over the temperature range from 273 to 400 K. The result again shows that the barrierless 1,4 O-H insertion reaction is predominant.

Equivalent to the case of  $\text{CH}_2\text{OO}$  reaction with HCOOH, the rate coefficient of each elementary pathway involved in the anti- $\text{CH}_3\text{CHOO} + \text{HCOOH}$  reaction also decreases with the temperature increasing (Table S4). This table shows that Entry 1 is kinetically favored over Entry 2, 3 and 4, and Entry 2 is competitive with Entry 4 in the range 273-400 K. Similar conclusion is also obtained from the results of the rate coefficients for the reactions of syn- $\text{CH}_3\text{CHOO}$  and  $(\text{CH}_3)_2\text{COO}$  with HCOOH that Entry 1 is the dominant pathway (Table S5-S6). It deserves mentioning that the competition of Entry 2 is significantly greater than that of Entry 4 in the syn-

*CH<sub>3</sub>CHOO + HCOOH and (CH<sub>3</sub>)<sub>2</sub>COO + HCOOH systems. At ambient temperature, the total rate coefficients of HCOOH reactions with anti-CH<sub>3</sub>CHOO, syn-CH<sub>3</sub>CHOO and (CH<sub>3</sub>)<sub>2</sub>COO are estimated to be 5.9, 2.7 and 4.8 × 10<sup>-10</sup> cm<sup>3</sup> molecule<sup>-1</sup> s<sup>-1</sup>, respectively, which are consistent with the prior experimental measurements of 5 ± 3, 2.5 ± 0.3 and 4.5 × 10<sup>-10</sup> cm<sup>3</sup> molecule<sup>-1</sup> s<sup>-1</sup> (Welz et al., 2014; Chung et al., 2019; Sipilä et al., 2014).*

2. Furthermore, this paper should also exhibit some extended discussions about atmospheric implications of these reactions and their products. For example, what is the role of the formed oligomers on the atmosphere? It follows in the requirements of ACP journal “The journal scope is focused on studies with important implications for our understanding of the state and behavior of the atmosphere. Articles with a local focus must clearly explain how the results extend and compare with current knowledge”.

**Response:** Based on the Reviewer’s suggestion, the atmospheric implication of the reactions of SCIs with hydroperoxide esters and the role of the formed oligomers have been added in the revised manuscript. It is well known that the reactions with trace species (e.g., H<sub>2</sub>O, HCOOH and SO<sub>2</sub>) are expected to be the dominant chemical sinks for SCIs in the atmosphere (Taatjes et al., 2013; Long et al., 2016). The relative importance of distinct SCIs reactions with hydroperoxide esters and trace species is taken into account. In the present study, the hydroperoxymethyl formate (HPMF) is selected as the model compound since it is the simplest hydroperoxide ester formed from the barrierless reaction of 1,4 O-H insertion of CH<sub>2</sub>OO into HCOOH. The reported concentrations of coreactant, the rate coefficients *k*, and the effective pseudo-first-order rate constants (*k*<sub>eff</sub> = *k*[coreactant]) for distinct SCI reactions with H<sub>2</sub>O, HCOOH, SO<sub>2</sub>, and HPMF are summarized in Table 2. As seen in Table 2, the rate coefficient of a particular SCI reaction with trace species is strongly dependent on its structure. The methyl group substitution may alter the rate coefficient by several to tens of times. The atmospheric concentrations of H<sub>2</sub>O, HCOOH and SO<sub>2</sub> in the tropical forest environments are measured to be 3.9-6.1 × 10<sup>17</sup>, 5.0-10 × 10<sup>10</sup>, and 1.7-9.0 × 10<sup>10</sup> molecules cm<sup>-3</sup>, respectively (Vereecken, 2012). For the reactions of CH<sub>2</sub>OO with H<sub>2</sub>O, HCOOH, and SO<sub>2</sub>, the experimental rate coefficients are determined to be < 1.5 × 10<sup>-15</sup>, [1.1 ± 0.1] × 10<sup>-10</sup>, and [3.9 ± 0.7] × 10<sup>-11</sup> cm<sup>3</sup> molecule<sup>-1</sup> s<sup>-1</sup>, respectively (Welz et al., 2012 and 2014; Chao et al., 2015), which translate into *k*<sub>eff(CH<sub>2</sub>OO+H<sub>2</sub>O)</sub>, *k*<sub>eff(CH<sub>2</sub>OO+HCOOH)</sub> and *k*<sub>eff(CH<sub>2</sub>OO+SO<sub>2</sub>)</sub> of 5.9-9.2 × 10<sup>2</sup>, 5.5-11, and 0.7-

3.5 s<sup>-1</sup>, respectively. The result reveals that the reaction of CH<sub>2</sub>OO with H<sub>2</sub>O is the most important bimolecular reaction.  $k_{\text{eff}}(\text{CH}_2\text{OO}+\text{HCOOH})$  is greater by a factor of 3-8 than  $k_{\text{eff}}(\text{CH}_2\text{OO}+\text{SO}_2)$ , indicating that the reaction of CH<sub>2</sub>OO with HCOOH is favored over reaction with SO<sub>2</sub>. Similar conclusion is also obtained from the results of  $k_{\text{eff}}$  for the reactions of *anti*-CH<sub>3</sub>CHOO, *syn*-CH<sub>3</sub>CHOO and (CH<sub>3</sub>)<sub>2</sub>COO with H<sub>2</sub>O, HCOOH and SO<sub>2</sub> that SCIs reactions with H<sub>2</sub>O are faster than with HCOOH, which, in turn, are faster than with SO<sub>2</sub>.

According to the results shown in the Table 2, the room temperature rate coefficient for the reaction of CH<sub>2</sub>OO with HPMF is calculated to be  $2.7 \times 10^{-11}$  cm<sup>3</sup> molecule<sup>-1</sup> s<sup>-1</sup>. However, to the best of our knowledge, the atmospheric concentration of HPMF has not been reported up to now. If we assume that the concentration of HPMF is the same as that of HCOOH,  $k_{\text{eff}}(\text{CH}_2\text{OO}+\text{HPMF})$  is estimated to be 1.4-2.7 s<sup>-1</sup>, which is significantly lower than  $k_{\text{eff}}(\text{CH}_2\text{OO}+\text{H}_2\text{O})$  and  $k_{\text{eff}}(\text{CH}_2\text{OO}+\text{HCOOH})$ .  $k_{\text{eff}}(\text{CH}_2\text{OO}+\text{HPMF})$  is nearly identical to  $k_{\text{eff}}(\text{CH}_2\text{OO}+\text{SO}_2)$ , indicating that the CH<sub>2</sub>OO + HPMF reaction is competitive with the CH<sub>2</sub>OO + SO<sub>2</sub> system. Previous model-measurement studies have estimated the surface-level SCIs concentrations in the range of  $1.0 \times 10^4$  to  $1.0 \times 10^5$  molecules cm<sup>-3</sup> (Khan et al., 2018; Novelli et al., 2017). If we assume that the concentration of HPMF is equal to that of SCIs,  $k_{\text{eff}}(\text{CH}_2\text{OO}+\text{HPMF})$  is calculated to be  $2.7\text{-}27 \times 10^{-7}$  s<sup>-1</sup>, which is several orders of magnitude lower than  $k_{\text{eff}}(\text{CH}_2\text{OO}+\text{H}_2\text{O})$ ,  $k_{\text{eff}}(\text{CH}_2\text{OO}+\text{HCOOH})$  and  $k_{\text{eff}}(\text{CH}_2\text{OO}+\text{SO}_2)$ . This result indicates that the reaction of CH<sub>2</sub>OO with HPMF is of less importance. Similar conclusion is also obtained from the reactions of *anti*-CH<sub>3</sub>CHOO, *syn*-CH<sub>3</sub>CHOO and (CH<sub>3</sub>)<sub>2</sub>COO with HPMF. Based on the above discussions, it can be concluded that the relative importance of carbonyl oxides reactions with hydroperoxide esters is significantly dependent on the concentrations of hydroperoxide esters. These reactions may play a certain role in the formation of organic new particle in some regions where low concentration of water vapour and high concentration of hydroperoxide esters occur.

The vapour pressure and volatility of the formed oligomers are estimated in the revised manuscript. The assessment of Barley and McFiggans (2010) and O'Meara et al. (2014) found that the combination of boiling point estimation from Nannoolal et al. (2004) and vapour pressure estimation from Nannoolal et al. (2008) gives the lowest mean bias error of vapour pressure for atmospherically relevant compounds. Therefore, the saturated vapour pressure (P<sup>0</sup>) of adduct products at room temperature is estimated by using the Nannoolal-Nannoolal method, and the results are listed in Table S10. From Table S10, it can be seen that the P<sup>0</sup> of adduct products involved

in the successive reactions of CH<sub>2</sub>OO with HCOOH increases first and then decreases with increasing the number of CH<sub>2</sub>OO. The P<sup>0</sup> of the adduct product HC(O)O(CH<sub>2</sub>OO)<sub>3</sub>H is maximum when the number of CH<sub>2</sub>OO is equal to three. The P<sup>0</sup> of adduct products included in the successive reactions of *anti*-CH<sub>3</sub>CHOO with HCOOH decreases significantly as the number of *anti*-CH<sub>3</sub>CHOO is increased. Similar phenomenon is also observed from the successive reactions of *syn*-CH<sub>3</sub>CHOO and (CH<sub>3</sub>)<sub>2</sub>COO with HCOOH. Notably, the P<sup>0</sup> of adduct products decreases obviously when the size of SCIs increases. For example, the P<sup>0</sup> of the adduct product HC(O)O(CH<sub>2</sub>OO)<sub>3</sub>H in the nCH<sub>2</sub>OO + HCOOH reaction is estimated to be 4.43 × 10<sup>-3</sup> atm, which is greater than those of the corresponding adduct products in the *nanti*-CH<sub>3</sub>CHOO + HCOOH (7.12 × 10<sup>-4</sup>), *nsyn*-CH<sub>3</sub>CHOO + HCOOH (7.12 × 10<sup>-4</sup>), and n(CH<sub>3</sub>)<sub>2</sub>COO + HCOOH (1.27 × 10<sup>-4</sup>) reactions by 6.22, 6.22 and 34.88 times, respectively.

A classify scheme of various organic compounds is based on their volatility, as presented by Donahue et al. (2012) The volatility of organic compounds is described by their effective saturation concentration. The saturated concentrations (c<sup>0</sup>) of adduct products formed from the successive reactions of SCIs with HCOOH are predicted with the SIMPOL.1 method proposed by Pankow and Asher (2008), and the results are listed in Table S10. As shown in Table S10, the c<sup>0</sup> of adduct products involved in the nCH<sub>2</sub>OO + HCOOH reaction decreases with increasing the number of CH<sub>2</sub>OO. According to the Volatility Basis Set (VBS) of organic compounds (Donahue et al., 2012), these adduct products belong to volatile organic compound (VOC) (c<sup>0</sup> > 3 × 10<sup>6</sup> ug/m<sup>3</sup>). Similarly, the c<sup>0</sup> of adduct products included in the *nanti*-CH<sub>3</sub>CHOO + HCOOH, *nsyn*-CH<sub>3</sub>CHOO + HCOOH, and n(CH<sub>3</sub>)<sub>2</sub>COO + HCOOH reactions decreases when the number of SCIs increases. It deserves mentioning that the adduct products in the *nanti*-CH<sub>3</sub>CHOO + HCOOH and *nsyn*-CH<sub>3</sub>CHOO + HCOOH reactions belong to intermediate volatility organic compounds (IVOC, 300 < c<sup>0</sup> < 3 × 10<sup>6</sup> ug/m<sup>3</sup>) when the number of SCIs is equal to five. However, the adduct products in the n(CH<sub>3</sub>)<sub>2</sub>COO + HCOOH reaction become IVOC when the number of (CH<sub>3</sub>)<sub>2</sub>COO is greater than or equal to two. Based on the above discussions, it can be concluded that the volatility of adduct products is significantly affected by the number and size of SCIs in the successive reaction of SCIs with HCOOH.

**Table 2** The reported concentrations of coreactant, the rate coefficients *k*, and the effective pseudo-first-order rate constants ( $k_{\text{eff}} = k[\text{coreactant}]$ ) for distinct SCI reactions with HPMF, H<sub>2</sub>O, HCOOH

and SO<sub>2</sub> at the tropical forest environments

SCIs	Coreactant	[Coreactant] (molecules cm <sup>-3</sup> )	<i>k</i> (cm <sup>3</sup> molecule <sup>-1</sup> s <sup>-1</sup> )	<i>k</i> <sub>eff</sub> (s <sup>-1</sup> )	Reference
CH <sub>2</sub> OO	H <sub>2</sub> O	3.9-6.1 × 10 <sup>17</sup>	< 1.5 × 10 <sup>-15</sup>	5.9-9.2 × 10 <sup>2</sup>	Chao et al., (2015)
	HCOOH	5.0-10.0 × 10 <sup>10</sup>	[1.1 ± 0.1] × 10 <sup>-10</sup>	5.5-11	Welz et al., (2014)
	SO <sub>2</sub>	1.7-9.0 × 10 <sup>10</sup>	[3.9 ± 0.7] × 10 <sup>-11</sup>	0.7-3.5	Welz et al., (2012)
	HPMF	-	2.7 × 10 <sup>-11</sup>	-	This work
<i>anti</i> -CH <sub>3</sub> CHOO	H <sub>2</sub> O	3.9-6.1 × 10 <sup>17</sup>	[1.0 ± 0.4] × 10 <sup>-14</sup>	3.9-6.1 × 10 <sup>3</sup>	Taatjes et al., (2013)
	HCOOH	5.0-10.0 × 10 <sup>10</sup>	[5 ± 3] × 10 <sup>-10</sup>	25.0-50.0	Welz et al., (2014)
	SO <sub>2</sub>	1.7-9.0 × 10 <sup>10</sup>	[6.7 ± 1.0] × 10 <sup>-11</sup>	1.1-6.0	Taatjes et al., (2013)
	HPMF	-	3.3 × 10 <sup>-10</sup>	-	This work
<i>syn</i> -CH <sub>3</sub> CHOO	H <sub>2</sub> O	3.9-6.1 × 10 <sup>17</sup>	< 4.0 × 10 <sup>-15</sup>	1.6-2.4 × 10 <sup>3</sup>	Taatjes et al., (2013)
	HCOOH	5.0-10.0 × 10 <sup>10</sup>	[2.5 ± 0.3] × 10 <sup>-10</sup>	12.5-25.0	Welz et al., (2014)
	SO <sub>2</sub>	1.7-9.0 × 10 <sup>10</sup>	[2.4 ± 0.3] × 10 <sup>-11</sup>	0.4-2.2	Taatjes et al., (2013)
	HPMF	-	1.7 × 10 <sup>-13</sup>	-	This work
(CH <sub>3</sub> ) <sub>2</sub> COO	H <sub>2</sub> O	3.9-6.1 × 10 <sup>17</sup>	< 1.5 × 10 <sup>-16</sup>	58.5-91.5	Huang et al., (2015)
	HCOOH	5.0-10.0 × 10 <sup>10</sup>	4.5 × 10 <sup>-10</sup>	22.5-45.0	Sipilä et al., (2014)
	SO <sub>2</sub>	1.7-9.0 × 10 <sup>10</sup>	1.3 × 10 <sup>-10</sup>	2.2-11.7	Huang et al., (2015)
	HPMF	-	2.2 × 10 <sup>-11</sup>	-	This work

**Table S10** Predicted saturated vapour pressure (P<sup>0</sup>) and saturated concentrations (c<sup>0</sup>) for the adduct products of the successive reactions of SCIs with HCOOH

	formula	P <sup>0</sup> (atm)	c <sup>0</sup> (ug/m <sup>3</sup> )
n CH <sub>2</sub> OO + HCOOH			
n = 1	HC(O)OCH <sub>2</sub> OOH	2.12 × 10 <sup>-3</sup>	7.86 × 10 <sup>7</sup>
n = 2	HC(O)O(CH <sub>2</sub> OO) <sub>2</sub> H	3.80 × 10 <sup>-3</sup>	3.99 × 10 <sup>7</sup>
n = 3	HC(O)O(CH <sub>2</sub> OO) <sub>3</sub> H	4.43 × 10 <sup>-3</sup>	3.91 × 10 <sup>7</sup>

n = 4	HC(O)O(CH <sub>2</sub> OO) <sub>4</sub> H	4.21 × 10 <sup>-3</sup>	3.29 × 10 <sup>7</sup>
n = 5	HC(O)O(CH <sub>2</sub> OO) <sub>5</sub> H	3.59 × 10 <sup>-3</sup>	2.12 × 10 <sup>7</sup>
n	<i>anti</i> -CH <sub>3</sub> CHOO + HCOOH		
n = 1	HC(O)OCH(CH <sub>3</sub> )OOH	1.25 × 10 <sup>-3</sup>	8.32 × 10 <sup>6</sup>
n = 2	HC(O)O(CH(CH <sub>3</sub> )OO) <sub>2</sub> H	1.13 × 10 <sup>-3</sup>	7.57 × 10 <sup>6</sup>
n = 3	HC(O)O(CH(CH <sub>3</sub> )OO) <sub>3</sub> H	7.12 × 10 <sup>-4</sup>	6.49 × 10 <sup>6</sup>
n = 4	HC(O)O(CH(CH <sub>3</sub> )OO) <sub>4</sub> H	3.90 × 10 <sup>-4</sup>	4.50 × 10 <sup>6</sup>
n = 5	HC(O)O(CH(CH <sub>3</sub> )OO) <sub>5</sub> H	2.01 × 10 <sup>-4</sup>	2.81 × 10 <sup>6</sup>
n	<i>syn</i> -CH <sub>3</sub> CHOO + HCOOH		
n = 1	HC(O)OCH(CH <sub>3</sub> )OOH	1.25 × 10 <sup>-3</sup>	8.32 × 10 <sup>6</sup>
n = 2	HC(O)O(CH(CH <sub>3</sub> )OO) <sub>2</sub> H	1.13 × 10 <sup>-3</sup>	7.57 × 10 <sup>6</sup>
n = 3	HC(O)O(CH(CH <sub>3</sub> )OO) <sub>3</sub> H	7.12 × 10 <sup>-4</sup>	6.49 × 10 <sup>6</sup>
n = 4	HC(O)O(CH(CH <sub>3</sub> )OO) <sub>4</sub> H	3.90 × 10 <sup>-4</sup>	4.50 × 10 <sup>6</sup>
n = 5	HC(O)O(CH(CH <sub>3</sub> )OO) <sub>5</sub> H	2.01 × 10 <sup>-4</sup>	2.81 × 10 <sup>6</sup>
n	(CH <sub>3</sub> ) <sub>2</sub> COO + HCOOH		
n = 1	HC(O)OC(CH <sub>3</sub> ) <sub>2</sub> OOH	7.23 × 10 <sup>-4</sup>	3.50 × 10 <sup>6</sup>
n = 2	HC(O)O(C(CH <sub>3</sub> ) <sub>2</sub> OO) <sub>2</sub> H	3.50 × 10 <sup>-4</sup>	2.74 × 10 <sup>6</sup>
n = 3	HC(O)O(C(CH <sub>3</sub> ) <sub>2</sub> OO) <sub>3</sub> H	1.27 × 10 <sup>-4</sup>	1.38 × 10 <sup>6</sup>
n = 4	HC(O)O(C(CH <sub>3</sub> ) <sub>2</sub> OO) <sub>4</sub> H	4.27 × 10 <sup>-5</sup>	5.90 × 10 <sup>5</sup>
n = 5	HC(O)O(C(CH <sub>3</sub> ) <sub>2</sub> OO) <sub>5</sub> H	1.40 × 10 <sup>-5</sup>	2.36 × 10 <sup>5</sup>

Corresponding descriptions have been added in the page 23 line 573-590, page 24 line 591-610, page 27 line 645-671 and page 28 line 672-682 of the revised manuscript:

*It is of interest to assess whether the reactions of distinct SCIs with HPMF can compete well with the losses to reactions with trace species (e.g., H<sub>2</sub>O, HCOOH and SO<sub>2</sub>), because it is well known that the reactions with trace species are expected to be the dominant chemical sinks for SCIs in the atmosphere (Taatjes et al., 2013; Long et al., 2016). The reported concentrations of coreactant, the rate coefficients *k*, and the effective pseudo-first-order rate constants (*k<sub>eff</sub>* = *k*[coreactant]) for distinct SCI reactions with H<sub>2</sub>O, HCOOH, SO<sub>2</sub>, and HPMF are summarized in Table 2. As seen in Table 2, the rate coefficient of a particular SCI reaction with trace species is strongly dependent on its structure. The methyl group substitution may alter the rate coefficient by several to tens of times. The atmospheric concentrations of H<sub>2</sub>O, HCOOH and SO<sub>2</sub> in the tropical forest environments are measured to be 3.9-6.1 × 10<sup>17</sup>, 5.0-10 × 10<sup>10</sup>, and 1.7-9.0 × 10<sup>10</sup> molecules cm<sup>-3</sup>, respectively (Vereecken, 2012). For the reactions of CH<sub>2</sub>OO with H<sub>2</sub>O, HCOOH, and SO<sub>2</sub>, the experimental rate coefficients are determined to be < 1.5 × 10<sup>-15</sup>, [1.1 ± 0.1] × 10<sup>-10</sup>, and [3.9 ± 0.7] × 10<sup>-11</sup> cm<sup>3</sup> molecule<sup>-1</sup> s<sup>-1</sup>, respectively (Welz et al., 2012 and 2014; Chao et al., 2015), which translate into*



$k_{\text{eff}}(\text{CH}_2\text{OO}+\text{H}_2\text{O})$ ,  $k_{\text{eff}}(\text{CH}_2\text{OO}+\text{HCOOH})$  and  $k_{\text{eff}}(\text{CH}_2\text{OO}+\text{SO}_2)$  of  $5.9\text{-}9.2 \times 10^2$ ,  $5.5\text{-}11$ , and  $0.7\text{-}3.5 \text{ s}^{-1}$ , respectively. The result reveals that the reaction of  $\text{CH}_2\text{OO}$  with  $\text{H}_2\text{O}$  is the most important bimolecular reaction.  $k_{\text{eff}}(\text{CH}_2\text{OO}+\text{HCOOH})$  is greater by a factor of 3-8 than  $k_{\text{eff}}(\text{CH}_2\text{OO}+\text{SO}_2)$ , indicating that the reaction of  $\text{CH}_2\text{OO}$  with  $\text{HCOOH}$  is favored over reaction with  $\text{SO}_2$ . Similar conclusion is also obtained from the results of  $k_{\text{eff}}$  for the reactions of anti- $\text{CH}_3\text{CHOO}$ , syn- $\text{CH}_3\text{CHOO}$  and  $(\text{CH}_3)_2\text{COO}$  with  $\text{H}_2\text{O}$ ,  $\text{HCOOH}$  and  $\text{SO}_2$  that SCIs reactions with  $\text{H}_2\text{O}$  are faster than with  $\text{HCOOH}$ , which, in turn, are faster than with  $\text{SO}_2$ .

According to the results shown in the Table 2, the room temperature rate coefficient for the reaction of  $\text{CH}_2\text{OO}$  with HPMF is calculated to be  $2.7 \times 10^{-11} \text{ cm}^3 \text{ molecule}^{-1} \text{ s}^{-1}$ . However, to the best of our knowledge, the atmospheric concentration of HPMF has not been reported up to now. If we assume that the concentration of HPMF is the same as that of  $\text{HCOOH}$ ,  $k_{\text{eff}}(\text{CH}_2\text{OO}+\text{HPMF})$  is estimated to be  $1.4\text{-}2.7 \text{ s}^{-1}$ , which is significantly lower than  $k_{\text{eff}}(\text{CH}_2\text{OO}+\text{H}_2\text{O})$  and  $k_{\text{eff}}(\text{CH}_2\text{OO}+\text{HCOOH})$ .  $k_{\text{eff}}(\text{CH}_2\text{OO}+\text{HPMF})$  is nearly identical to  $k_{\text{eff}}(\text{CH}_2\text{OO}+\text{SO}_2)$ , indicating that the  $\text{CH}_2\text{OO} + \text{HPMF}$  reaction is competitive with the  $\text{CH}_2\text{OO} + \text{SO}_2$  system. Previous model-measurement studies have estimated the surface-level SCIs concentrations in the range of  $1.0 \times 10^4$  to  $1.0 \times 10^5 \text{ molecules cm}^{-3}$  (Khan et al., 2018; Novelli et al., 2017). If we assume that the concentration of HPMF is equal to that of SCIs,  $k_{\text{eff}}(\text{CH}_2\text{OO}+\text{HPMF})$  is calculated to be  $2.7\text{-}27 \times 10^{-7} \text{ s}^{-1}$ , which is several orders of magnitude lower than  $k_{\text{eff}}(\text{CH}_2\text{OO}+\text{H}_2\text{O})$ ,  $k_{\text{eff}}(\text{CH}_2\text{OO}+\text{HCOOH})$  and  $k_{\text{eff}}(\text{CH}_2\text{OO}+\text{SO}_2)$ . This result indicates that the reaction of  $\text{CH}_2\text{OO}$  with HPMF is of less importance. Similar conclusion is also obtained from the reactions of anti- $\text{CH}_3\text{CHOO}$ , syn- $\text{CH}_3\text{CHOO}$  and  $(\text{CH}_3)_2\text{COO}$  with HPMF. Based on the above discussions, it can be concluded that the relative importance of carbonyl oxides reactions with hydroperoxide esters is significantly dependent on the concentrations of hydroperoxide esters. These reactions may play a certain role in the formation of organic new particle in some regions where low concentration of water vapour and high concentration of hydroperoxide esters occur.

The assessment of Barley and McFiggans (2010) and O'Meara et al. (2014) found that the combination of boiling point estimation from Nannoolal et al. (2004) and vapour pressure estimation from Nannoolal et al. (2008) gives the lowest mean bias error of vapour pressure for atmospherically relevant compounds. Therefore, the saturated vapour pressure ( $P^0$ ) of adduct products at room temperature is estimated by using the Nannoolal-Nannoolal method, and the results are listed in Table S10. From Table S10, it can be seen that the  $P^0$  of adduct products involved

in the successive reactions of  $\text{CH}_2\text{OO}$  with  $\text{HCOOH}$  increases first and then decreases with increasing the number of  $\text{CH}_2\text{OO}$ . The  $P^0$  of the adduct product  $\text{HC(O)O(CH}_2\text{OO)}_3\text{H}$  is maximum when the number of  $\text{CH}_2\text{OO}$  is equal to three. The  $P^0$  of adduct products included in the successive reactions of anti- $\text{CH}_3\text{CHOO}$  with  $\text{HCOOH}$  decreases significantly as the number of anti- $\text{CH}_3\text{CHOO}$  is increased. Similar phenomenon is also observed from the successive reactions of syn- $\text{CH}_3\text{CHOO}$  and  $(\text{CH}_3)_2\text{COO}$  with  $\text{HCOOH}$ . Notably, the  $P^0$  of adduct products decreases obviously when the size of SCIs increases. For example, the  $P^0$  of the adduct product  $\text{HC(O)O(CH}_2\text{OO)}_3\text{H}$  in the  $n\text{CH}_2\text{OO} + \text{HCOOH}$  reaction is estimated to be  $4.43 \times 10^{-3}$  atm, which is greater than those of the corresponding adduct products in the nanti- $\text{CH}_3\text{CHOO} + \text{HCOOH}$  ( $7.12 \times 10^{-4}$ ), nsyn- $\text{CH}_3\text{CHOO} + \text{HCOOH}$  ( $7.12 \times 10^{-4}$ ), and  $n(\text{CH}_3)_2\text{COO} + \text{HCOOH}$  ( $1.27 \times 10^{-4}$ ) reactions by 6.22, 6.22 and 34.88 times, respectively.

A classify scheme of various organic compounds is based on their volatility, as presented by Donahue et al. (2012) The volatility of organic compounds is described by their effective saturation concentration. The saturated concentrations ( $c^0$ ) of adduct products formed from the successive reactions of SCIs with  $\text{HCOOH}$  are predicted by using the SIMPOL.1 method proposed by Pankow and Asher (2008), and the results are listed in Table S10. As shown in Table S10, the  $c^0$  of adduct products involved in the  $n\text{CH}_2\text{OO} + \text{HCOOH}$  reaction decreases with increasing the number of  $\text{CH}_2\text{OO}$ . According to the Volatility Basis Set (VBS) of organic compounds (Donahue et al., 2012), these adduct products belong to VOC ( $c^0 > 3 \times 10^6$  ug/m<sup>3</sup>). Similarly, the  $c^0$  of adduct products included in the nanti- $\text{CH}_3\text{CHOO} + \text{HCOOH}$ , nsyn- $\text{CH}_3\text{CHOO} + \text{HCOOH}$ , and  $n(\text{CH}_3)_2\text{COO} + \text{HCOOH}$  reactions decreases when the number of SCIs increases. It deserves mentioning that the adduct products in the nanti- $\text{CH}_3\text{CHOO} + \text{HCOOH}$  and nsyn- $\text{CH}_3\text{CHOO} + \text{HCOOH}$  reactions belong to intermediate volatility organic compounds (IVOC,  $300 < c^0 < 3 \times 10^6$  ug/m<sup>3</sup>) when the number of SCIs is equal to five. However, the adduct products in the  $n(\text{CH}_3)_2\text{COO} + \text{HCOOH}$  reaction become IVOC when the number of  $(\text{CH}_3)_2\text{COO}$  is greater than or equal to two. Based on the above discussions, it can be concluded that the volatility of adduct products is significantly affected by the number and size of SCIs in the successive reaction of SCIs with  $\text{HCOOH}$ .

3. Hence, as a quick assessment, some deeper and extended discussions should be required and strengthened, such as the nature of the reactions, the detailed atmospheric implications, if this paper

is published in the ACP journal.

**Response:** Based on the Reviewer's suggestion, the deeper discussions on the nature of the reactions of SCIs with hydroperoxide esters have been added in the revised manuscript. A schematic potential energy surface (PES) for the addition reaction  $2\text{CH}_2\text{OO} + \text{Pent1a}$  is drawn in Fig. 2. As seen in Fig. 2, the successive insertion of  $\text{CH}_2\text{OO}$  into Pent1a eventually leads to the formation of oligomers P2a and P2b composed of  $\text{CH}_2\text{OO}$  as the repeat unit. These oligomerization reactions are strongly exothermic and spontaneous ( $> 83 \text{ kcal}\cdot\text{mol}^{-1}$ ), implying that they are feasible thermodynamically. The addition reaction  $2\text{CH}_2\text{OO} + \text{Pent1a}$  initially proceeds through two possible pathways, namely (1)  $-\text{OOH}$  insertion reaction R1a, and (2)  $-\text{CH}$  insertion reaction R1b. For the  $-\text{OOH}$  insertion reaction R1a, the pre-reactive intermediate IM1a with a seven-membered ring structure is formed in the entrance channel, which is stabilized by the hydrogen bond interactions between the  $\text{H}_4$  atom of Pent1a and the  $\text{O}_6$  atom of  $\text{CH}_2\text{OO}$  ( $D_{(\text{O}_6-\text{H}_4)} = 1.706 \text{ \AA}$ ), and between the  $\text{H}_6$  atom of  $\text{CH}_2\text{OO}$  and the  $\text{O}_3$  atom of Pent1a ( $D_{(\text{O}_3-\text{H}_6)} = 2.115 \text{ \AA}$ ). Then IM1a converts into P1a ( $\text{C}_3\text{H}_6\text{O}_6$ ,  $\text{HC}(\text{O})-(\text{CH}_2\text{OO})_2-\text{H}$ ) via a concerted process of  $\text{O}_4-\text{H}_4$  bond breaking in the Pent1a and  $\text{O}_4-\text{C}_3$  and  $\text{H}_4-\text{O}_6$  bonds forming with a barrier of  $8.1 \text{ kcal}\cdot\text{mol}^{-1}$ . For the  $-\text{CH}$  insertion reaction R1b, the pre-reactive intermediate IM1b with a seven-membered ring structure is formed in the entrance channel, which is stabilized by the van der Waals (vdW) interactions between the  $\text{O}_3$  atom of Pent1a and the  $\text{C}_3$  atom of  $\text{CH}_2\text{OO}$  ( $D_{(\text{O}_3-\text{C}_3)} = 2.602 \text{ \AA}$ ), and between the  $\text{O}_6$  atom of  $\text{CH}_2\text{OO}$  and the  $\text{C}_1$  atom of Pent1a ( $D_{(\text{O}_6-\text{C}_1)} = 2.608 \text{ \AA}$ ). Due to the absence of hydrogen bond in IM1b, the energy of IM1b is lower than that of IM1a by  $3.0 \text{ kcal}\cdot\text{mol}^{-1}$ . IM1b transforms into P1b ( $\text{C}_3\text{H}_6\text{O}_6$ ,  $\text{HO}_2\text{CH}_2\text{OC}(\text{O})\text{CH}_2\text{OOH}$ ) via a concerted process of  $\text{C}_1-\text{H}_1$  bond breaking in the Pent1a and  $\text{C}_1-\text{C}_3$  and  $\text{H}_1-\text{O}_6$  bonds forming with a barrier of  $21.5 \text{ kcal}\cdot\text{mol}^{-1}$ . By comparing the barriers of R1a and R1b, it can be concluded that the  $-\text{OOH}$  insertion reaction is favored over the  $-\text{CH}$  insertion reaction. The high reaction barrier of R1b is attributed to the large bond dissociation energy (BDE) of C-H bond in the Pent1a. To further insight into the reaction mechanism of R1a, the natural bond orbital (NBO) analysis of the donor-accepter orbitals involved in the TS1a is performed using the M06-2X wave function. The possible donor-accepter interactions are estimated by using the second order perturbation theory. As illustrated in Fig. S4, the strong interactions are identified as the interaction of the lone pair orbital of  $\text{O}_6$  atom and the antibonding orbital of  $\text{O}_4-\text{H}_4$  bond, and the interaction of the lone pair orbital of  $\text{O}_4$  atom and the antibonding orbital of  $\text{C}_3-\text{O}_5$  bond.

Similarly, the addition reaction  $\text{CH}_2\text{OO} + \text{P1a}$  proceeds through the formation of the pre-reactive intermediates IM2a and IM2b in the entrance channel, which are stabilized by a hydrogen bond between the terminal oxygen atom of  $\text{CH}_2\text{OO}$  and the reacting hydrogen atom of P1a, and a van der Waals (vdW) interaction between the central carbon atom of  $\text{CH}_2\text{OO}$  and the carbonyl oxygen atom of P1a. The relative energies of IM2a and IM2b with respect to the separate reactants P1a and  $\text{CH}_2\text{OO}$  are  $-1.2$  and  $3.2$   $\text{kcal}\cdot\text{mol}^{-1}$ , respectively, below the energies of the initial reactants  $2\text{CH}_2\text{OO}$  and Pent1a are  $41.6$  and  $37.2$   $\text{kcal}\cdot\text{mol}^{-1}$ , respectively. Then they immediately transform into the respective products P2a and P2b through the  $-\text{OOH}$  and  $-\text{CH}$  insertion transition states TS2a and TS2b with the barriers of  $10.1$  and  $21.6$   $\text{kcal}\cdot\text{mol}^{-1}$ . This result again shows that the  $-\text{OOH}$  insertion reaction is favored kinetically. It deserves mentioning that the barrier of  $-\text{OOH}$  insertion reaction increases as the number of  $\text{CH}_2\text{OO}$  is increased. From the viewpoint of the geometrical parameters of TS2a and TS2b, the breaking O-H and C-H bonds are elongated by  $14.8\%$  and  $20.6\%$ , respectively, with respect to the equilibrium structures of IM2a and IM2b, while the forming C-O and C-C bond length are  $2.013$  and  $2.264$  Å, respectively. The result reveals that TS2a and TS2b are structurally reactant-like, which are consistent with the Hammond's hypothesis that the earlier transition states are generally exothermic (Hammond, 1955).

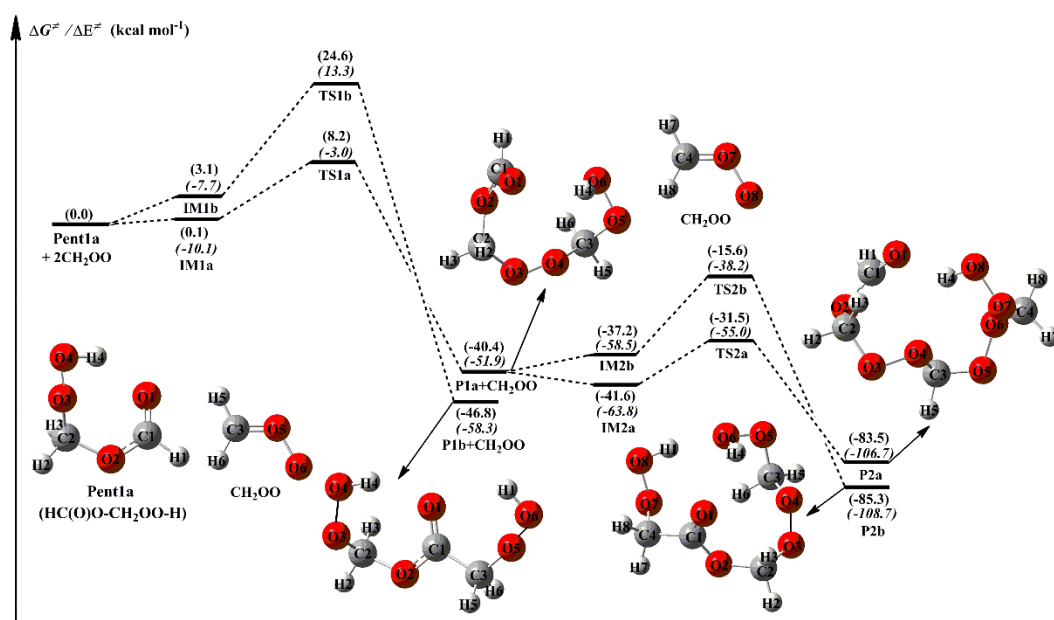


**Figure 2.** PES ( $\Delta G$  and  $\Delta E$ , in italics) for the  $2\text{CH}_2\text{OO} + \text{Pent1a}$  reaction at the M06-2X/ma-TZVP//M06-2X/6-311+G(2df,2p) level of theory

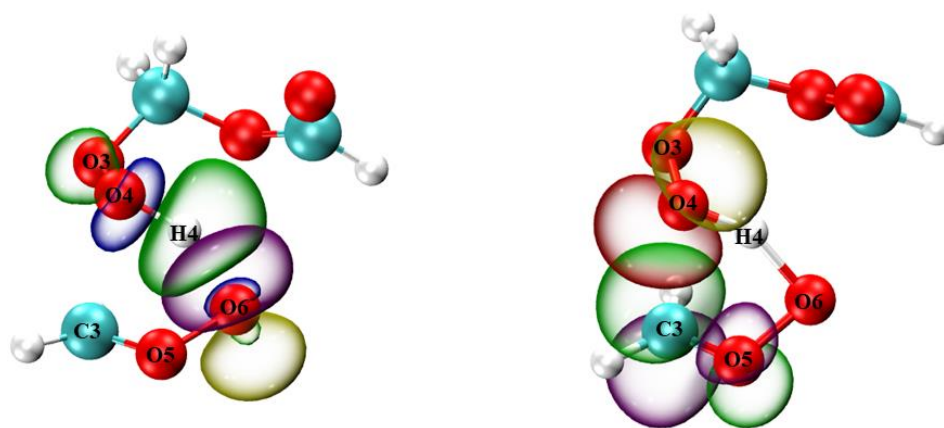


**Figure S4.** Natural bond orbital (NBO) analysis of the donor-acceptor orbitals involved in the TS1a

To further elucidate the effect of the number and location of methyl substituents on the reactivity of carbonyl oxides toward hydroperoxide esters, Pent1a (also called as HPMF) is selected as the model compound since it is the simplest hydroperoxide ester formed from the barrierless reaction of 1,4 O-H insertion of  $\text{CH}_2\text{OO}$  into  $\text{HCOOH}$ . As mentioned above,  $-\text{OOH}$  insertion reaction in the oligomerization reactions is the most favorable pathway. Therefore, this type of reaction is merely considered in the reactions of distinct SCIs with Pent1a. The corresponding PES is displayed in Fig. 6. As shown in Fig. 6, each pathway starts with the formation of a pre-reactive intermediate, and then it overcomes a modest barrier to reaction. The barrier of the reaction of  $\text{CH}_2\text{OO}$  with Pent1a is calculated to be  $8.1 \text{ kcal}\cdot\text{mol}^{-1}$ , which is higher than that of the *anti*- $\text{CH}_3\text{CHOO} + \text{Pent1a}$  reaction by  $2.5 \text{ kcal}\cdot\text{mol}^{-1}$ . The reason of low barrier can be explained by the NPA atomic charges, as presented in Fig. S9. As seen in Fig. S9, the charges of the central carbon atom  $\text{C}_1$  and the terminal oxygen atom  $\text{O}_1$  of  $\text{CH}_2\text{OO}$  are  $0.186e$  and  $-0.459e$ , respectively, indicating that  $\text{CH}_2\text{OO}$  is indeed a zwitterion. The  $\text{C}_1$  atom charge becomes more positive ( $0.393e$ ), while the  $\text{O}_1$  atom charge becomes more negative ( $-0.497e$ ) when a methyl substituent occurs at the *anti*-position. This result suggests that the *anti*-methyl substituent enhances the characteristic of carbonyl oxides zwitterion and reduces the reaction barriers. Compared with the barrier of the  $\text{CH}_2\text{OO} + \text{Pent1a}$  reaction, the barriers increase by about  $3.0 \text{ kcal}\cdot\text{mol}^{-1}$  when a methyl group is introduced at the *syn*-position and dimethyl substituent. Although *syn*-methyl and dimethyl substituent promote the raise of carbonyl oxides zwitterion, the steric hindrance effect and intramolecular hydrogen bond are obviously dominant for *syn*- $\text{CH}_3\text{CHOO}$  and  $(\text{CH}_3)_2\text{COO}$ , that are not thus conducive to the nucleophilic attack of hydroperoxide esters. It is worth noting that the exothermicity of distinct SCIs reactions with Pent1a obviously decreases as the number of methyl group is increased, and the

exothermicity of *anti*-methyl substituent is higher than that of *syn*-methyl substituent.

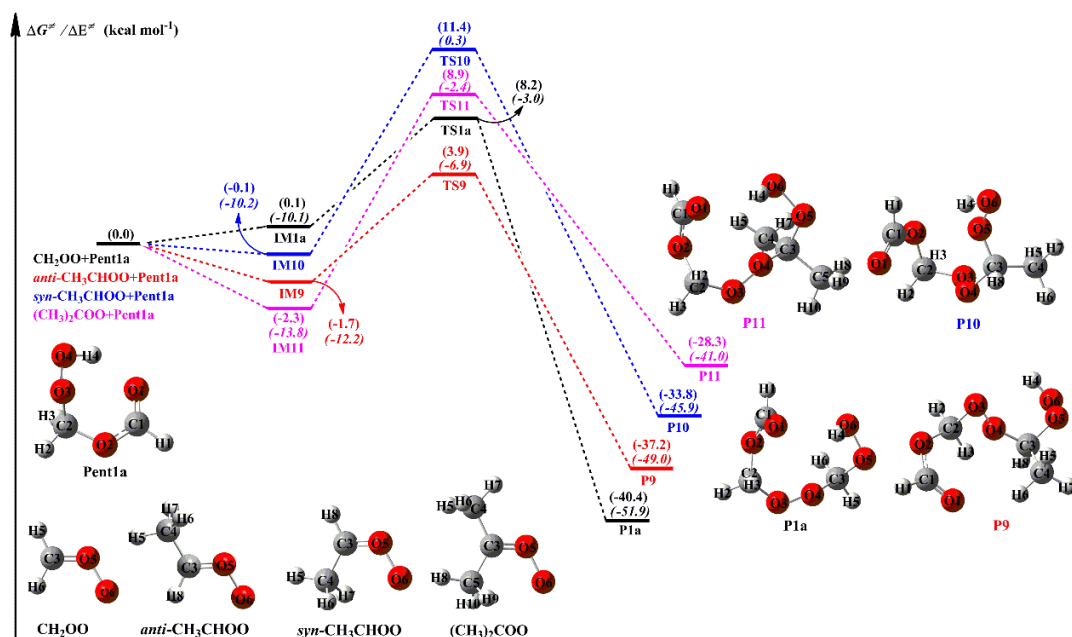


**Figure 6.** PES ( $\Delta G$  and  $\Delta E$ , in italics) for the distinct SCIs + Pent1a reactions at the M06-2X/ma-TZVP//M06-2X/6-311+G(2df,2p) level of theory

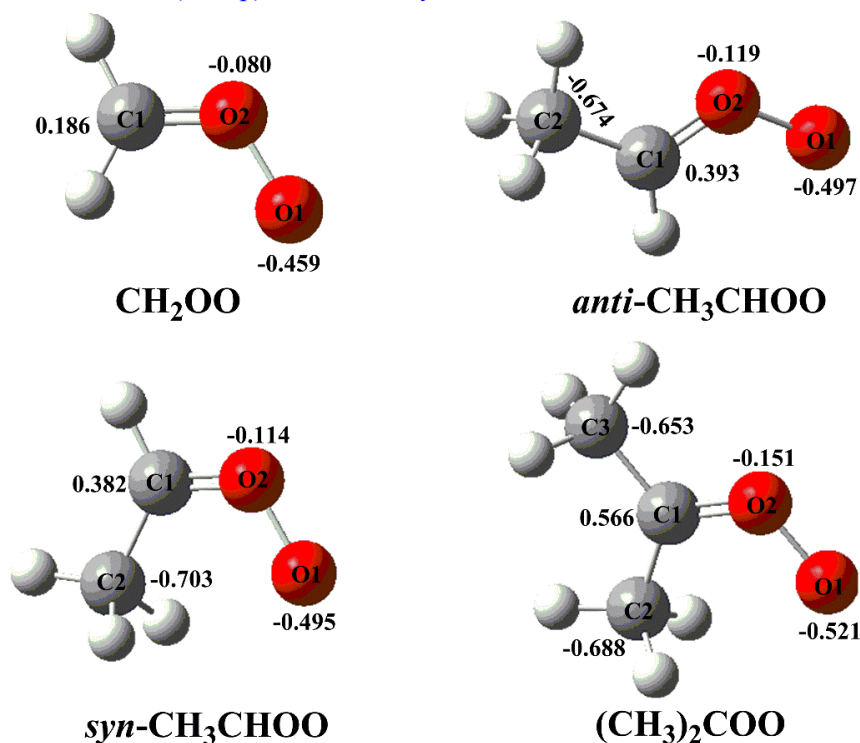


**Figure S9** The NPA charges of different atoms in the distinct SCIs computed at the M06-2X/6-311+g(2df,2p) level of theory

Corresponding descriptions have been added in the page 15 line 388-398, page 16 line 399-438 and page 21 line 530-556 of the revised manuscript:

*A schematic PES for the addition reaction 2CH<sub>2</sub>OO + Pent1a is drawn in Fig. 2. As seen in*

Fig. 2, the successive insertion of CH<sub>2</sub>OO into Pent1a eventually leads to the formation of oligomers P2a and P2b composed of CH<sub>2</sub>OO as the repeat unit. These oligomerization reactions are strongly exothermic and spontaneous ( $> 83 \text{ kcal}\cdot\text{mol}^{-1}$ ), implying that they are feasible thermodynamically. The addition reaction  $2\text{CH}_2\text{OO} + \text{Pent1a}$  initially proceeds through two possible pathways, namely (1) –OOH insertion reaction R1a, and (2) –CH insertion reaction R1b. For the –OOH insertion reaction R1a, the pre-reactive intermediate IM1a with a seven-membered ring structure is formed in the entrance channel, which is stabilized by the hydrogen bond interactions between the H<sub>4</sub> atom of Pent1a and the O<sub>6</sub> atom of CH<sub>2</sub>OO ( $D_{(\text{O}_6\text{-H}_4)} = 1.706 \text{ \AA}$ ), and between the H<sub>6</sub> atom of CH<sub>2</sub>OO and the O<sub>3</sub> atom of Pent1a ( $D_{(\text{O}_3\text{-H}_6)} = 2.115 \text{ \AA}$ ). Then IM1a converts into P1a (C<sub>3</sub>H<sub>6</sub>O<sub>6</sub>, HC(O)O–(CH<sub>2</sub>OO)<sub>2</sub>–H) via a concerted process of O<sub>4</sub>–H<sub>4</sub> bond breaking in the Pent1a and O<sub>4</sub>–C<sub>3</sub> and H<sub>4</sub>–O<sub>6</sub> bonds forming with a barrier of  $8.1 \text{ kcal}\cdot\text{mol}^{-1}$ . For the –CH insertion reaction R1b, the pre-reactive intermediate IM1b with a seven-membered ring structure is formed in the entrance channel, which is stabilized by the van der Waals (vdW) interactions between the O<sub>3</sub> atom of Pent1a and the C<sub>3</sub> atom of CH<sub>2</sub>OO ( $D_{(\text{O}_3\text{-C}_3)} = 2.602 \text{ \AA}$ ), and between the O<sub>6</sub> atom of CH<sub>2</sub>OO and the C<sub>1</sub> atom of Pent1a ( $D_{(\text{O}_6\text{-C}_1)} = 2.608 \text{ \AA}$ ). Due to the absence of hydrogen bond in IM1b, the energy of IM1b is lower than that of IM1a by  $3.0 \text{ kcal}\cdot\text{mol}^{-1}$ . IM1b transforms into P1b (C<sub>3</sub>H<sub>6</sub>O<sub>6</sub>, HO<sub>2</sub>CH<sub>2</sub>OC(O)CH<sub>2</sub>OOH) via a concerted process of C<sub>1</sub>–H<sub>1</sub> bond breaking in the Pent1a and C<sub>1</sub>–C<sub>3</sub> and H<sub>1</sub>–O<sub>6</sub> bonds forming with a barrier of  $21.5 \text{ kcal}\cdot\text{mol}^{-1}$ . By comparing the barriers of R1a and R1b, it can be concluded that the –OOH insertion reaction is favored over the –CH insertion reaction. The high reaction barrier of R1b is attributed to the large bond dissociation energy (BDE) of C–H bond in the Pent1a. To further insight into the reaction mechanism of R1a, the natural bond orbital (NBO) analysis of the donor-accepter orbitals involved in the TS1a is performed using the M06-2X wave function. The possible donor-accepter interactions are estimated by using the second order perturbation theory. As illustrated in Fig. S4, the strong interactions are identified as the interaction of the lone pair orbital of O<sub>6</sub> atom and the antibonding orbital of O<sub>4</sub>–H<sub>4</sub> bond, and the interaction of the lone pair orbital of O<sub>4</sub> atom and the antibonding orbital of C<sub>3</sub>–O<sub>5</sub> bond.

Similarly, the addition reaction  $\text{CH}_2\text{OO} + \text{P1a}$  proceeds through the formation of the pre-reactive intermediates IM2a and IM2b in the entrance channel, which are stabilized by a hydrogen bond between the terminal oxygen atom of CH<sub>2</sub>OO and the reacting hydrogen atom of P1a, and a van der Waals (vdW) interaction between the central carbon atom of CH<sub>2</sub>OO and the carbonyl

oxygen atom of P1a. The relative energies of IM2a and IM2b with respect to the separate reactants P1a and CH<sub>2</sub>OO are -1.2 and 3.2 kcal·mol<sup>-1</sup>, respectively, below the energies of the initial reactants 2CH<sub>2</sub>OO and Pent1a are 41.6 and 37.2 kcal·mol<sup>-1</sup>, respectively. Then they immediately transform into the respective products P2a and P2b through the -OOH and -CH insertion transition states TS2a and TS2b with the barriers of 10.1 and 21.6 kcal·mol<sup>-1</sup>. This result again shows that the -OOH insertion reaction is favored kinetically. It deserves mentioning that the barrier of -OOH insertion reaction increases as the number of CH<sub>2</sub>OO is increased. From the viewpoint of the geometrical parameters of TS2a and TS2b, the breaking O-H and C-H bonds are elongated by 14.8% and 20.6%, respectively, with respect to the equilibrium structures of IM2a and IM2b, while the forming C-O and C-C bond length are 2.013 and 2.264 Å, respectively. The result reveals that TS2a and TS2b are structurally reactant-like, which are consistent with the Hammond's hypothesis that the earlier transition states are generally exothermic (Hammond, 1955).

To further elucidate the effect of the number and location of methyl substituents on the reactivity of carbonyl oxides toward hydroperoxide esters, Pent1a (also called as HPMF) is selected as the model compound since it is the simplest hydroperoxide ester formed from the barrierless reaction of 1,4 O-H insertion of CH<sub>2</sub>OO into HCOOH. As mentioned above, -OOH insertion reaction in the oligomerization reactions is the most favorable pathway. Therefore, this type of reaction is merely considered in the reactions of distinct SCIs with Pent1a. The corresponding PES and the optimized geometries of all stationary points are displayed in Figs. 6 and S8, respectively. As seen in Fig. 6, each pathway starts with the formation of a pre-reactive intermediate, and then it overcomes a modest barrier to reaction. The barrier of the reaction of CH<sub>2</sub>OO with Pent1a is calculated to be 8.1 kcal·mol<sup>-1</sup>, which is higher than that of the anti-CH<sub>3</sub>CHOO + Pent1a reaction by 2.5 kcal·mol<sup>-1</sup>. The reason of low barrier can be explained by the NPA atomic charges, as presented in Fig. S9. As seen in Fig. S9, the charges of the central carbon atom C<sub>1</sub> and the terminal oxygen atom O<sub>1</sub> of CH<sub>2</sub>OO are 0.186e and -0.459e, respectively, indicating that CH<sub>2</sub>OO is indeed a zwitterion. The C<sub>1</sub> atom charge becomes more positive (0.393e), while the O<sub>1</sub> atom charge becomes more negative (-0.497e) when a methyl substituent occurs at the anti-position. This result suggests that the anti-methyl substituent enhances the characteristic of carbonyl oxides zwitterion and reduces the reaction barriers. Compared with the barrier of the CH<sub>2</sub>OO + Pent1a reaction, the barriers increase by about 3.0 kcal·mol<sup>-1</sup> when a methyl group is introduced at the syn-position and



*dimethyl substituent. Although syn-methyl and dimethyl substituent promote the raise of carbonyl oxides zwitterion, the steric hindrance effect and intramolecular hydrogen bond are obviously dominant for syn-CH<sub>3</sub>CHOO and (CH<sub>3</sub>)<sub>2</sub>COO, that are not thus conducive to the nucleophilic attack of hydroperoxide esters. It is worth noting that the exothermicity of distinct SCIs reactions with Pent1a obviously decreases as the number of methyl group is increased, and the exothermicity of anti-methyl substituent is higher than that of syn-methyl substituent.*

## Reference

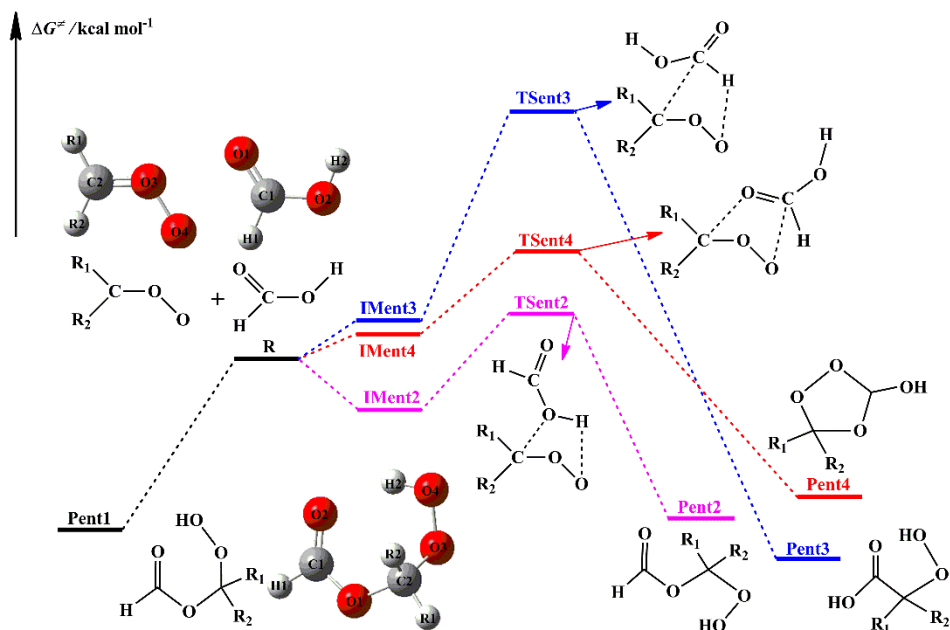
- Barley, M. H., and McFiggans, G.: The critical assessment of vapour pressure estimation methods for use in modelling the formation of atmospheric organic aerosol, *Atmos. Chem. Phys.*, 10, 749-767, <https://doi.org/10.5194/acp-10-749-2010>, 2010.
- Canneaux, S., Bohr, F., and Henon, E.: KiSThelP: a program to predict thermodynamic properties and rate constants from quantum chemistry results, *J. Comput. Chem.*, 35, 82-93, <https://doi.org/10.1002/jcc.23470>, 2013.
- Chao, W., Hsieh, J. T., Chang, C. H., and Lin, J. J. M.: Direct kinetic measurement of the reaction of the simplest Criegee intermediate with water vapor, *Science*, 347, 751-754, <https://doi.org/10.1126/science.1261549>, 2015.
- Chung, C. A., Su, J. W., and Lee, Y. P.: Detailed mechanism and kinetics of the reaction of Criegee intermediate CH<sub>2</sub>OO with HCOOH investigated via infrared identification of conformers of hydroperoxymethyl formate and formic acid anhydride, *Phys. Chem. Chem. Phys.*, 21, 21445-21455, <https://doi.org/10.1039/c9cp04168k>, 2019.
- Donahue, N. M., Kroll, J. H., Pandis, S. N., and Robinson, A. L.: A two-dimensional volatility basis set – Part 2: Diagnostics of organic-aerosol evolution, *Atmos. Chem. Phys.*, 12, 615-634, <https://doi.org/10.5194/acp-12-615-2012>, 2012.
- Gilbert, R. G., and Smith, S. C.: *Theory of unimolecular and recombination reactions*; Blackwell Scientific: Carlton, Australia, 1990.
- Glowacki, D. R., Liang, C. H., Morley, C., Pilling, M. J., and Robertson, S. H.: MESMER: an open-source master equation solver for multi-energy well reactions, *J. Phys. Chem. A*, 116, 9545-9560, <https://doi.org/10.1021/jp3051033>, 2012.
- Hammond, G. S.: A correlation of reaction rates, *J. Am. Chem. Soc.*, 77, 334-338, <https://doi.org/10.1021/ja01607a027>, 1955.
- Huang, H. L., Chao, W., and Lin, J. J. M.: Kinetics of a Criegee intermediate that would survive high humidity and may oxidize atmospheric SO<sub>2</sub>, *Proc. Natl. Acad. Sci. U.S.A.*, 112, 10857-10862, <https://doi.org/10.1073/pnas.1513149112>, 2015.
- Khan, M. A. H., Percival, C. J., Caravan, R. L., Taatjes, C. A., and Shallcross, D. E.: Criegee intermediates and their impacts on the troposphere, *Environ. Sci.: Processes Impacts*, 20, 437-453, <https://doi.org/10.1039/C7EM00585G>, 2018.
- Long, B., Bao, J. L., and Truhlar, D. G.: Atmospheric chemistry of Criegee intermediates: unimolecular reactions and reactions with water, *J. Am. Chem. Soc.*, 138, 14409-14422, <https://doi.org/10.1021/jacs.6b08655>, 2016.
- Nannoolal, Y., Rarey, J., and Ramjugernatha, D.: Estimation of pure component properties Part 3. Estimation of the vapor pressure of non-electrolyte organic compounds via group contributions and group interactions, *Fluid Phase Equilibria*, 269, 117-133, <https://doi.org/10.1016/j.fluid.2008.04.020>, 2008.
- Nannoolal, Y., Rarey, J., Ramjugernatha, D., and Cordesb, W.: Estimation of pure component properties Part 1. Estimation of the normal boiling point of non-electrolyte organic compounds via group contributions and group interactions, *Fluid Phase Equilibria*, 226, 45-63, <https://doi.org/10.1016/j.fluid.2004.09.001>, 2004.
- Novelli, A., Hens, K., Ernest, C. T., Martinez, M., Nölscher, A. C., Sinha, V., Paasonen, P., Petäjä, T., Sipilä, M., Elste, T., Plass-Dülmer, C., Phillips, G. J., Kubistin, D., Williams, J., Vereecken, L., Lelieveld, J., and Harder, H.: Estimating the atmospheric concentration of Criegee

- intermediates and their possible interference in a FAGE-LIF instrument, *Atmos. Chem. Phys.*, **17**, 7807-7826, <https://doi.org/10.5194/acp-17-7807-2017>, 2017.
- O'Meara, S., Booth, A. M., Barley, M. H., Topping, D., and McFiggans, G.: An assessment of vapour pressure estimation methods, *Phys. Chem. Chem. Phys.*, **16**, 19453-19469, <https://doi.org/10.1039/C4CP00857J>, 2014.
- Pankow, J. F., and Asher, W. E.: SIMPOL.1: a simple group contribution method for predicting vapor pressures and enthalpies of vaporization of multifunctional organic compounds, *Atmos. Chem. Phys.*, **8**, 2773-2796, <https://doi.org/10.5194/acp-8-2773-2008>, 2008.
- Peltola, J., Seal, P., Inkilä, A., and Eskola, A.: Time-resolved, broadband UV-absorption spectrometry measurements of Criegee intermediate kinetics using a new photolytic precursor: unimolecular decomposition of CH<sub>2</sub>OO and its reaction with formic acid, *Phys. Chem. Chem. Phys.*, **22**, 11797-11808, <https://doi.org/10.1039/d0cp00302f>, 2020.
- Raghunath, P., Lee, Y. P., and Lin, M. C.: Computational chemical kinetics for the reaction of Criegee intermediate CH<sub>2</sub>OO with HNO<sub>3</sub> and its catalytic conversion to OH and HCO, *J. Phys. Chem. A*, **121**, 3871-3878, <https://doi.org/10.1021/acs.jpca.7b02196>, 2017.
- Sipilä, M., Jokinen, T., Berndt, T., Richters, S., Makkonen, R., Donahue, N. M., Mauldin III, R. L., Kurtén, T., Paasonen, P., Sarnela, N., Ehn, M., Junninen, H., Rissanen, M. P., Thornton, J., Stratmann, F., Herrmann, H., Worsnop, D. R., Kulmala, M., Kerminen, V. M., and Petäjä, T.: Reactivity of stabilized Criegee intermediates (sCIs) from isoprene and monoterpene ozonolysis toward SO<sub>2</sub> and organic acids, *Atmos. Chem. Phys.*, **14**, 12143-12153, <https://doi.org/10.5194/acp-14-12143-2014>, 2014.
- Taatjes, C. A., Welz, O., Eskola, A. J., Savee, J. D., Scheer, A. M., Shallcross, D. E., Rotavera, B., Lee, E. P. F., Dyke, J. M., Mok, D. K. W., Osborn, D. L., and Percival, C. J.: Direct measurements of conformer-dependent reactivity of the Criegee intermediate CH<sub>3</sub>CHOO, *Science*, **340**, 177-180, <https://doi.org/10.1126/science.1234689>, 2013.
- Vereecken, L., Harder, H., and Novelli, A.: The reaction of Criegee intermediates with NO, RO<sub>2</sub>, and SO<sub>2</sub>, and their fate in the atmosphere, *Phys. Chem. Chem. Phys.*, **14**, 14682-14695, <https://doi.org/10.1039/c2cp42300f>, 2012.
- Welz, O., Eskola, A. J., Sheps, L., Rotavera, B., Savee, J. D., Scheer, A. M., Osborn, D. L., Lowe, D., Booth, A. M., Xiao, P., Khan, M. A. H., Percival, C. J., Shallcross, D. E., and Taatjes, C. A.: Rate coefficients of C(1) and C(2) Criegee intermediate reactions with formic and acetic acid near the collision limit: direct kinetics measurements and atmospheric implications, *Angew. Chem. Int. Ed.*, **53**, 4547-4550, <https://doi.org/10.1002/anie.201400964>, 2014.
- Welz, O., Savee, J. D., Osborn, D. L., Vasu, S. S., Percival, C. J., Shallcross, D. E., and Taatjes, C. A.: Direct kinetic measurements of Criegee intermediate (CH<sub>2</sub>OO) formed by reaction of CH<sub>2</sub>I with O<sub>2</sub>, *Science*, **335**, 204-207, <https://doi.org/10.1126/science.1213229>, 2012.

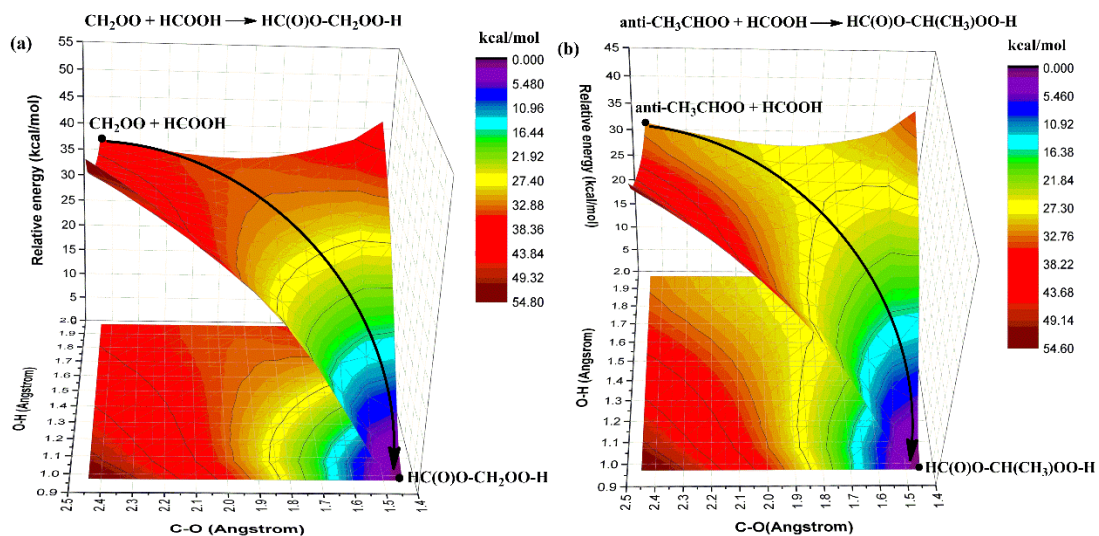
### Comments of reviewer #3

1. For Entry 1 of the initiation reaction, how is it validated that 1,4 O-H insertion is barrierless? Is there a multi-point potential energy surface showing that no barrier is found along the reaction coordinate?

**Response:** Based on the Reviewer's suggestion, the relevance descriptions on the barrierless 1,4 O-H insertion reactions have been added in the revised manuscript. The potential energy surface (PES) of the initiation reactions of distinct stabilized Criegee intermediates (SCIs) ( $\text{CH}_2\text{OO}$ , *syn*-, *anti*- $\text{CH}_3\text{CHOO}$  and  $(\text{CH}_3)_2\text{COO}$ ) with  $\text{HCOOH}$  is drawn in Fig. 1. As shown in Fig. 1, the bimolecular reaction of distinct SCIs with  $\text{HCOOH}$  proceeds via four possible pathways, namely (1) 1,4 O-H insertion (Entry 1), (2) 1,2 O-H insertion (Entry 2), (3) C-H insertion (Entry 3), and (4) C=O cycloaddition (Entry 4). For Entry 1, the addition reaction of  $\text{CH}_2\text{OO}$  with  $\text{HCOOH}$  proceeds through the 1,4 O-H insertion of  $\text{CH}_2\text{OO}$  into  $\text{HCOOH}$  to form a hydroperoxide ester  $\text{HC(O)O-CH}_2\text{OO-H}$  with a exoergicity of  $37.6 \text{ kcal}\cdot\text{mol}^{-1}$ . The formation of  $\text{HC(O)O-CH}_2\text{OO-H}$  is obtained through a concerted process of  $\text{O}_2\text{-H}_2$  bond breaking in the  $\text{HCOOH}$  and  $\text{O}_4\text{-H}_2$  and  $\text{C}_2\text{-O}_1$  bonds forming. Despite an attempt by various methods, the corresponding transition state is still not located in the effort of optimization. To further validate the barrierless process of 1,4 O-H insertion reaction, a relaxed scan over the  $\text{O}_4\text{-H}_2$  and  $\text{C}_2\text{-O}_1$  bonds is performed at the M06-2X/6-311+G(2df,2p) level of theory. The scans start from the optimized structure of the adduct product  $\text{HC(O)O-CH}_2\text{OO-H}$ , and the  $\text{O}_4\text{-H}_2$  and  $\text{C}_2\text{-O}_1$  bond length are then increased in steps of  $0.10 \text{ \AA}$ . The relaxed scan energy profiles are presented in Fig. S2. As seen in Fig. S2a, the relative energy of the minimum energy path from reactant to product decreases monotonically when the bond length of  $\text{O}_4\text{-H}_2$  and  $\text{C}_2\text{-O}_1$  bonds decreases, suggesting that the transition state is not exist in the 1,4 O-H insertion reaction of  $\text{CH}_2\text{OO}$  with  $\text{HCOOH}$ . Similar conclusion is also obtained from the relaxed scan energy profiles for the  $\text{HCOOH} + \textit{anti}\text{-CH}_3\text{CHOO}$ ,  $\text{HCOOH} + \textit{syn}\text{-CH}_3\text{CHOO}$  and  $\text{HCOOH} + (\text{CH}_3)_2\text{COO}$  (Fig. S2b-d) reactions that 1,4 O-H insertion reactions are barrierless. This conclusion is further supported by the analogous reaction systems that 1,4 O-H insertion reactions of carbonyl oxides with carboxylic acids are a barrierless process including concerted hydrogen atom transfer and new bond formation (Long et al., 2009; Vereecken, 2017; Cabezas and Endo, 2019; Lin et al., 2019; Chhantyal-Pun et al., 2017).



**Figure 1.** Schematic PES for the possible entrance pathways of the initiation reactions of HCOOH with various SCIs (black, pink, blue, and red lines represent 1,4 O-H insertion, 1,2 O-H insertion, C-H insertion, and C=O cycloaddition reactions, respectively)



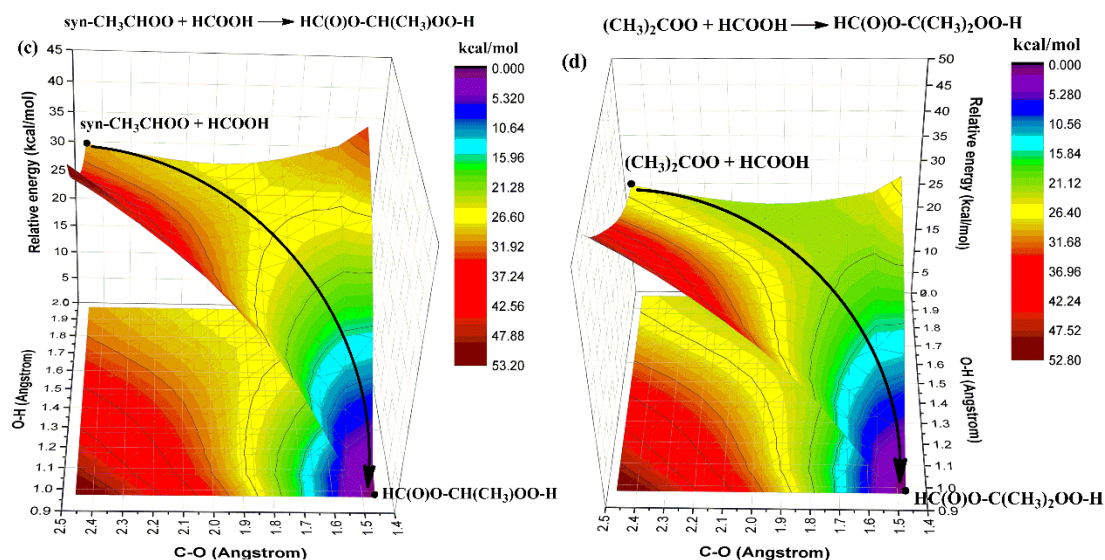


**Figure S2.** Relaxed scan energy profiles calculated using the M06-2X/6-311+G(2df,2p) method for varying the C-O and O-H bonds in the 1,4-insertion reactions  $\text{CH}_2\text{OO} + \text{HCOOH}$  (a), *anti*- $\text{CH}_3\text{CHOO} + \text{HCOOH}$  (b), *syn*- $\text{CH}_3\text{CHOO} + \text{HCOOH}$  (c) and  $(\text{CH}_3)_2\text{COO} + \text{HCOOH}$  (d) (the black solid line represents the minimum energy path)

Corresponding descriptions have been added in the page 8 line 215-239 of the revised manuscript:

The potential energy surface (PES) of distinct SCIs ( $\text{CH}_2\text{OO}$ , *syn*-, *anti*- $\text{CH}_3\text{CHOO}$  and  $(\text{CH}_3)_2\text{COO}$ ) reactions with  $\text{HCOOH}$  is drawn in Fig. 1. As shown in Fig. 1, the bimolecular reaction of distinct SCIs with  $\text{HCOOH}$  proceeds via four possible pathways, namely (1) 1,4 O-H insertion (Entry 1), (2) 1,2 O-H insertion (Entry 2), (3) C-H insertion (Entry 3), and (4) C=O cycloaddition (Entry 4). For Entry 1, the addition reaction of  $\text{CH}_2\text{OO}$  with  $\text{HCOOH}$  proceeds through the 1,4 O-H insertion of  $\text{CH}_2\text{OO}$  into  $\text{HCOOH}$  to form a hydroperoxide ester  $\text{HC(O)O-CH}_2\text{OO-H}$  with a exoergicity of  $37.6 \text{ kcal}\cdot\text{mol}^{-1}$ . The formation of  $\text{HC(O)O-CH}_2\text{OO-H}$  is obtained through a concerted process of  $\text{O}_2\text{-H}_2$  bond breaking in the  $\text{HCOOH}$  and  $\text{O}_4\text{-H}_2$  and  $\text{C}_2\text{-O}_1$  bonds forming. Despite an attempt by various methods, the corresponding transition state is still not located in the effort of optimization. To further validate the barrierless process of 1,4 O-H insertion reaction, a relaxed scan over the  $\text{O}_4\text{-H}_2$  and  $\text{C}_2\text{-O}_1$  bonds is performed at the M06-2X/6-311+G(2df,2p) level of theory. The scans start from the optimized structure of the adduct product  $\text{HC(O)O-CH}_2\text{OO-H}$ , and the  $\text{O}_4\text{-H}_2$  and  $\text{C}_2\text{-O}_1$  bond length are then increased in steps of  $0.10 \text{ \AA}$ . The relaxed scan energy profiles are presented in Fig. S2. As seen in Fig. S2a, the relative energy of the minimum energy path from reactant to product decreases monotonically when the bond length of  $\text{O}_4\text{-H}_2$  and  $\text{C}_2\text{-O}_1$  bonds decreases, suggesting that the transition state is not exist in the 1,4 O-H

*insertion reaction of CH<sub>2</sub>OO with HCOOH. Similar conclusion is also obtained from the relaxed scan energy profiles for the HCOOH + anti-CH<sub>3</sub>CHOO, HCOOH + syn-CH<sub>3</sub>CHOO and HCOOH + (CH<sub>3</sub>)<sub>2</sub>COO (Fig. S2b-d) reactions that 1,4 O-H insertion reactions are barrierless. This conclusion is further supported by the analogous reaction systems that 1,4 O-H insertion reactions of carbonyl oxides with carboxylic acids are a barrierless process including concerted hydrogen atom transfer and new C-O bond formation (Chhantyal-Pun et al., 2017; Long et al., 2009; Vereecken, 2017; Cabezas and Endo, 2019; Lin et al., 2019).*

2. The calculated  $k_{\text{tot}}$  in this study is greater by a factor of  $\sim 3$  than several previous studies. Since this is related to one of the major conclusions of the paper, the authors should carefully validate this result. For example, what could be the reason they underestimate the value? Which value can have a better interpretation of the experimental or atmospheric data?

**Response:** In the original manuscript, the rate coefficients for the barrierless reactions are calculated by employing the variational transition state theory (VTST), and the rate coefficients for the bimolecular reactions with the tight transition states are computed by using the canonical transition state theory (CTST) along with one-dimensional asymmetric Eckart tunneling correction. For the initiation reactions of distinct SCIs with HCOOH, there are four possible pathways, namely (1) 1,4 O-H insertion (Entry 1), (2) 1,2 O-H insertion (Entry 2), (3) C-H insertion (Entry 3), and (4) C=O cycloaddition (Entry 4), in which Entry 1 is barrierless and Entry 2-4 have the tight transition states. The total rate coefficient for the reaction of SCIs with HCOOH is equal to the sum of the rate coefficient of each pathway. For the barrierless 1,4 O-H insertion reaction, the VTST is approximated with a Morse potential function,  $V(R) = D_e\{1 - \exp[-\beta(R - R_e)]\}^2$ , along with an anisotropy potential function to stand for the minimum energy path, which is used to calculate the rate coefficients (Raghunath et al., 2017). Here,  $D_e$  is the bond energy excluding the zero-point energy,  $R$  is the reaction coordinate, and  $R_e$  is the equilibrium value of  $R$ . It is assumed that the stretching potential in an anisotropy potential is used in conjunction with a potential form of  $V_{\text{anisotropy}} = V_0[1 - \cos^2(\theta_1 - \theta_{1e}) \times \cos^2(\theta_2 - \theta_{2e})]$  (Raghunath et al., 2017). Here,  $V_0$  is the stretching potential, which stands for by a Morse potential,  $\theta_1$  and  $\theta_{1e}$  represent the rotational angle between fragment 1 and the reference axis and the equilibrium bond angle of fragment 1,  $\theta_2$  and  $\theta_{2e}$  stand for the rotational angle between fragment 2 and the reference axis and the equilibrium bond angle of

fragment 2. The association curve for the reaction of 1,4 O-H insertion of SCIs into HCOOH is computed at the M06-2X/6-311+G(2df,2p) level of theory to cover a range from 0.97 to 1.97 Å at step size 0.1 Å for O-H bond and from 1.44 to 2.44 Å at step size 0.1 Å for C-O bond, while other structural parameters are fully optimized. The computed potential energies are fitted to the Morse potential function. However, the calculated rate coefficients for the reactions of SCIs with HCOOH are higher than the prior experimental measurements. The reason is ascribed to the fact that the approximation of VTST using a Morse potential function in conjunction with an anisotropy potential function is unsuitable to predict the rate coefficients for the barrierless 1,4 O-H insertion reaction.

In the revised manuscript, the rate coefficients for the barrierless reactions are computed by employing the inverse Laplace transformation (ILT) method, and the rate coefficients for the bimolecular reactions with the tight transition states are calculated by utilizing CTST in conjunction with Eckart tunneling correction. The ILT and CTST/Eckart calculations are performed by using the MESMER 6.0 and KiSTheIP 2019 programs, respectively (Glowacki et al., 2012; Canneaux et al., 2013). In the ILT treatment, the rotational constants, vibrational frequencies, molecular weights, energies and other input parameters are obtained from the M06-2X/6-311+G(2df,2p) or M06-2X/ma-TZVP methods. For the barrierless reaction of 1,4 O-H insertion of SCIs into HCOOH, SCIs and HCOOH are assigned as the deficient and excess reactants, respectively. The concentration of HCOOH is given a value of  $5.0 \times 10^{10}$  molecules  $\text{cm}^{-3}$  in the simulation, which is taken from the typical concentration of HCOOH in the tropical forest environments (Vereecken et al., 2012).  $\text{N}_2$  is applied as the buffer gas. A single exponential down model is employed to simulate the collision transfer ( $\langle \Delta E \rangle_{\text{down}} = 200 \text{ cm}^{-1}$ ). The collisional Lennard-Jones parameters are estimated with the empirical formula described by Gilbert and Smith (1990).

The rate coefficients of each elementary pathway included in the initiation reactions of distinct SCIs with HCOOH are calculated in the temperature range of 273-400 K, as listed in Table S3-S6. As shown in Table S3, the total rate coefficients  $k_{\text{tot-CH}_2\text{OO}}$  of  $\text{CH}_2\text{OO}$  reaction with HCOOH are in excess of  $1.0 \times 10^{-10} \text{ cm}^3 \text{ molecule}^{-1} \text{ s}^{-1}$ , and they exhibit a slightly negative temperature dependence in the temperature range studied.  $k_{\text{tot-CH}_2\text{OO}}$  is estimated to be  $1.4 \times 10^{-10} \text{ cm}^3 \text{ molecule}^{-1} \text{ s}^{-1}$  at 298 K, which is in good agreement with the experimental values reported by Welz et al. (2014) ( $[1.1 \pm 0.1] \times 10^{-10}$ ), Chung et al. (2019) ( $[1.4 \pm 0.3] \times 10^{-10}$ ), and Peltola et al. (2020) ( $[1.0 \pm 0.03] \times 10^{-10}$ ).  $k(\text{TS}_{\text{ent1}})$  is approximately equal to  $k_{\text{tot-CH}_2\text{OO}}$  in the whole temperature range, and it decreases in the



range of  $1.7 \times 10^{-10}$  (273 K) to  $1.2 \times 10^{-10}$  (400 K)  $\text{cm}^3 \text{ molecule}^{-1} \text{ s}^{-1}$  with increasing temperature.  $k(\text{TS}_{\text{ent1}})$  is several orders of magnitude greater than  $k(\text{TS}_{\text{ent2}})$ ,  $k(\text{TS}_{\text{ent3}})$  and  $k(\text{TS}_{\text{ent4}})$  over the temperature range from 273 to 400 K. The result again shows that the barrierless 1,4 O-H insertion reaction is predominant. Similar conclusion is also obtained from the results of the rate coefficients for the reactions of HCOOH with *anti*-CH<sub>3</sub>CHOO, *syn*-CH<sub>3</sub>CHOO and (CH<sub>3</sub>)<sub>2</sub>COO (Table S4-S6). At ambient temperature, the total rate coefficients of HCOOH reactions with *anti*-CH<sub>3</sub>CHOO, *syn*-CH<sub>3</sub>CHOO and (CH<sub>3</sub>)<sub>2</sub>COO are estimated to be 5.9, 2.7 and  $4.8 \times 10^{-10} \text{ cm}^3 \text{ molecule}^{-1} \text{ s}^{-1}$ , respectively, which are consistent with the prior experimental measurements of  $5 \pm 3$ ,  $2.5 \pm 0.3$  and  $4.5 \times 10^{-10} \text{ cm}^3 \text{ molecule}^{-1} \text{ s}^{-1}$  (Welz et al., 2014; Chung et al., 2019; Sipilä et al., 2014).

**Table S3** Rate coefficients ( $\text{cm}^3 \text{ molecule}^{-1} \text{ s}^{-1}$ ) of each elementary pathway involved in the initiation reaction of CH<sub>2</sub>OO with HCOOH computed at different temperatures

T/K	$k(\text{TS}_{\text{ent1}})$	$k(\text{TS}_{\text{ent2}})$	$k(\text{TS}_{\text{ent3}})$	$k(\text{TS}_{\text{ent4}})$	$k_{\text{tot-CH2OO}}$
273	$1.7 \times 10^{-10}$	$3.6 \times 10^{-12}$	$1.0 \times 10^{-22}$	$3.6 \times 10^{-12}$	$1.8 \times 10^{-10}$
280	$1.6 \times 10^{-10}$	$2.9 \times 10^{-12}$	$1.2 \times 10^{-22}$	$3.1 \times 10^{-12}$	$1.7 \times 10^{-10}$
298	$1.4 \times 10^{-10}$	$1.9 \times 10^{-12}$	$2.2 \times 10^{-22}$	$2.3 \times 10^{-12}$	$1.4 \times 10^{-10}$
300	$1.4 \times 10^{-10}$	$1.8 \times 10^{-12}$	$2.4 \times 10^{-22}$	$2.2 \times 10^{-12}$	$1.4 \times 10^{-10}$
320	$1.3 \times 10^{-10}$	$1.2 \times 10^{-12}$	$4.9 \times 10^{-22}$	$1.6 \times 10^{-12}$	$1.3 \times 10^{-10}$
340	$1.3 \times 10^{-10}$	$8.2 \times 10^{-13}$	$1.0 \times 10^{-21}$	$1.3 \times 10^{-12}$	$1.3 \times 10^{-10}$
360	$1.2 \times 10^{-10}$	$5.9 \times 10^{-13}$	$2.2 \times 10^{-21}$	$1.0 \times 10^{-12}$	$1.2 \times 10^{-10}$
380	$1.2 \times 10^{-10}$	$4.5 \times 10^{-13}$	$4.5 \times 10^{-21}$	$8.2 \times 10^{-13}$	$1.2 \times 10^{-10}$
400	$1.2 \times 10^{-10}$	$3.5 \times 10^{-13}$	$9.0 \times 10^{-21}$	$6.9 \times 10^{-13}$	$1.2 \times 10^{-10}$

**Table S4** Rate coefficients ( $\text{cm}^3 \text{ molecule}^{-1} \text{ s}^{-1}$ ) of each elementary pathway involved in the initiation reaction of *anti*-CH<sub>3</sub>CHOO with HCOOH computed at different temperatures

T/K	$k(\text{TS}_{\text{ent1-anti}})$	$k(\text{TS}_{\text{ent2-anti}})$	$k(\text{TS}_{\text{ent3-anti}})$	$k(\text{TS}_{\text{ent4-anti}})$	$k_{\text{tot-anti}}$
273	$5.9 \times 10^{-10}$	$4.2 \times 10^{-11}$	$5.5 \times 10^{-22}$	$6.1 \times 10^{-11}$	$6.9 \times 10^{-10}$
280	$5.7 \times 10^{-10}$	$3.8 \times 10^{-11}$	$6.7 \times 10^{-22}$	$4.9 \times 10^{-11}$	$6.6 \times 10^{-10}$
298	$5.4 \times 10^{-10}$	$2.3 \times 10^{-11}$	$1.2 \times 10^{-21}$	$3.0 \times 10^{-11}$	$5.9 \times 10^{-10}$
300	$5.3 \times 10^{-10}$	$2.0 \times 10^{-11}$	$1.3 \times 10^{-21}$	$2.8 \times 10^{-11}$	$5.8 \times 10^{-10}$
320	$5.0 \times 10^{-10}$	$1.5 \times 10^{-11}$	$2.6 \times 10^{-21}$	$1.7 \times 10^{-11}$	$5.3 \times 10^{-10}$
340	$4.7 \times 10^{-10}$	$9.4 \times 10^{-12}$	$5.4 \times 10^{-21}$	$1.1 \times 10^{-11}$	$4.9 \times 10^{-10}$

360	$4.5 \times 10^{-10}$	$7.0 \times 10^{-12}$	$1.1 \times 10^{-20}$	$7.8 \times 10^{-12}$	$4.7 \times 10^{-10}$
380	$4.4 \times 10^{-10}$	$3.6 \times 10^{-12}$	$2.1 \times 10^{-20}$	$5.6 \times 10^{-12}$	$4.5 \times 10^{-10}$
400	$4.3 \times 10^{-10}$	$2.0 \times 10^{-12}$	$4.0 \times 10^{-20}$	$4.2 \times 10^{-12}$	$4.4 \times 10^{-10}$

**Table S5** Rate coefficients ( $\text{cm}^3 \text{ molecule}^{-1} \text{ s}^{-1}$ ) of each elementary pathway involved in the initiation reaction of *syn*-CH<sub>3</sub>CHOO with HCOOH computed at different temperatures

T/K	$k(\text{TS}_{\text{ent1-}syn})$	$k(\text{TS}_{\text{ent2-}syn})$	$k(\text{TS}_{\text{ent3-}syn})$	$k(\text{TS}_{\text{ent4-}syn})$	$k_{\text{tot-}syn}$
273	$3.1 \times 10^{-10}$	$9.5 \times 10^{-13}$	$4.6 \times 10^{-27}$	$7.5 \times 10^{-16}$	$3.1 \times 10^{-10}$
280	$2.8 \times 10^{-10}$	$8.0 \times 10^{-13}$	$7.1 \times 10^{-27}$	$6.4 \times 10^{-16}$	$2.8 \times 10^{-10}$
298	$2.7 \times 10^{-10}$	$5.4 \times 10^{-13}$	$8.9 \times 10^{-26}$	$5.5 \times 10^{-16}$	$2.7 \times 10^{-10}$
300	$2.7 \times 10^{-10}$	$5.2 \times 10^{-13}$	$9.9 \times 10^{-26}$	$4.6 \times 10^{-16}$	$2.7 \times 10^{-10}$
320	$2.5 \times 10^{-10}$	$3.6 \times 10^{-13}$	$3.0 \times 10^{-25}$	$3.8 \times 10^{-16}$	$2.5 \times 10^{-10}$
340	$2.5 \times 10^{-10}$	$2.6 \times 10^{-13}$	$9.1 \times 10^{-25}$	$3.1 \times 10^{-16}$	$2.5 \times 10^{-10}$
360	$2.3 \times 10^{-10}$	$2.0 \times 10^{-13}$	$2.6 \times 10^{-24}$	$3.0 \times 10^{-16}$	$2.3 \times 10^{-10}$
380	$2.2 \times 10^{-10}$	$1.5 \times 10^{-13}$	$7.2 \times 10^{-24}$	$2.4 \times 10^{-16}$	$2.2 \times 10^{-10}$
400	$2.2 \times 10^{-10}$	$1.2 \times 10^{-13}$	$1.8 \times 10^{-23}$	$2.2 \times 10^{-16}$	$2.2 \times 10^{-10}$

**Table S6** Rate coefficients ( $\text{cm}^3 \text{ molecule}^{-1} \text{ s}^{-1}$ ) of each elementary pathway involved in the initiation reaction of (CH<sub>3</sub>)<sub>2</sub>OO with HCOOH computed at different temperatures

T/K	$k(\text{TS}_{\text{ent1-}dim})$	$k(\text{TS}_{\text{ent2-}dim})$	$k(\text{TS}_{\text{ent3-}dim})$	$k(\text{TS}_{\text{ent4-}dim})$	$k_{\text{tot-}dim}$
273	$5.3 \times 10^{-10}$	$6.8 \times 10^{-12}$	$1.4 \times 10^{-26}$	$4.4 \times 10^{-15}$	$5.4 \times 10^{-10}$
280	$5.1 \times 10^{-10}$	$5.2 \times 10^{-12}$	$2.2 \times 10^{-26}$	$4.2 \times 10^{-15}$	$5.2 \times 10^{-10}$
298	$4.8 \times 10^{-10}$	$2.8 \times 10^{-12}$	$8.0 \times 10^{-26}$	$4.0 \times 10^{-15}$	$4.8 \times 10^{-10}$
300	$4.7 \times 10^{-10}$	$2.6 \times 10^{-12}$	$9.2 \times 10^{-26}$	$3.9 \times 10^{-15}$	$4.7 \times 10^{-10}$
320	$4.5 \times 10^{-10}$	$1.4 \times 10^{-12}$	$3.6 \times 10^{-25}$	$3.7 \times 10^{-15}$	$4.5 \times 10^{-10}$
340	$4.2 \times 10^{-10}$	$8.6 \times 10^{-13}$	$1.3 \times 10^{-24}$	$3.6 \times 10^{-15}$	$4.2 \times 10^{-10}$
360	$3.9 \times 10^{-10}$	$5.5 \times 10^{-13}$	$4.5 \times 10^{-24}$	$3.5 \times 10^{-15}$	$3.9 \times 10^{-10}$
380	$3.7 \times 10^{-10}$	$3.7 \times 10^{-13}$	$1.4 \times 10^{-23}$	$3.4 \times 10^{-15}$	$3.7 \times 10^{-10}$
400	$3.7 \times 10^{-10}$	$2.6 \times 10^{-13}$	$3.9 \times 10^{-23}$	$3.4 \times 10^{-15}$	$3.7 \times 10^{-10}$

Corresponding descriptions have been added in the page 7 line 173-190, page 11 line 303-315, page 12 line 330-338 and page 13 line 346-351 of the revised manuscript:

The rate coefficients for the barrierless reactions are determined by employing the inverse Laplace transformation (ILT) method. The ILT calculations are performed with the MESMER 6.0 program (Glowacki et al., 2012). In the ILT treatment, the rotational constants, vibrational frequencies, molecular weights, energies and other input parameters are obtained from the M06-2X/6-311+G(2df,2p) or M06-2X/ma-TZVP methods. For the barrierless reaction of 1,4 O-H insertion of SCIs into HCOOH, SCIs and HCOOH are assigned as the deficient and excess reactants, respectively. The concentration of HCOOH is given a value of  $5.0 \times 10^{10}$  molecules  $\text{cm}^{-3}$  in the simulation, which is taken from the typical concentration of HCOOH in the tropical forest environments (Vereecken et al., 2012).  $\text{N}_2$  is applied as the buffer gas. A single exponential down model is employed to simulate the collision transfer ( $\langle \Delta E \rangle_{\text{down}} = 200 \text{ cm}^{-1}$ ). The collisional Lennard-Jones parameters are estimated with the empirical formula described by Gilbert and Smith (1990).

The rate coefficients for the bimolecular reactions with the tight transition states are calculated by using the canonical transition state theory (CTST) along with one-dimensional asymmetric Eckart tunneling correction (Truhlar et al., 1996; Eckart, 1930). The CTST/Eckart calculations are performed with the KiSThelP 2019 program (Canneaux et al., 2013).

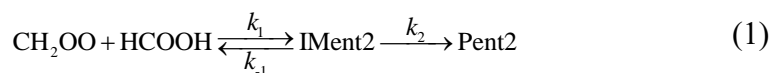
The rate coefficients of each elementary pathway included in the initiation reactions of distinct SCIs with HCOOH are calculated in the temperature range of 273-400 K, as listed in Table S3-S6. As shown in Table S3, the total rate coefficients  $k_{\text{tot-CH}_2\text{OO}}$  of  $\text{CH}_2\text{OO}$  reaction with HCOOH are in excess of  $1.0 \times 10^{-10} \text{ cm}^3 \text{ molecule}^{-1} \text{ s}^{-1}$ , and they exhibit a slightly negative temperature dependence in the temperature range studied.  $k_{\text{tot-CH}_2\text{OO}}$  is estimated to be  $1.4 \times 10^{-10} \text{ cm}^3 \text{ molecule}^{-1} \text{ s}^{-1}$  at 298 K, which is in good agreement with the experimental values reported by Welz et al. (2014) ( $[1.1 \pm 0.1] \times 10^{-10}$ ), Chung et al. (2019) ( $[1.4 \pm 0.3] \times 10^{-10}$ ), and Peltola et al. (2020) ( $[1.0 \pm 0.03] \times 10^{-10}$ ).  $k(\text{TS}_{\text{ent}1})$  is approximately equal to  $k_{\text{tot-CH}_2\text{OO}}$  in the whole temperature range, and it decreases in the range of  $1.7 \times 10^{-10}$  (273 K) to  $1.2 \times 10^{-10}$  (400 K)  $\text{cm}^3 \text{ molecule}^{-1} \text{ s}^{-1}$  with increasing temperature.  $k(\text{TS}_{\text{ent}1})$  is several orders of magnitude greater than  $k(\text{TS}_{\text{ent}2})$ ,  $k(\text{TS}_{\text{ent}3})$  and  $k(\text{TS}_{\text{ent}4})$  over the temperature range from 273 to 400 K. The result again shows that the barrierless 1,4 O-H insertion reaction is predominant.

Equivalent to the case of  $\text{CH}_2\text{OO}$  reaction with HCOOH, the rate coefficient of each elementary pathway involved in the anti- $\text{CH}_3\text{CHOO} + \text{HCOOH}$  reaction also decreases with the

temperature increasing (Table S4). This table shows that Entry 1 is kinetically favored over Entry 2, 3 and 4, and Entry 2 is competitive with Entry 4 in the range 273-400 K. Similar conclusion is also obtained from the results of the rate coefficients for the reactions of *syn*-CH<sub>3</sub>CHOO and (CH<sub>3</sub>)<sub>2</sub>COO with HCOOH that Entry 1 is the dominant pathway (Table S5-S6). It deserves mentioning that the competition of Entry 2 is significantly greater than that of Entry 4 in the *syn*-CH<sub>3</sub>CHOO + HCOOH and (CH<sub>3</sub>)<sub>2</sub>COO + HCOOH systems. At ambient temperature, the total rate coefficients of HCOOH reactions with *anti*-CH<sub>3</sub>CHOO, *syn*-CH<sub>3</sub>CHOO and (CH<sub>3</sub>)<sub>2</sub>COO are estimated to be 5.9, 2.7 and 4.8 × 10<sup>-10</sup> cm<sup>3</sup> molecule<sup>-1</sup> s<sup>-1</sup>, respectively, which are consistent with the prior experimental measurements of 5 ± 3, 2.5 ± 0.3 and 4.5 × 10<sup>-10</sup> cm<sup>3</sup> molecule<sup>-1</sup> s<sup>-1</sup> (Welz et al., 2014; Chung et al., 2019; Sipilä et al., 2014).

3. Why are  $k(\text{TS}_{\text{ent}2})$  and  $k(\text{TS}_{\text{ent}4})$  decrease with increasing temperature as they both have positive energy barrier? (Table S3)

**Response:** Based on the Reviewer's suggestion, the relevance descriptions on the negative temperature dependence of  $k(\text{TS}_{\text{ent}2})$  and  $k(\text{TS}_{\text{ent}4})$  in Table S3 have been added in the revised manuscript. The rate coefficients for the bimolecular reactions with the tight transition states are calculated by using the canonical transition state theory (CTST) along with one-dimensional asymmetric Eckart tunneling correction. The initiation reaction of CH<sub>2</sub>OO with HCOOH proceeds through four possible pathways, namely (1) 1,4 O-H insertion (Entry 1), (2) 1,2 O-H insertion (Entry 2), (3) C-H insertion (Entry 3), and (4) C=O cycloaddition (Entry 4). A schematic PES for the possible entrance pathways is drawn in Fig. 1. As shown in Fig. 1, the entrance pathway Entry2 consists of two elementary steps: (i) an intermediate IMent2 is formed via a barrierless process; (ii) then, it rearranges to the product Pent2 through a tight transition state TSent2. The whole reaction process can be described as Eq. (1):



Assuming the rapid equilibrium is established between the IMent2 and reactants. According to the steady-state approximation (SSA), the total rate coefficient is approximately expressed as Eq. (2):

$$k_{\text{tot}} = \frac{k_1}{k_{-1} + k_2} k_2 \approx \frac{k_1}{k_{-1}} k_2 = K_{\text{eq}} k_2 \quad (2)$$

The equilibrium constant  $K_{\text{eq}}$  is written as Eq. (3):

$$K_{\text{eq}} = \sigma \frac{Q_{\text{IM}}(T)}{Q_{\text{R1}}(T)Q_{\text{R2}}(T)} \exp\left(\frac{G_{\text{R}} - G_{\text{IM}}}{RT}\right) \quad (3)$$

where  $\sigma$  refers to the reaction symmetry number,  $Q_{\text{IM}}(T)$ ,  $Q_{\text{R1}}(T)$  and  $Q_{\text{R2}}(T)$  denote the partition functions of intermediate, reactants R1 and R2, which are equal to the multiplication of translational, rotational, vibrational and electronic partition functions ( $Q = Q_{\text{rot}}Q_{\text{vib}}Q_{\text{trans}}Q_{\text{elec}}$ ).  $T$  is the temperature in Kelvin,  $R$  is the ideal gas constant,  $G_{\text{R}}$  and  $G_{\text{IM}}$  are the total Gibbs free energies of reactant and intermediate, respectively. Similar methodology is adopted to calculate the rate coefficient of each elementary pathway in Entry 4.

The calculated  $K_{\text{eq-ent2}}$ ,  $k_{2\text{-ent2}}$ , and  $k(\text{TS}_{\text{ent2}})$  ( $k(\text{TS}_{\text{ent2}}) = K_{\text{eq-ent2}} \times k_{2\text{-ent2}}$ ) in Entry 2 are listed in Table S7. This table shows that  $K_{\text{eq-ent2}}$  significantly decreases with increasing temperature, and  $k_{2\text{-ent2}}$  increases as the temperature is increased. However, the decreased value in  $K_{\text{eq-ent2}}$  is greater than the increased value in  $k_{2\text{-ent2}}$  under the same temperature range. For example,  $K_{\text{eq-ent2}}$  decreases by a factor of 6.3 and  $k_{2\text{-ent2}}$  increases by a factor of 2.9 at 298 K compared with the values of  $K_{\text{eq-ent2}}$  and  $k_{2\text{-ent2}}$  at 273 K. It is therefore that  $k(\text{TS}_{\text{ent2}})$  decreases with the temperature increasing. Similar conclusion is also obtained from the results of the rate coefficients in Entry 4 that  $k(\text{TS}_{\text{ent4}})$  exhibits a negative temperature dependence in the temperature range studied (Table S8). The aforementioned results imply that  $k(\text{TS}_{\text{ent2}})$  and  $k(\text{TS}_{\text{ent4}})$  are mediated by the pre-reactive complexes IMent2 and IMent4 in the Entry 2 and 4 of the  $\text{CH}_2\text{OO} + \text{HCOOH}$  reaction.

**Table S7**  $K_{\text{eq-ent2}}$  ( $\text{cm}^3 \text{ molecule}^{-1}$ ),  $k_{2\text{-ent2}}$  ( $\text{s}^{-1}$ ) and  $k(\text{TS}_{\text{ent2}})$  ( $\text{cm}^3 \text{ molecule}^{-1} \text{ s}^{-1}$ ) in Entry 2 computed at different temperatures

T/K	$K_{\text{eq-ent2}}$	$k_{2\text{-ent2}}$	$k(\text{TS}_{\text{ent2}})$
273	$8.2 \times 10^{-17}$	$4.4 \times 10^4$	$3.6 \times 10^{-12}$
280	$4.7 \times 10^{-17}$	$6.3 \times 10^4$	$2.9 \times 10^{-12}$
298	$1.3 \times 10^{-17}$	$1.5 \times 10^5$	$1.9 \times 10^{-12}$
300	$1.1 \times 10^{-17}$	$1.6 \times 10^5$	$1.8 \times 10^{-12}$
320	$3.2 \times 10^{-18}$	$3.7 \times 10^5$	$1.2 \times 10^{-12}$
340	$1.1 \times 10^{-18}$	$7.6 \times 10^5$	$8.2 \times 10^{-13}$

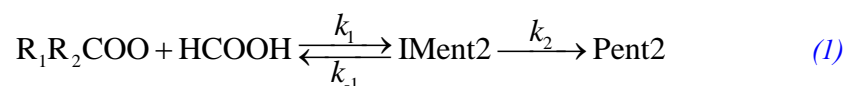
360	$4.1 \times 10^{-19}$	$1.5 \times 10^6$	$5.9 \times 10^{-13}$
380	$1.7 \times 10^{-19}$	$2.6 \times 10^6$	$4.5 \times 10^{-13}$
400	$8.0 \times 10^{-20}$	$4.4 \times 10^6$	$3.5 \times 10^{-13}$

**Table S8**  $K_{\text{eq-ent4}}$  ( $\text{cm}^3 \text{ molecule}^{-1}$ ),  $k_{2\text{-ent4}}$  ( $\text{s}^{-1}$ ) and  $k(\text{TS}_{\text{ent4}})$  ( $\text{cm}^3 \text{ molecule}^{-1} \text{ s}^{-1}$ ) in Entry 4 computed at different temperatures

T/K	$K_{\text{eq-ent4}}$	$k_{2\text{-ent4}}$	$k(\text{TS}_{\text{ent4}})$
273	$6.3 \times 10^{-20}$	$5.7 \times 10^7$	$3.6 \times 10^{-12}$
280	$4.5 \times 10^{-20}$	$7.0 \times 10^7$	$3.1 \times 10^{-12}$
298	$2.0 \times 10^{-20}$	$1.1 \times 10^8$	$2.3 \times 10^{-12}$
300	$1.8 \times 10^{-20}$	$1.2 \times 10^8$	$2.2 \times 10^{-12}$
320	$8.4 \times 10^{-21}$	$1.9 \times 10^8$	$1.6 \times 10^{-12}$
340	$4.3 \times 10^{-21}$	$2.9 \times 10^8$	$1.3 \times 10^{-12}$
360	$2.4 \times 10^{-21}$	$4.2 \times 10^8$	$1.0 \times 10^{-12}$
380	$1.4 \times 10^{-21}$	$5.9 \times 10^8$	$8.2 \times 10^{-13}$
400	$8.8 \times 10^{-22}$	$7.9 \times 10^8$	$6.9 \times 10^{-13}$

Corresponding descriptions have been added in the page 7 line 186-206 and page 12 line 315-326 of the revised manuscript:

*The rate coefficients for the bimolecular reactions with the tight transition states are calculated by using the canonical transition state theory (CTST) along with one-dimensional asymmetric Eckart tunneling correction (Truhlar et al., 1996; Eckart, 1930). The CTST/Eckart calculations are performed with the KiSThelP 2019 program (Canneaux et al., 2013). As shown in Fig. 1, the entrance pathway Entry2 of  $R_1R_2\text{COO}$  reaction with  $\text{HCOOH}$  consists of two steps: (i) an intermediate  $\text{IMent2}$  is formed via a barrierless process; (ii) then, it rearranges to the product  $\text{Pent2}$  through a tight transition state  $\text{TSent2}$ . The whole reaction process can be described as Eq. (1):*



*Assuming the rapid equilibrium is established between the  $\text{IMent2}$  and reactants. According to the steady-state approximation (SSA), the total rate coefficient is approximately expressed as Eq. (2) (Zhang et al., 2012):*

$$k_{\text{tot}} = \frac{k_1}{k_{-1} + k_2} k_2 \approx \frac{k_1}{k_{-1}} k_2 = K_{\text{eq}} k_2 \quad (2)$$

The equilibrium constant  $K_{\text{eq}}$  is written as Eq. (3):

$$K_{\text{eq}} = \sigma \frac{Q_{\text{IM}}(T)}{Q_{\text{R1}}(T)Q_{\text{R2}}(T)} \exp\left(\frac{G_{\text{R}} - G_{\text{IM}}}{RT}\right) \quad (3)$$

where  $\sigma$  refers to reaction symmetry number,  $Q_{\text{IM}}(T)$ ,  $Q_{\text{R1}}(T)$  and  $Q_{\text{R2}}(T)$  denote the partition functions of intermediate, reactants R1 and R2, which are equal to the multiplication of translational, rotational, vibrational and electronic partition functions ( $Q = Q_{\text{rot}}Q_{\text{vib}}Q_{\text{trans}}Q_{\text{elec}}$ ) (Mendes et al., 2014),  $T$  is the temperature in Kelvin,  $R$  is the ideal gas constant,  $G_{\text{R}}$  and  $G_{\text{IM}}$  are the total Gibbs free energies of reactant and intermediate, respectively.

The calculated  $K_{\text{eq-ent2}}$ ,  $k_{2\text{-ent2}}$ , and  $k(\text{TS}_{\text{ent2}})$  ( $k(\text{TS}_{\text{ent2}}) = K_{\text{eq-ent2}} \times k_{2\text{-ent2}}$ ) in Entry 2 are listed in Table S7. This table shows that  $K_{\text{eq-ent2}}$  significantly decreases with increasing temperature, and  $k_{2\text{-ent2}}$  increases as the temperature is increased. However, the decreased value in  $K_{\text{eq-ent2}}$  is greater than the increased value in  $k_{2\text{-ent2}}$  under the same temperature range. For example,  $K_{\text{eq-ent2}}$  decreases by a factor of 6.3 and  $k_{2\text{-ent2}}$  increases by a factor of 2.9 at 298 K compared with the values of  $K_{\text{eq-ent2}}$  and  $k_{2\text{-ent2}}$  at 273 K. It is therefore that  $k(\text{TS}_{\text{ent2}})$  decreases with the temperature increasing. Similar conclusion is also obtained from the results of the rate coefficients in Entry 4 that  $k(\text{TS}_{\text{ent4}})$  exhibits a negative temperature dependence in the temperature range studied (Table S8). The aforementioned results imply that  $k(\text{TS}_{\text{ent2}})$  and  $k(\text{TS}_{\text{ent4}})$  are mediated by the pre-reactive complexes  $\text{IMent2}$  and  $\text{IMent4}$  in the Entry 2 and 4.

4. The oligomerization reactions are highly dependent on the concentration of the monomers. Here the monomer are highly reactive SCIs and usually has very low concentration in the atmosphere. It seems that the high exothermicity of the oligomerization reaction results from the “stabilization” of SCIs in oligomerization. Also, the calculated free energies represent standard condition. Could the authors correct the Gibbs free energies by incorporating the atmospheric concentrations of SCIs (i.e.,  $RT\ln(P/\text{Pref})$ ) to check whether this oligomerization is favored in the atmospheric conditions?

**Response:** Based on the Reviewer’s suggestion, the relative importance of distinct SCIs reactions with hydroperoxide esters and trace species (e.g.,  $\text{H}_2\text{O}$ ,  $\text{HCOOH}$  and  $\text{SO}_2$ ) has been added in the revised manuscript. It is well known that the reactions with trace species are expected to be

the dominant chemical sinks for SCIs in the atmosphere (Taatjes et al., 2013; Long et al., 2016). In the present study, the hydroperoxymethyl formate (HPMF) is selected as the model compound since it is the simplest hydroperoxide ester formed from the barrierless reaction of 1,4 O-H insertion of CH<sub>2</sub>OO into HCOOH. The reported concentrations of coreactant, the rate coefficients  $k$ , and the effective pseudo-first-order rate constants ( $k_{\text{eff}} = k[\text{coreactant}]$ ) for distinct SCI reactions with H<sub>2</sub>O, HCOOH, SO<sub>2</sub>, and HPMF are summarized in Table 2. As seen in Table 2, the rate coefficient of a particular SCI reaction with trace species is strongly dependent on its structure. The methyl group substitution may alter the rate coefficient by several to tens of times. The atmospheric concentrations of H<sub>2</sub>O, HCOOH and SO<sub>2</sub> in the tropical forest environments are measured to be  $3.9\text{--}6.1 \times 10^{17}$ ,  $5.0\text{--}10 \times 10^{10}$ , and  $1.7\text{--}9.0 \times 10^{10}$  molecules cm<sup>-3</sup>, respectively (Vereecken et al., 2012). For the reactions of CH<sub>2</sub>OO with H<sub>2</sub>O, HCOOH, and SO<sub>2</sub>, the experimental rate coefficients are determined to be  $< 1.5 \times 10^{-15}$ ,  $[1.1 \pm 0.1] \times 10^{-10}$ , and  $[3.9 \pm 0.7] \times 10^{-11}$  cm<sup>3</sup> molecule<sup>-1</sup> s<sup>-1</sup>, respectively (Welz et al, 2012 and 2014; Chao et al., 2015), which translate into  $k_{\text{eff}(\text{CH}_2\text{OO}+\text{H}_2\text{O})}$ ,  $k_{\text{eff}(\text{CH}_2\text{OO}+\text{HCOOH})}$  and  $k_{\text{eff}(\text{CH}_2\text{OO}+\text{SO}_2)}$  of  $5.9\text{--}9.2 \times 10^2$ ,  $5.5\text{--}11$ , and  $0.7\text{--}3.5$  s<sup>-1</sup>, respectively. The result reveals that the reaction of CH<sub>2</sub>OO with H<sub>2</sub>O is the most important bimolecular reaction.  $k_{\text{eff}(\text{CH}_2\text{OO}+\text{HCOOH})}$  is greater by a factor of 3-8 than  $k_{\text{eff}(\text{CH}_2\text{OO}+\text{SO}_2)}$ , indicating that the reaction of CH<sub>2</sub>OO with HCOOH is favored over reaction with SO<sub>2</sub>. Similar conclusion is also obtained from the results of  $k_{\text{eff}}$  for the reactions of *anti*-CH<sub>3</sub>CHOO, *syn*-CH<sub>3</sub>CHOO and (CH<sub>3</sub>)<sub>2</sub>COO with H<sub>2</sub>O, HCOOH and SO<sub>2</sub> that SCIs reactions with H<sub>2</sub>O are faster than with HCOOH, which, in turn, are faster than with SO<sub>2</sub>.

According to the results shown in the Table 2, the room temperature rate coefficient for the reaction of CH<sub>2</sub>OO with HPMF is calculated to be  $2.7 \times 10^{-11}$  cm<sup>3</sup> molecule<sup>-1</sup> s<sup>-1</sup>. However, to the best of our knowledge, the atmospheric concentration of HPMF has not been reported up to now. If we assume that the concentration of HPMF is the same as that of HCOOH,  $k_{\text{eff}(\text{CH}_2\text{OO}+\text{HPMF})}$  is estimated to be  $1.4\text{--}2.7$  s<sup>-1</sup>, which is significantly lower than  $k_{\text{eff}(\text{CH}_2\text{OO}+\text{H}_2\text{O})}$  and  $k_{\text{eff}(\text{CH}_2\text{OO}+\text{HCOOH})}$ .  $k_{\text{eff}(\text{CH}_2\text{OO}+\text{HPMF})}$  is nearly identical to  $k_{\text{eff}(\text{CH}_2\text{OO}+\text{SO}_2)}$ , indicating that the CH<sub>2</sub>OO + HPMF reaction is competitive with the CH<sub>2</sub>OO + SO<sub>2</sub> system. Previous model-measurement studies have estimated the surface-level SCIs concentrations in the range of  $1.0 \times 10^4$  to  $1.0 \times 10^5$  molecules cm<sup>-3</sup> (Khan et al., 2018; Novelli et al., 2017). If we assume that the concentration of HPMF is equal to that of SCIs,  $k_{\text{eff}(\text{CH}_2\text{OO}+\text{HPMF})}$  is calculated to be  $2.7\text{--}27 \times 10^{-7}$  s<sup>-1</sup>, which is several orders of magnitude lower than



$k_{\text{eff}}(\text{CH}_2\text{OO}+\text{H}_2\text{O})$ ,  $k_{\text{eff}}(\text{CH}_2\text{OO}+\text{HCOOH})$  and  $k_{\text{eff}}(\text{CH}_2\text{OO}+\text{SO}_2)$ . This result indicates that the reaction of  $\text{CH}_2\text{OO}$  with HPMF is of less importance. Similar conclusion is also obtained from the reactions of *anti*- $\text{CH}_3\text{CHOO}$ , *syn*- $\text{CH}_3\text{CHOO}$  and  $(\text{CH}_3)_2\text{COO}$  with HPMF. Based on the above discussions, it can be concluded that the relative importance of carbonyl oxides reactions with hydroperoxide esters is significantly dependent on the concentrations of hydroperoxide esters. These reactions may play a certain role in the formation of organic new particle in some regions where low concentration of water vapour and high concentration of hydroperoxide esters occur.

**Table 2** The reported concentrations of coreactant, the rate coefficients  $k$ , and the effective pseudo-first-order rate constants ( $k_{\text{eff}} = k[\text{coreactant}]$ ) for distinct SCI reactions with HPMF,  $\text{H}_2\text{O}$ ,  $\text{HCOOH}$  and  $\text{SO}_2$  at the tropical forest environments

SCIs	Coreactant	[Coreactant] (molecules $\text{cm}^{-3}$ )	$k$ ( $\text{cm}^3 \text{ molecule}^{-1} \text{ s}^{-1}$ )	$k_{\text{eff}}$ ( $\text{s}^{-1}$ )	Reference
$\text{CH}_2\text{OO}$	$\text{H}_2\text{O}$	$3.9\text{-}6.1 \times 10^{17}$	$< 1.5 \times 10^{-15}$	$5.9\text{-}9.2 \times 10^2$	Chao et al., (2015)
	$\text{HCOOH}$	$5.0\text{-}10.0 \times 10^{10}$	$[1.1 \pm 0.1] \times 10^{-10}$	5.5-11	Welz et al., (2014)
	$\text{SO}_2$	$1.7\text{-}9.0 \times 10^{10}$	$[3.9 \pm 0.7] \times 10^{-11}$	0.7-3.5	Welz et al., (2012)
	HPMF	-	$2.7 \times 10^{-11}$	-	This work
<i>anti</i> - $\text{CH}_3\text{CHOO}$	$\text{H}_2\text{O}$	$3.9\text{-}6.1 \times 10^{17}$	$[1.0 \pm 0.4] \times 10^{-14}$	$3.9\text{-}6.1 \times 10^3$	Taatjes et al., (2013)
	$\text{HCOOH}$	$5.0\text{-}10.0 \times 10^{10}$	$[5 \pm 3] \times 10^{-10}$	25.0-50.0	Welz et al., (2014)
	$\text{SO}_2$	$1.7\text{-}9.0 \times 10^{10}$	$[6.7 \pm 1.0] \times 10^{-11}$	1.1-6.0	Taatjes et al., (2013)
	HPMF	-	$3.3 \times 10^{-10}$	-	This work
<i>syn</i> - $\text{CH}_3\text{CHOO}$	$\text{H}_2\text{O}$	$3.9\text{-}6.1 \times 10^{17}$	$< 4.0 \times 10^{-15}$	$1.6\text{-}2.4 \times 10^3$	Taatjes et al., (2013)
	$\text{HCOOH}$	$5.0\text{-}10.0 \times 10^{10}$	$[2.5 \pm 0.3] \times 10^{-10}$	12.5-25.0	Welz et al., (2014)
	$\text{SO}_2$	$1.7\text{-}9.0 \times 10^{10}$	$[2.4 \pm 0.3] \times 10^{-11}$	0.4-2.2	Taatjes et al., (2013)
	HPMF	-	$1.7 \times 10^{-13}$	-	This work
$(\text{CH}_3)_2\text{COO}$	$\text{H}_2\text{O}$	$3.9\text{-}6.1 \times 10^{17}$	$< 1.5 \times 10^{-16}$	58.5-91.5	Huang et al., (2015)
	$\text{HCOOH}$	$5.0\text{-}10.0 \times 10^{10}$	$4.5 \times 10^{-10}$	22.5-45.0	Sipilä et al., (2014)

SO <sub>2</sub>	1.7-9.0 × 10 <sup>10</sup>	1.3 × 10 <sup>-10</sup>	2.2-11.7	Huang et al., (2015)
HPMF	-	2.2 × 10 <sup>-11</sup>	-	This work

Corresponding descriptions have been added in the page 23 line 573-590 and page 24 line 591-610 of the revised manuscript:

*It is of interest to assess whether the reactions of distinct SCIs with HPMF can compete well with the losses to reactions with trace species (e.g., H<sub>2</sub>O, HCOOH and SO<sub>2</sub>), because it is well known that the reactions with trace species are expected to be the dominant chemical sinks for SCIs in the atmosphere (Taatjes et al., 2013; Long et al., 2016). The reported concentrations of coreactant, the rate coefficients  $k$ , and the effective pseudo-first-order rate constants ( $k_{\text{eff}} = k[\text{coreactant}]$ ) for distinct SCI reactions with H<sub>2</sub>O, HCOOH, SO<sub>2</sub>, and HPMF are summarized in Table 2. As seen in Table 2, the rate coefficient of a particular SCI reaction with trace species is strongly dependent on its structure. The methyl group substitution may alter the rate coefficient by several to tens of times. The atmospheric concentrations of H<sub>2</sub>O, HCOOH and SO<sub>2</sub> in the tropical forest environments are measured to be 3.9-6.1 × 10<sup>17</sup>, 5.0-10 × 10<sup>10</sup>, and 1.7-9.0 × 10<sup>10</sup> molecules cm<sup>-3</sup>, respectively (Vereecken, 2012). For the reactions of CH<sub>2</sub>OO with H<sub>2</sub>O, HCOOH, and SO<sub>2</sub>, the experimental rate coefficients are determined to be < 1.5 × 10<sup>-15</sup>, [1.1 ± 0.1] × 10<sup>-10</sup>, and [3.9 ± 0.7] × 10<sup>-11</sup> cm<sup>3</sup> molecule<sup>-1</sup> s<sup>-1</sup>, respectively (Welz et al., 2012 and 2014; Chao et al., 2015), which translate into  $k_{\text{eff}}(\text{CH}_2\text{OO}+\text{H}_2\text{O})$ ,  $k_{\text{eff}}(\text{CH}_2\text{OO}+\text{HCOOH})$  and  $k_{\text{eff}}(\text{CH}_2\text{OO}+\text{SO}_2)$  of 5.9-9.2 × 10<sup>2</sup>, 5.5-11, and 0.7-3.5 s<sup>-1</sup>, respectively. The result reveals that the reaction of CH<sub>2</sub>OO with H<sub>2</sub>O is the most important bimolecular reaction.  $k_{\text{eff}}(\text{CH}_2\text{OO}+\text{HCOOH})$  is greater by a factor of 3-8 than  $k_{\text{eff}}(\text{CH}_2\text{OO}+\text{SO}_2)$ , indicating that the reaction of CH<sub>2</sub>OO with HCOOH is favored over reaction with SO<sub>2</sub>. Similar conclusion is also obtained from the results of  $k_{\text{eff}}$  for the reactions of anti-CH<sub>3</sub>CHOO, syn-CH<sub>3</sub>CHOO and (CH<sub>3</sub>)<sub>2</sub>COO with H<sub>2</sub>O, HCOOH and SO<sub>2</sub> that SCIs reactions with H<sub>2</sub>O are faster than with HCOOH, which, in turn, are faster than with SO<sub>2</sub>.*

*According to the results shown in the Table 2, the room temperature rate coefficient for the reaction of CH<sub>2</sub>OO with HPMF is calculated to be 2.7 × 10<sup>-11</sup> cm<sup>3</sup> molecule<sup>-1</sup> s<sup>-1</sup>. However, to the best of our knowledge, the atmospheric concentration of HPMF has not been reported up to now. If we assume that the concentration of HPMF is the same as that of HCOOH,  $k_{\text{eff}}(\text{CH}_2\text{OO}+\text{HPMF})$  is*

estimated to be  $1.4\text{-}2.7\text{ s}^{-1}$ , which is significantly lower than  $k_{\text{eff}(\text{CH}_2\text{OO}+\text{H}_2\text{O})}$  and  $k_{\text{eff}(\text{CH}_2\text{OO}+\text{HCOOH})}$ .  $k_{\text{eff}(\text{CH}_2\text{OO}+\text{HPMF})}$  is nearly identical to  $k_{\text{eff}(\text{CH}_2\text{OO}+\text{SO}_2)}$ , indicating that the  $\text{CH}_2\text{OO} + \text{HPMF}$  reaction is competitive with the  $\text{CH}_2\text{OO} + \text{SO}_2$  system. Previous model-measurement studies have estimated the surface-level SCIs concentrations in the range of  $1.0 \times 10^4$  to  $1.0 \times 10^5$  molecules  $\text{cm}^{-3}$  (Khan et al., 2018; Novelli et al., 2017). If we assume that the concentration of HPMF is equal to that of SCIs,  $k_{\text{eff}(\text{CH}_2\text{OO}+\text{HPMF})}$  is calculated to be  $2.7\text{-}27 \times 10^{-7}\text{ s}^{-1}$ , which is several orders of magnitude lower than  $k_{\text{eff}(\text{CH}_2\text{OO}+\text{H}_2\text{O})}$ ,  $k_{\text{eff}(\text{CH}_2\text{OO}+\text{HCOOH})}$  and  $k_{\text{eff}(\text{CH}_2\text{OO}+\text{SO}_2)}$ . This result indicates that the reaction of  $\text{CH}_2\text{OO}$  with HPMF is of less importance. Similar conclusion is also obtained from the reactions of anti- $\text{CH}_3\text{CHOO}$ , syn- $\text{CH}_3\text{CHOO}$  and  $(\text{CH}_3)_2\text{COO}$  with HPMF. Based on the above discussions, it can be concluded that the relative importance of carbonyl oxides reactions with hydroperoxide esters is significantly dependent on the concentrations of hydroperoxide esters. These reactions may play a certain role in the formation of organic new particle in some regions where low concentration of water vapour and high concentration of hydroperoxide esters occur.

5. Additionally, it would be helpful if there is some estimation about how much the oligomerization process could contribute to the regional or global SOA.

**Response:** Sakamoto et al. (2013) investigated the ozonolysis of ethylene in a Teflon bag reactor, and found that  $\text{CH}_2\text{OO}$  plays a critical role in the formations of oligomers and secondary organic aerosol (SOA) in the gas phase and particle phase. They proposed a possible formation mechanism for the oligomeric hydroperoxides, which includes the successive addition of  $\text{CH}_2\text{OO}$  to hydroperoxides. Sadezky et al. (2008) studied the gas-phase ozonolysis of small enol ethers in a 570 l spherical glass reactor at atmospheric conditions in the absence of seed aerosol. They found that the oligomers composed of Criegee intermediate as the repeated chain unit are the main constituents of SOA. Zhao et al. (2015) studied the ozonolysis of trans-3-hexene in both the static Teflon chamber and glass flow reactor under different relative humidity conditions. It was found that the oligomers having Criegee intermediate as the chain unit are the dominant components of SOA. These findings may help in understanding the potential pathway for the formation of SOA in the atmosphere. However, to the best of our knowledge, the contribution of the oligomerization reaction composed of Criegee intermediate as the chain unit to SOA remains unknown. In the future work, we will adopt the combination of quantum chemistry and numerical simulation to estimate

the contribution of oligomerization reaction to the regional and global SOA.

6. Line 39, “with increasing the number of SCIs” is a bit confusing, it would be better to say “with increasing the number of SCIs added to the oligomer”.

**Response:** The sentence “with increasing the number of SCIs” has been replaced by “with increasing the number of SCIs added to the oligomer” in the revised manuscript.

7. Line 491, “netative” should be “negative”.

**Response:** The word “netative” has been replaced by “negative” in the revised manuscript.

8. Line 499, “neartly” should be “nearly”.

**Response:** The word “neartly” has been replaced by “nearly” in the revised manuscript.

## References

- Cabezas, C., and Endo, Y.: The Criegee intermediate-formic acid reaction explored by rotational spectroscopy, *Phys. Chem. Chem. Phys.*, 21, 18059-18064, <https://doi.org/10.1039/c9cp03001h>, 2019.
- Canneaux, S., Bohr, F., and Henon, E.: KiSThelP: a program to predict thermodynamic properties and rate constants from quantum chemistry results, *J. Comput. Chem.*, 35, 82-93, <https://doi.org/10.1002/jcc.23470>, 2013.
- Chao, W., Hsieh, J. T., Chang, C. H., and Lin, J. J. M.: Direct kinetic measurement of the reaction of the simplest Criegee intermediate with water vapor, *Science*, 347, 751-754, <https://doi.org/10.1126/science.1261549>, 2015.
- Chhantyal-Pun, R., McGillen, M. R., Beames, J. M., Khan, M. A. H., Percival, C. J., Shallcross, D. E., and Orr-Ewing, A. J.: Temperature Dependence of the Rates of Reaction of Trifluoroacetic Acid with Criegee Intermediates, *Angew. Chem. Int. Ed.*, 129, 9172-9175, <https://doi.org/10.1002/anie.201703700>, 2017.
- Chung, C. A., Su, J. W., and Lee, Y. P.: Detailed mechanism and kinetics of the reaction of Criegee intermediate CH<sub>2</sub>OO with HCOOH investigated via infrared identification of conformers of hydroperoxymethyl formate and formic acid anhydride, *Phys. Chem. Chem. Phys.*, 21, 21445-21455, <https://doi.org/10.1039/c9cp04168k>, 2019.
- Gilbert, R. G., and Smith, S. C.: *Theory of unimolecular and recombination reactions*; Blackwell Scientific: Carlton, Australia, 1990.
- Glowacki, D. R., Liang, C. H., Morley, C., Pilling, M. J., and Robertson, S. H.: MESMER: an open-source master equation solver for multi-energy well reactions, *J. Phys. Chem. A*, 116, 9545-9560, <https://doi.org/10.1021/jp3051033>, 2012.
- Huang, H. L., Chao, W., and Lin, J. J. M.: Kinetics of a Criegee intermediate that would survive high humidity and may oxidize atmospheric SO<sub>2</sub>, *Proc. Natl. Acad. Sci. U.S.A.*, 112, 10857-10862, <https://doi.org/10.1073/pnas.1513149112>, 2015.
- Khan, M. A. H., Percival, C. J., Caravan, R. L., Taatjes, C. A., and Shallcross, D. E.: Criegee intermediates and their impacts on the troposphere, *Environ. Sci.: Processes Impacts*, 20, 437-453, <https://doi.org/10.1039/C7EM00585G>, 2018.
- Lin, X., Meng, Q., Feng, B., Zhai, Y., Li, Y., Yu, Y., Li, Z., Shan, X., Liu, F., Zhang, L., and Sheng, L.: Theoretical study on Criegee intermediate's role in ozonolysis of acrylic acid, *J. Phys. Chem. A*, 123, 1929-1936, <https://doi.org/10.1021/acs.jpca.8b11671>, 2019.
- Long, B., Bao, J. L., and Truhlar, D. G.: Atmospheric chemistry of Criegee intermediates: unimolecular reactions and reactions with water, *J. Am. Chem. Soc.*, 138, 14409-14422, <https://doi.org/10.1021/jacs.6b08655>, 2016.
- Long, B., Cheng, J. R., Tan, X. F., and Zhang, W. J.: Theoretical study on the detailed reaction mechanisms of carbonyl oxide with formic acid, *J. Mol. Struct.: Theochem*, 916, 159-167, <https://doi.org/10.1016/j.theochem.2009.09.028>, 2009.
- Novelli, A., Hens, K., Ernest, C. T., Martinez, M., Nölscher, A. C., Sinha, V., Paasonen, P., Petäjä, T., Sipilä, M., Elste, T., Plass-Dülmer, C., Phillips, G. J., Kubistin, D., Williams, J., Vereecken, L., Lelieveld, J., and Harder, H.: Estimating the atmospheric concentration of Criegee intermediates and their possible interference in a FAGE-LIF instrument, *Atmos. Chem. Phys.*, 17, 7807-7826, <https://doi.org/10.5194/acp-17-7807-2017>, 2017.
- Peltola, J., Seal, P., Inkilä, A., and Eskola, A.: Time-resolved, broadband UV-absorption

- spectrometry measurements of Criegee intermediate kinetics using a new photolytic precursor: unimolecular decomposition of  $\text{CH}_2\text{OO}$  and its reaction with formic acid, *Phys. Chem. Chem. Phys.*, 22, 11797-11808, <https://doi.org/10.1039/d0cp00302f>, 2020.
- Raghunath, P., Lee, Y. P., and Lin, M. C.: Computational chemical kinetics for the reaction of Criegee intermediate  $\text{CH}_2\text{OO}$  with  $\text{HNO}_3$  and its catalytic conversion to OH and HCO, *J. Phys. Chem. A*, 121, 3871-3878, <https://doi.org/10.1021/acs.jpca.7b02196>, 2017.
- Sadezky, A., Winterhalter, R., Kanawati, B., Rompp, A., Spengler, B., Mellouki, A., Bras, G. L., Chaimbault, P., and Moortgat, G. K.: Oligomer formation during gas-phase ozonolysis of small alkenes and enol ethers: new evidence for the central role of the Criegee Intermediate as oligomer chain unit, *Atmos. Chem. Phys.*, 8, 2667-2699, <https://doi.org/10.5194/acp-8-2667-2008>, 2008.
- Sakamoto, Y., Inomata, S., and Hirokawa, J.: Oligomerization reaction of the Criegee intermediate leads to secondary organic aerosol formation in ethylene ozonolysis, *J. Phys. Chem. A*, 117, 12912-12921, <https://doi.org/10.1021/jp408672m>, 2013.
- Sipilä, M., Jokinen, T., Berndt, T., Richters, S., Makkonen, R., Donahue, N. M., Mauldin III, R. L., Kurtén, T., Paasonen, P., Sarnela, N., Ehn, M., Junninen, H., Rissanen, M. P., Thornton, J., Stratmann, F., Herrmann, H., Worsnop, D. R., Kulmala, M., Kerminen, V. M., and Petäjä, T.: Reactivity of stabilized Criegee intermediates (sCIs) from isoprene and monoterpene ozonolysis toward  $\text{SO}_2$  and organic acids, *Atmos. Chem. Phys.*, 14, 12143-12153, <https://doi.org/10.5194/acp-14-12143-2014>, 2014.
- Taatjes, C. A., Welz, O., Eskola, A. J., Savee, J. D., Scheer, A. M., Shallcross, D. E., Rotavera, B., Lee, E. P. F., Dyke, J. M., Mok, D. K. W., Osborn, D. L., and Percival, C. J.: Direct measurements of conformer-dependent reactivity of the Criegee intermediate  $\text{CH}_3\text{CHOO}$ , *Science*, 340, 177-180, <https://doi.org/10.1126/science.1234689>, 2013.
- Vereecken, L., Harder, H., and Novelli, A.: The reaction of Criegee intermediates with NO,  $\text{RO}_2$ , and  $\text{SO}_2$ , and their fate in the atmosphere, *Phys. Chem. Chem. Phys.*, 14, 14682-14695, <https://doi.org/10.1039/c2cp42300f>, 2012.
- Vereecken, L.: The reaction of Criegee intermediates with acids and enols, *Phys. Chem. Chem. Phys.*, 19, 28630-28640, <https://doi.org/10.1039/c7cp05132h>, 2017.
- Welz, O., Eskola, A. J., Sheps, L., Rotavera, B., Savee, J. D., Scheer, A. M., Osborn, D. L., Lowe, D., Booth, A. M., Xiao, P., Khan, M. A. H., Percival, C. J., Shallcross, D. E., and Taatjes, C. A.: Rate coefficients of C(1) and C(2) Criegee intermediate reactions with formic and acetic acid near the collision limit: direct kinetics measurements and atmospheric implications, *Angew. Chem. Int. Ed.*, 53, 4547-4550, <https://doi.org/10.1002/anie.201400964>, 2014.
- Welz, O., Savee, J. D., Osborn, D. L., Vasu, S. S., Percival, C. J., Shallcross, D. E., and Taatjes, C. A.: Direct kinetic measurements of Criegee intermediate ( $\text{CH}_2\text{OO}$ ) formed by reaction of  $\text{CH}_2\text{I}$  with  $\text{O}_2$ , *Science*, 335, 204-207, <https://doi.org/10.1126/science.1213229>, 2012.
- Zhao, Y., Wingen, L. M., Perraud, V., Greaves, J., and Finlayson-Pitts, B. J.: Role of the reaction of stabilized Criegee intermediates with peroxy radicals in particle formation and growth in air, *Phys. Chem. Chem. Phys.*, 17, 12500-12514, <https://doi.org/10.1039/c5cp01171j>, 2015.